NASA TECHNICAL NOTE

NASA TN D-5476

TRANSPORT PROPERTIES AT HIGH TEMPERATURES OF CO_2-N_2-O_2-Ar GAS MIXTURES FOR PLANETARY ENTRY APPLICATIONS

by Jerry S. Lee and Percy J. Bobbitt

Langley Research Center
Langley Station, Hampton, Va.

NATIONAL AERONAUTICS AND SPACE ADMINISTRATION • WASHINGTON, D. C. • NOVEMBER 1969

1. Report No. NASA TN D-5476	2. Government Accession No.	3. Recipient's Catalog No.
4. Title and Subtitle TRANSPORT PROPERTIES AT HIGH TEMPERATURES OF CO_2-N_2-O_2-Ar GAS MIXTURES FOR PLANETARY ENTRY APPLICATIONS		5. Report Date November 1969 6. Performing Organization Code
7. Author(s) Jerry S. Lee (North Carolina State University at Raleigh) and Percy J. Bobbitt		8. Performing Organization Report No. L-6395 10. Work Unit No. 129-01-22-10-23
9. Performing Organization Name and Address NASA Langley Research Center Hampton, Va. 23365		11. Contract or Grant No. 13. Type of Report and Period Covered Technical Note
12. Sponsoring Agency Name and Address National Aeronautics and Space Administration Washington, D.C. 20546		14. Sponsoring Agency Code

15. Supplementary Notes

16. Abstract

The equations and assumptions employed to compute the viscosity, thermal conductivity, and Prandtl number for high-temperature gas mixtures which, at low temperatures, may be composed of arbitrary percentages of CO_2, N_2, O_2, and Ar are presented. Ionization phenomena are not considered; hence, the results are limited to pressures and temperatures where dissociation reactions dominate. Numerical results are obtained for three different "atmospheric" gas mixtures: air, 100 percent CO_2, and a mixture of 43 percent CO_2, 25 percent N_2, and 32 percent Ar (by vol.). Comparisons of the latter two mixtures with air and, also, of air and CO_2 with the results of other investigations are given. In addition, transport properties computed from the full equations of the first approximation of the Chapman-Enskog rigorous kinetic theory are compared to those computed from first and second approximations to these equations.

17. Key Words Suggested by Author(s) CO_2-N_2-O_2-Ar gas mixture High-temperature transport properties Viscosity Prandtl number Thermal conductivity	18. Distribution Statement Unclassified – Unlimited		
19. Security Classif. (of this report) Unclassified	20. Security Classif. (of this page) Unclassified	21. No. of Pages 114	22. Price* $3.00

*For sale by the Clearinghouse for Federal Scientific and Technical Information Springfield, Virginia 22151

TRANSPORT PROPERTIES AT HIGH TEMPERATURES OF CO_2-N_2-O_2-Ar GAS MIXTURES FOR PLANETARY ENTRY APPLICATIONS

By Jerry S. Lee* and Percy J. Bobbitt
Langley Research Center

SUMMARY

The equations and assumptions employed to compute the viscosity, thermal conductivity, and Prandtl number for high-temperature gas mixtures which, at low temperatures, may be composed of arbitrary percentages of CO_2, N_2, O_2, and Ar are presented. Ionization phenomena are not considered; hence, the results are limited to pressures and temperatures where dissociation reactions dominate. Numerical results are obtained for three different "atmospheric" gas mixtures: air, 100 percent CO_2, and a mixture of 43 percent CO_2, 25 percent N_2, and 32 percent Ar (by vol.). Comparisons of the latter two mixtures with air and, also, of air and CO_2 with the results of other investigations are given. In addition, transport properties computed from the full equations of the first approximation of the Chapman-Enskog rigorous kinetic theory are compared to those computed from first and second approximations to these equations.

INTRODUCTION

The Martian atmosphere, as well as other planetary atmospheres, is believed to consist primarily of carbon dioxide, nitrogen, and argon. In order to perform meaningful boundary layer and wake analyses for entry spacecraft, reasonably accurate values of the high-temperature thermodynamic and transport properties of these atmospheres are required. Thermodynamic properties of several NASA Mars model atmospheres have already been calculated (refs. 1 to 4). In this report, attention is focused on the calculation of viscosity, thermal conductivity, and Prandtl number of dilute, ideal gas mixtures in a state of local chemical equilibrium. The mixtures consist of a maximum of nine chemical species: CO_2, O_2, N_2, NO, CO, O, N, C, and Ar. A specific mixture need not contain all nine of these species.

There are several approaches to the computation of transport properties of multicomponent mixtures. The first approach, such as presented by Kennard (ref. 5), makes

*Assistant Professor, North Carolina State University at Raleigh.

use of simple kinetic theory based on mean free path concepts. The second approach makes use of the more precise Chapman-Enskog theory (ref. 6) which was extended to multicomponent mixtures by Hirschfelder, Curtiss, and Bird (ref. 7) and which was modified to account for multiple atomic interactions by Mason, Vanderslice, and Yos (ref. 8). The third approach makes use of the kinetic theory of polyatomic gas mixtures developed by Monchick, Yun, and Mason (ref. 9).

The first two approaches apply rigorously only to dilute, nonreactive, monatomic gas mixtures, and the third applies to dilute, nonreactive, polyatomic gas mixtures. Thus, in a strict sense, none of these theories can be used for the mixtures under consideration without modification. Of the three approaches, the third is the most applicable. However, utilization of this theory requires extensive knowledge of rotational and vibrational relaxation times which, unfortunately, are not currently available for all of the polyatomic species. In this work, a slight modification of the second monatomic gas theory, referred to as the rigorous kinetic theory, is used.

The principal modification consists of the introduction of an expression (ref. 10) to account for the effects of internal degrees of freedom on thermal conductivity. For viscosity and the translational portion of the thermal conductivity, the equations resulting from the first approximation (i.e., the lowest Sonine approximation leading to nonzero results for the transport properties) of first-order Chapman-Enskog perturbation theory (ref. 7) are used directly. In other words, internal degrees of freedom and chemical reactions are assumed to have negligible perturbing effects on these equations. The results of Butler and Brokaw (ref. 11) are used to compute a reactive contribution to the thermal conductivity. It is also assumed that the collision integrals involved in all these equations, referred to herein as the full kinetic-theory equations, can be evaluated from orientation-averaged interaction potentials.

Although the basic equations for calculating transport properties are well known (refs. 7 and 10 to 14), the collision integrals needed in these equations have not yet been determined for all pairs of species present in the atmospheric models. Fortunately, many of the interactions of importance also occur in air, and these have received considerable study (refs. 15 to 19). Herein, the tables of Yun and Mason (ref. 19), containing the most important air-collision integrals, are used.

The procedure followed in obtaining collision integrals for the remaining interactions – namely those associated with CO_2, CO, C, and Ar – is a modification of the technique employed by Amdur and Mason (ref. 20). For each interaction, appropriate low-temperature and high-temperature potentials are obtained from experimental data and/or approximate calculations. Then, the low-temperature and high-temperature collision integrals determined by these potentials are plotted as a function of temperature, and the two branches are joined by a smooth curve. Although this curve is not uniquely defined,

the technique should be markedly superior to using collision integrals generated from low-temperature potentials throughout the entire temperature range.

Numerical results for viscosity, thermal conductivity, and Prandtl number are obtained for three different atmospheres: air, 100 percent CO_2, and a mixture (referred to herein as the Mars model atmosphere) of 43 percent CO_2, 25 percent N_2, and 32 percent Ar (by vol.). Comparisons of the latter two atmospheres with air and of the present air results with those of Hansen (ref. 21) and Yos (ref. 22) are shown. The CO_2 results are compared with those of Thomas (ref. 23) and Van Tassell (ref. 24). Transport properties obtained from the full kinetic-theory equations are compared with those obtained from first and second approximations to these equations.

SYMBOLS

A parameter in exponential repulsive potential (eq. (6)), electron volts

A_{ij}^* collision integral ratio

a parameter in exponential repulsive potential (eq. (6)), 1/angstrom

B_{ij}^* collision integral ratio

b impact parameter

$C_{1,ij}, C_{2,ij}, C_{3,ij}, C_{4,ij}, C_{5,ij}$ constant defined by equation (B10), (B11), (B12), (B24), and (B25), respectively

c_p mixture specific heat at constant pressure (per mole of undissociated mixture)

c_p^* nondimensional mixture specific heat at constant pressure, $\frac{c_p}{R}$

$c_{p,i}$ molar specific heat at constant pressure of species i

$c_{p,i}^*$ nondimensional specific heat at constant pressure of species i, $\frac{c_{p,i}}{R}$

D_{ij} binary diffusion coefficient of species i and j

d parameter in point center of repulsive force potential (eq. (5))

d_O, d_N	distance from center of mass of molecule to O or N atom
E_{ik}	element in reactive conductivity determinants (eqs. (B30) and (B31))
E^*_{ik}	nondimensional element in reactive conductivity determinants (eqs. (41) and (42)), $\frac{\lambda_O}{R} E_{ik}$
g	initial relative speed of colliding particles
ΔH_i	enthalpy of reaction for reaction i
ΔH^*_i	nondimensional enthalpy of reaction for reaction i, $\frac{\Delta H_i}{RT}$
H_{ij}	element in viscosity determinants (eqs. (B2) and (B3))
H^*_{ij}	nondimensional element in viscosity determinants (eqs. (25) and (26)), $\eta_O H_{ij}$
h_i	molar enthalpy of species i
h^*_i	nondimensional molar enthalpy of species i, $\frac{h_i}{RT}$
i,j,k,m,p	indices
k	Boltzmann's constant
L_{ij}	elements in translational conductivity determinants (eqs. (B17) and (B18))
L^*_{ij}	nondimensional elements in translational conductivity (eqs. (31) and (32)), $\lambda_O L_{ij}$
M_i	molecular weight of species i
M_u	molecular weight of undissociated mixture
m	mass per particle, grams
N_A	Avogadro's number

N_{Pr}	Prandtl number
$N_{Pr,I}$	first approximation to Prandtl number
$N_{Pr,II}$	second approximation to Prandtl number
n	parameter in point center of repulsive force potential (eq. (5))
n_{ij}	stoichiometric coefficient of species j in reaction i
p	pressure, atmospheres
R	universal gas constant, ergs per ^{o}K-mole
r	distance between colliding particles, angstroms
r_m	value of r at potential energy minimum
r'_m	distance of closest approach of particles
T	absolute temperature, ^{o}K
T^*	nondimensional absolute temperature, $\frac{T}{\epsilon/k}$
t	number of independent reactions
$[X]_i$	symbolic representation of chemical symbol for species i
x_i	mole fraction of species i
α	parameter controlling steepness of repulsive part of exp-6 potential
α_i	exp-6 parameter for binary collision of particles of species i
α_{ij}	exp-6 parameter for binary collisions of particles of species i and j
β	temperature parameter used in finding collision integrals for exponential repulsive potential (eq. (22))

γ^* nondimensional relative velocity, $\left(\frac{\mu}{2kT}\right)^{1/2} g$

Δ_{ij} parameter in reactive conductivity equations

Δ_{ij}^* nondimensional parameter in reactive conductivity equations, $\frac{\lambda_o}{R} \Delta_{ij}$

ϵ depth of potential well, electron volts

ϵ_i depth of potential well for interaction of two particles of species i, electron volts

ϵ_{ij} depth of potential well for interaction of two particles of different species i and j, electron volts

η viscosity

η^* nondimensional viscosity, $\frac{\eta}{\eta_o}$

η_I^* first approximation to viscosity

η_{II}^* second approximation to viscosity

η_i viscosity of pure species i

η_o reference viscosity, $3.20295 \times 10^{-5} \sqrt{T}$, grams per centimeter-second

λ total thermal conductivity

λ^* nondimensional total thermal conductivity, $\frac{\lambda}{\lambda_o}$

λ_I^* first approximation to total thermal conductivity

λ_{II}^* second approximation to total thermal conductivity

λ_f frozen thermal conductivity, $\lambda_t + \lambda_{int}$

$\lambda_{f,I}$ first approximation to frozen thermal conductivity

$\lambda_{f,II}$ second approximation to frozen thermal conductivity

λ_f^* nondimensional frozen thermal conductivity, $\frac{\lambda_f}{\lambda_o}$

λ_i conductivity of pure species i

λ_{int} internal contribution to total thermal conductivity

λ_{int}^* nondimensional internal conductivity, $\frac{\lambda_{int}}{\lambda_o}$

λ_o reference thermal conductivity, $4.16118 \times 10^3 \sqrt{T}$, ergs per centimeter-$^oK$-second

λ_r reactive contribution to total thermal conductivity

λ_r^* nondimensional reactive conductivity, $\frac{\lambda_r}{\lambda_o}$

$\lambda_{r,I}^*$ first approximation to reactive conductivity

λ_t translational contribution to total thermal conductivity

λ_t^* nondimensional translational conductivity, $\frac{\lambda_t}{\lambda_o}$

$\lambda_{t,I}^*$ first approximation to translational conductivity

$\lambda_{t,II}^*$ second approximation to translational conductivity

μ reduced mass, $\frac{m_i m_j}{m_i + m_j}$

ν total number of species considered

σ collision diameter, angstroms

σ_i collision diameter for binary collision of species i

σ_{ij} collision diameter for binary collision of species i and j

ϕ interaction potential, electron volts

χ angle of deflection

$\Omega^{(l,s)}$ collision integral

$\Omega^{(l,s)^*}$ nondimensional collision integral, $\dfrac{\Omega^{(l,s)}}{\Omega^{(l,s)}_{\text{rigid sphere}}}$

$\overline{\Omega}^{(l,s)}$ modified collision integral, $\sigma^2\Omega^{(l,s)^*}$, angstroms^2

ANALYSIS

Thermodynamic Properties

The thermodynamic properties required in calculating mixture transport properties are the mole fractions, the mixture constant-pressure specific heat, the species constant-pressure specific heats, and the species enthalpies. For each mixture, these properties were calculated by using the computer program developed by Allison (ref. 3) and Newman and Allison (ref. 4). Figures 1, 2, and 3 show the dependence of the mole fractions on temperature for pressures of 0.001, 0.01, 0.1, 1.0, and 10 atm for air, CO_2, and the Mars model atmosphere (43% CO_2, 25% N_2, 32% Ar (by vol.)), respectively. Figures 4, 5, and 6 show the variation of the nondimensional specific heat of these mixtures with temperature for the same pressures. The nondimensional species specific heats and species enthalpies are shown in figures 7 and 8, respectively, and apply for all three mixtures.

Inspection of figures 1 to 3 reveals that electrons and ionized atoms become important at the higher temperatures, especially at low pressure. Since ionization is not included in subsequent transport-property calculations, it is necessary to specify regions of validity for these properties. More is said about this in the section "Results and Discussion."

Potentials

As noted in the Introduction, transport properties depend upon the collision integrals for each pair of chemical species in the mixture. These collision integrals, in turn, depend upon the interaction potentials for the possible binary encounters. It is therefore

appropriate at this point to enumerate all possible binary interactions for a mixture of CO_2, O_2, N_2, NO, CO, O, N, C, and Ar. These interactions are given in table 1.

With reference to table 1, parentheses around a pair designate that its interaction potential has been considered previously and that the corresponding collision integrals can be obtained from the tabular values of Yun and Mason (ref. 19). Brackets around a pair mean that an accurate interaction potential for the pair is not critical because one or both of the mole fractions associated with the pair are always small. Table 2 summarizes the potentials used in the computations. The atom-atom potentials listed in this table apply to the interaction of atoms in their ground electronic states. For the limited temperature range considered herein, such potentials are adequate.

In the following paragraphs, some general comments are made about the interaction potentials. Then attention is focused on specific cases with special emphasis placed on pointing out the difficulties encountered and the assumptions invoked.

The potentials used at low temperature are the Lennard-Jones 6-12 potential,

$$\phi = 4\epsilon\left[\left(\frac{\sigma}{r}\right)^{12} - \left(\frac{\sigma}{r}\right)^{6}\right] \tag{1}$$

and the modified Buckingham exp-6 potential

$$\phi = \frac{\epsilon}{1 - \frac{6}{\alpha}}\left[\frac{6}{\alpha} e^{\alpha\left(1 - \frac{r}{r_m}\right)} - \left(\frac{r_m}{r}\right)^{6}\right] \tag{2}$$

Potential parameters (i.e., ϵ, σ, α, and r_m) for many of the like-like interactions were obtained from references 7 and 25 for the 6-12 and exp-6 potentials, respectively. In the absence of experimental data, potential parameters for interactions of unlike molecules were generated from those for like molecules by using empirical combining rules. For the 6-12 potential,

$$\sigma_{ij} = \frac{\sigma_i + \sigma_j}{2} \tag{3a}$$

$$\epsilon_{ij} = \sqrt{\epsilon_i \epsilon_j} \tag{3b}$$

and for the exp-6 potential,

$$r_{m,ij} = \frac{r_{m,i} + r_{m,j}}{2} \tag{4a}$$

$$\epsilon_{ij} = \sqrt{\epsilon_i \epsilon_j} \tag{4b}$$

$$\alpha_{ij} = \frac{\alpha_i + \alpha_j}{2} \tag{4c}$$

These rules hold well for the interaction of molecules i and j provided these molecules have essentially spherically symmetric force fields. The sources from which potential parameters were obtained are given in table 2.

At high temperatures the repulsive portion of the potential primarily determines the collision integrals (ref. 7). Under these conditions, two potential forms were used: the point center of repulsive force potential

$$\phi = \frac{d}{r^n} \tag{5}$$

and the exponential repulsive potential

$$\phi = Ae^{-ar} \tag{6}$$

where d, n, A, and a are constants for a given interaction. Potentials derived from molecular beam scattering experiments are normally cast in the first form, although the second can be used. Results of semiempirical quantum mechanical calculations are usually presented in the second form which has some theoretical basis. According to Amdur and Mason (ref. 20), equation (6) usually remains valid over a wider range of r than equation (5). For both potentials, experiment seems to confirm a geometric mean rule for finding potentials for unlike atoms from those for like atoms (ref. 20). That is, if ϕ(D-D) denotes the interaction potential for two D atoms and if ϕ(E-E) denotes the interaction potential for two E atoms, then the interaction potential for atoms D and E is given by (refs. 20, 26, 27, and 28)

$$\phi(\text{D-E}) = \sqrt{\phi(\text{D-D})\ \phi(\text{E-E})} \tag{7}$$

It should be emphasized that this rule does not apply to atom-molecule or molecule-molecule interactions.

Many of the high-temperature atom-molecule and molecule-molecule interaction potentials listed in table 2 were obtained by averaging appropriate atom-atom potentials over all orientations as was done in references 19 and 28 for binary interactions of atoms with diatomic molecules and diatomic molecules with diatomic molecules. Appendix A extends this technique to include interactions with the triatomic CO_2 molecule. Specific cases are treated in the following sections.

Carbon monoxide interactions.- Figures 2 and 3 show that CO is a major constituent in the CO_2 and CO_2-N_2-Ar mixtures throughout most of the temperature range considered. Consequently, reliable transport property computations hinge strongly on knowledge of potentials for the various CO-molecule and CO-atom interactions. Yet there exists only a meager amount of information on these potentials, especially at high temperature. Specifically, molecular beam scattering experiments on the Ar-CO system yield (ref. 29)

$$\phi(\text{Ar-CO}) = \frac{551}{r^{6.99}} \text{ eV} \qquad (2.09 \text{ Å} \leqq r \leqq 2.68 \text{ Å}) \qquad (8)$$

To the authors' knowledge, no high-temperature potentials are presently available for the remaining CO interactions.

Because of this lack of data, it was necessary to resort to reasonable approximations. The logic used proceeds as follows. Since CO and N_2 have very similar nuclear and electronic structures and since these factors play a dominant role in determining intermolecular potentials, it appears plausible to assume that CO and N_2 behave similarly during molecular encounters. An indication of the validity of this assumption is provided in figure 9 where the high-temperature scattering potential for Ar-N_2[1] (ref. 29),

$$\phi(\text{Ar-N}_2) = \frac{567}{r^{7.06}} \text{ eV} \qquad (2.04 \text{ Å} \leqq r \leqq 2.53 \text{ Å}) \qquad (9)$$

is compared to the Ar-CO potential given by equation (8). The percent difference in energy varies from about 3 percent at the smallest common value of r to about 4 percent at the highest common value of r. From the standpoint of transport-property computations, the comparison is extremely favorable because the potentials enter these computations solely through collision integrals, and these quantities are relatively insensitive to the magnitude of the potentials. Figures 10 and 11, which compare the two most important collision integrals for the potentials of equations (8) and (9), clearly demonstrate this point. The percent difference in corresponding collision integrals never exceeds 3.1 percent. Figures 12 and 13 compare low-temperature collision integrals for CO-CO and N_2-N_2 interactions. The Lennard-Jones 6-12 potential with parameters derived from viscosity measurements (ref. 7) was used for each interaction. Again the agreement is remarkable.

[1]The high-temperature potential listed in table 2 for Ar-N_2 differs from equation (9). Equation (9) is valid for a higher temperature range than considered in the transport-property computations. It is used here simply because its range of validity is very nearly the same as that of equation (8). Were this not true, the comparisons would be meaningless.

Based on these comparisons, it was assumed that the potential for each CO interaction could be replaced by the potential for the analogous N_2 interaction; for example, CO-O_2 was treated as N_2-O_2. This assumption is incorporated in table 2.

Argon interactions.- With the exception of the Ar-CO_2, Ar-C, Ar-O, and Ar-NO interactions, table 2 provides adequate explanation of the methods employed to formulate interaction potentials for the various argon interactions. Potentials for Ar-CO_2 and Ar-C interactions are considered in later sections dealing with carbon dioxide and carbon interactions, respectively. This section deals with high-temperature potentials for the Ar-O and Ar-NO interactions.

The high-temperature Ar-O potential was calculated from the geometric mean rule (eq. (7)) with

$$\phi(\text{Ar-Ar}) = 3.23 \times 10^4 \, e^{-4.464r} \text{ eV} \tag{10}$$

and

$$\phi(\text{O-O}) = 32.56 \, e^{-2.197r} \text{ eV} \tag{11}$$

where ϕ(Ar-Ar) was taken directly from reference 20 and ϕ(O-O) was obtained from a least-squares curve fit of Meador's results (ref. 18).

It should be noted that Vanderslice, Mason, and Maisch (ref. 17) also present a potential for the O-O interaction. When their result is used, ϕ(Ar-O) differs appreciably from that given in table 2. However, the collision integrals corresponding to the two potentials differ very little. Meador's result for ϕ(O-O) was chosen primarily because it leads to greater consistency with known low-temperature potentials when it is used in the construction of high-temperature potentials for more complex interactions, such as CO_2-O_2, by the orientation-averaging technique. The same situation exists for the N-N interaction, which arises in the computation of the Ar-N interaction.

To calculate the high-temperature Ar-NO potential, the technique of averaging individual atom-atom interaction potentials over all molecular orientations was employed (ref. 19). This procedure yields

$$\phi(\text{Ar-NO}) = \frac{A_{ArO} e^{-a_{ArO} r}}{a_{ArO}^2 d_O r} \left[\left(a_{ArO} r + 1 \right) \sinh \left(a_{ArO} d_O \right) - a_{ArO} d_O \cosh \left(a_{ArO} d_O \right) \right]$$

$$+ \frac{A_{ArN} e^{-a_{ArN} r}}{a_{ArN}^2 d_N r} \left[\left(a_{ArN} r + 1 \right) \sinh a_{ArN} d_N - a_{ArN} d_N \cosh \left(a_{ArN} d_N \right) \right] \tag{12}$$

where A_{ArO}, a_{ArO}, A_{ArN}, and a_{ArN} are exponential repulsive potential parameters for the Ar-O and Ar-N potentials (eq. (6)); r is the distance from the center of mass of the nitric oxide molecule to the argon atom; and d_O and d_N are the distances from the center of mass of the nitric oxide molecule to its oxygen and nitrogen atoms, respectively. The Ar-O parameters can be obtained by inspection of ϕ(Ar-O) in table 2. The Ar-N parameters come from

$$\phi(\text{Ar-N}) = 2025e^{-3.59r} \text{ eV} \tag{13}$$

Equation (13) was obtained from the geometric mean rule using the Ar-Ar potential presented in equation (10) and Meador's result for the N-N potential (ref. 18),

$$\phi(\text{N-N}) = 127e^{-2.716r} \text{ eV} \tag{14}$$

According to Herzberg (ref. 30),

$$d_O = 0.53667 \text{ Å}$$

$$d_N = 0.61333 \text{ Å}$$

In order to make use of available tables of collision integrals, a least-squares curve fit of equation (12) was performed to obtain the exponential repulsive potential presented in table 2.

Carbon dioxide interactions.- All low-temperature potentials in table 2 for CO_2 interactions except those for CO_2-CO_2, CO_2-NO, and CO_2-Ar are based on experimental diffusion coefficient determinations (ref. 31). Lack of such data for CO_2-NO and CO_2-Ar interactions necessitated use of viscosity data and the combining rules given in equations (3).

The validity of using the low-temperature CO_2-CO_2 potential in table 2 in the calculation of multicomponent mixture transport properties is open to question. Recent self-diffusion coefficient measurements for CO_2 between 1103° K and 1944° K indicate that different sets of 6-12 parameters are required to correlate viscosity and self-diffusion data (refs. 32 and 33). Use of the potential from viscosity measurements in the prediction of self-diffusion coefficients, and vice versa, can produce errors as high as 30 percent or 40 percent at temperatures around 2000° K. Quite likely the need for two distinct potentials to correlate experimental results arises from the fact that CO_2 is a long linear molecule with a nonspherical force field. Based on this evidence, one must conclude that the theory does not yield uniformly good results for CO_2.

In an effort to decide whether the viscosity or self-diffusion potential was more appropriate for present purposes, the low-temperature viscosity and thermal conductivity of pure CO_2 were calculated by using both potentials. The viscosity potential led to good agreement with experimental viscosity and conductivity correlations (ref. 34) for CO_2, and the diffusion potential led to poor agreement. Therefore, it was assumed that the viscosity potential should also be more appropriate for mixture computations. It should be noted, however, that the situation might be reversed in the computation of multicomponent diffusion-coefficient properties which are not considered herein.

With the exception of the CO_2-N and CO_2-C interactions, the high-temperature CO_2-molecule and CO_2-atom potentials in table 2 were derived by averaging atomic interactions over all orientations. Appendix A contains all pertinent equations used in this procedure. Since these equations contain the C-O, C-C, C-N, and C-Ar interaction potentials and since these potentials are not currently available, it was necessary to introduce further approximations. The C-O potential was approximated with the N-N potential; and in the last three interactions, the carbon atom was treated as a nitrogen atom. These approximations are not as critical as it might appear because the averaging process automatically emphasizes the interactions of the peripheral atoms. Finally, establishment of CO_2-N_2 and CO_2-NO potentials requires knowledge of ϕ(N-O). For both potentials,

$$\phi(\text{N-O}) = 69.17e^{-2.556r} \text{ eV} \tag{15}$$

was used. This potential was found by curve-fitting Meador's results (ref. 18). After the introduction of these approximate potentials into the equations of appendix A, each orientation-averaged potential was replaced by a least-squares curve fit to obtain the results presented in table 2.

Carbon interactions.- The assumption that carbon atoms can be replaced by nitrogen atoms was also utilized in obtaining potentials for the interaction of carbon atoms with the various atoms and molecules. This assumption is much more critical because carbon—other-atom potentials occur in every term of the orientation-averaged potentials.

Collision Integrals

As noted previously, interaction potentials enter transport-property computations through a set of collision integrals. For the interaction of particles i and j along a single potential ϕ, the integrals are defined by the following formulas (ref. 7):

$$\chi = \pi - 2b \int_{r'_m}^{\infty} \frac{dr}{r^2 \sqrt{1 - \frac{b^2}{r^2} - \frac{\phi}{\frac{1}{2}\mu g^2}}} \tag{16}$$

$$\Omega^{(l,s)} = \sqrt{\frac{2\pi kT}{\mu}} \int_0^\infty \int_0^\infty e^{-\gamma^{*2}} \gamma^{*2s+3} \left(1 - \cos^l \chi\right) b \, db \, d\gamma^* \tag{17}$$

In general, two ground state atoms can interact along any one of several potential energy curves. For this situation, equations (16) and (17) must be evaluated for each curve, and then all of the resulting collision integrals with the same superscripts are averaged with a priori assigned weighting factors to yield an effective set of collision integrals for the interaction (ref. 8). These computations have been performed for the atom-atom interactions of importance in dissociating air (ref. 19), and fortunately, many of the same results also apply for the mixtures under consideration.

The basic-mixture transport-property equations are usually expressed in terms of reduced collision integrals. In reference 7, which is probably the most widely used reference for gaseous transport theory, the transport properties are formulated in terms of a set of quantities $\Omega^{(l,s)^*}$, defined as the ratio of equation (17) to the corresponding expression for the rigid sphere model; that is,

$$\Omega^{(l,s)^*} = \frac{\Omega^{(l,s)}}{\Omega^{(l,s)}_{\text{rigid sphere}}} \tag{18}$$

In the tabulations of the collision integrals of air, Yun and Mason (ref. 19) employed the slightly modified form,

$$\overline{\Omega}^{(l,s)} = \sigma^2 \Omega^{(l,s)^*} \tag{19}$$

where σ denotes the collision diameter. Since these tabulations were used in the present work, this notation was adopted for all interactions.

The following collision integrals and collision integral ratios are required to compute mixture viscosity and thermal conductivity:

$$\overline{\Omega}^{(1,1)}_{ij} \tag{20a}$$

$$\overline{\Omega}^{(2,2)}_{ij} \tag{20b}$$

$$A^*_{ij} = \frac{\overline{\Omega}^{(2,2)}_{ij}}{\overline{\Omega}^{(1,1)}_{ij}} \tag{20c}$$

$$B^*_{ij} = \frac{5\overline{\Omega}^{(1,2)}_{ij} - 4\overline{\Omega}^{(1,3)}_{ij}}{\overline{\Omega}^{(1,1)}_{ij}} \tag{20d}$$

In these equations, subscripts i and j designate quantities associated with the interaction of species i and j.

For a given pair of species, that is for fixed i and j, $\overline{\Omega}_{ij}^{(1,1)}$ and $\overline{\Omega}_{ij}^{(2,2)}$ vary considerably with temperature. In addition, at a fixed temperature, both quantities differ significantly for different pairs of species. On the other hand, A_{ij}^* and B_{ij}^* vary little regardless of the temperature or of the pair of species considered. This fact is illustrated in figures 14 and 15 where these quantities are plotted for the Lennard-Jones 6-12 and modified Buckingham exp-6 potentials. Figure 16 shows the quantities for the exponential repulsive potential. The abscissa in figures 14 and 15 is defined as

$$T^* = \frac{T}{\epsilon/k} \tag{21}$$

and that in figure 16 as

$$\beta = \ln\left(\frac{A}{kT}\right) \tag{22}$$

Generally, for the low-temperature potentials in table 2, the extreme right-hand portions of figures 14 and 15 apply. Furthermore, β normally ranges between 7 and 10. As can be seen from the graphs, little error should incur if A_{ij}^* and B_{ij}^* are arbitrarily assigned the constant values

$$A_{ij}^* = 1.18 \tag{23a}$$

$$B_{ij}^* = 1.15 \tag{23b}$$

These values give slight emphasis to the exponential repulsive potential (fig. 16) because of its appropriateness at the higher temperatures of interest. At any rate, actual values should deviate from the assigned ones by less than 5 percent. These results were used in all transport-property calculations.

For $\overline{\Omega}_{ij}^{(1,1)}$ and $\overline{\Omega}_{ij}^{(2,2)}$ no simple approximations hold because of the significant variations mentioned; consequently, it was necessary to consider each individual interaction. Collision integrals for interactions that occur in air were taken directly from reference 19. Collision integrals for the remaining interactions, given in table 3, were obtained by essentially the same method employed in references 19 and 20. The principal steps followed in this procedure were as follows. For each interaction, $\overline{\Omega}^{(1,1)}$ was computed for both the low- and high-temperature potentials and plotted as a function of temperature. This produced a curve consisting of two branches whose ranges of validity were estimated by using the technique of Hirschfelder and Eliason (ref. 35). The

branches were then joined by a single smooth curve from which values of $\overline{\Omega}^{(1,1)}$ were read. This procedure was also used for $\overline{\Omega}^{(2,2)}$. Collision integrals for the Lennard-Jones 6-12 potential were obtained from reference 7; those for the modified Buckingham exp-6 potential from references 7 and 25; those for the point center of repulsive force potential from reference 36; and those for the exponential repulsive potential from reference 37.

Although there is no way of checking the absolute accuracy of the results presented in table 3, it should be pointed out that the calculation procedure outlined is intrinsically more accurate for some interactions than others because of variation in the lengths of the "faired-in" curves. To illustrate this point, curves used for the Ar-O_2 and CO_2-O_2 interactions are shown in figures 17 to 19. Figure 20 gives $\overline{\Omega}^{(2,2)}$ for the CO_2-O_2 interaction computed from both the high- and low-temperature potentials. No faired curve is given, however, since the upper curve does not become valid until the temperature exceeds the range considered. Clearly, the Ar-O_2 results should be more accurate than the CO_2-O_2 results. Actually, the CO_2-O_2 curves are typical of all curves encountered for CO_2 interactions. This further bears out the point made earlier concerning the uncertainty associated with CO_2 interactions.

Transport Properties

In the preceding sections all requisite data for computing viscosity, thermal conductivity, and Prandtl number have been presented. This section summarizes convenient forms of the equations for these properties. In addition, possible causes of numerical inaccuracy are pointed out, and techniques for alleviating inaccuracy are given.

Because of the complexity of the kinetic-theory equations for viscosity and thermal conductivity of multicomponent mixtures, investigators (refs. 38 and 39, for example) have developed a number of relatively simple approximations, which "normally" yield values within a few percent of those attained from the full equations. In this note, the full equations were employed for the following reasons:

1. As pointed out by Brokaw (ref. 14), inherent deviations in individual properties introduced by the use of approximate formulas may be such that errors are magnified in forming such ratios as the Prandtl number.

2. The systems under consideration are simple enough that the full equations can be solved very rapidly with the aid of a high-speed computer.

For purposes of assessing the validity of using approximate equations and also of comparing the final results with those of other authors, first and second approximations to the viscosity, translational thermal conductivity, and a first approximation to reactive conductivity are included in the following subsections. These equations as well as the

special forms of the full equations are derived from more familiar equations in appendix B.

Viscosity.- It is shown in appendix B that the full kinetic-theory expression for the viscosity of a ν-component, monatomic gas mixture can be expressed in dimensionless forms as

$$\eta^* = -\frac{\begin{vmatrix} H_{11}^* & H_{12}^* & \cdots & H_{1\nu}^* & x_1 \\ H_{12}^* & H_{22}^* & \cdots & H_{2\nu}^* & x_2 \\ \cdot & \cdot & \cdot & \cdot & \cdot \\ \cdot & \cdot & \cdot & \cdot & \cdot \\ \cdot & \cdot & \cdot & \cdot & \cdot \\ H_{1\nu}^* & H_{2\nu}^* & \cdots & H_{\nu\nu}^* & x_\nu \\ x_1 & x_2 & \cdots & x_\nu & 0 \end{vmatrix}}{\left|H_{ij}^*\right|} \tag{24}$$

where

$$H_{ii}^* = \frac{1.2\overline{\Omega}_{ii}^{(2,2)}}{\sqrt{M_i}} x_i^2 + 2 \sum_{\substack{j=1 \\ j \neq i}}^{\nu} x_i x_j C_{1,ij} \overline{\Omega}_{ij}^{(1,1)} \tag{25}$$

$$H_{ij}^* = -2x_i x_j C_{2,ij} \overline{\Omega}_{ij}^{(1,1)} \left(1 - \frac{3}{5} A_{ij}^*\right) \qquad (i \neq j) \tag{26}$$

and C_1 and C_2 are defined by equations (B10) and (B11).

Also shown in appendix B are the first and second approximations to equation (24),

$$\eta_I^* = \sum_{i=1}^{\nu} \frac{x_i^2}{H_{ii}^*} \tag{27}$$

and

$$\eta_{II}^* = \sum_{i=1}^{\nu} \frac{x_i^2}{H_{ii}^*} - \sum_{i=1}^{\nu} \sum_{\substack{j=1 \\ j \neq i}}^{\nu} \frac{x_i x_j H_{ij}^*}{H_{ii}^* H_{jj}^*} \tag{28}$$

Although equation (24) applies rigorously only to dilute monatomic gas mixtures, it is well known that the presence of internal degrees of freedom has very little influence on viscosity (ref. 7). Hence, this result was applied without modification to the mixtures of monatomic, diatomic, and triatomic species under consideration.

In using equation (24), care must be exercised to obtain meaningful results. Inspections of equations (25) and (26) reveals that both H_{ii}^* and H_{ij}^* approach 0 as x_i approaches 0. Under these conditions, both the numerator and denominator in equation (24) become small and the ratio approaches the indeterminant form 0/0. To apply the equation correctly, only those rows and columns associated with chemical species actually present in the mixture should be included. This means that the orders of the determinants may change with changes in temperature and pressure. In other words, when a given species disappears because of dissociation, its row and column must be omitted, and the remaining rows and columns must be shifted to fill the void. Likewise, when a new species appears, a new row and column must be included. However, the inclusion of new rows and columns can be avoided by initially formulating equation (24) so as to account for all possible species. Then one is concerned only with omitting appropriate rows and columns. This process can be actuated either by inspecting the magnitude of x_i or H_{ii}^* and was employed herein.

In addition to providing a means of avoiding numerical difficulty, the deletion process inherently results in greater flexibility. Thus, a single general formulation including many species can easily be specialized to simpler mixtures with fewer species.

Thermal conductivity.- As noted in the Introduction, the rigorous kinetic theory applies strictly to monatomic gases; thus, it does not account for the presence of internal degrees of freedom. Although these degrees of freedom do not significantly affect viscosity and diffusion, energy transition among the several degrees of freedom does markedly influence thermal conductivity. At present, however, available polyatomic mixture theories remain intractable so far as practical computations are concerned; therefore approximations must be invoked. Energy transport due to the combined effects of diffusion and chemical reactions can become extremely large under certain conditions; hence, it must be taken into account.

All these effects can be included in approximate fashion by expressing the total conductivity as (ref. 10)

$$\lambda = \lambda_t + \lambda_{int} + \lambda_r \tag{29}$$

where λ_t designates the translational contribution; λ_{int}, the internal contribution; and λ_r, the reactive contribution. A frozen conductivity is also used in the calculations and is defined as

$$\lambda_f = \lambda_t + \lambda_{int}$$

First and second approximations $\lambda_{f,I}$ and $\lambda_{f,II}$ are determined by replacing λ_t in the equation for λ_f with $\lambda_{t,I}$ and $\lambda_{t,II}$, respectively. The following paragraphs set forth the equations used to compute each contribution.

According to appendix B, the results of Muckenfuss and Curtiss (ref. 13) for the translational conductivity[2] can be expressed in nondimensional form as

$$\lambda_t^* = 4 \frac{\begin{vmatrix} L_{11}^* & L_{12}^* & \cdots & L_{1\nu}^* & x_1 \\ L_{12}^* & L_{22}^* & \cdots & L_{2\nu}^* & x_2 \\ \cdot & \cdot & \cdot & \cdot & \cdot \\ \cdot & \cdot & \cdot & \cdot & \cdot \\ \cdot & \cdot & \cdot & \cdot & \cdot \\ L_{1\nu}^* & L_{2\nu}^* & \cdots & L_{\nu\nu}^* & x_\nu \\ x_1 & x_2 & \cdots & x_\nu & 0 \end{vmatrix}}{\left| L_{ij}^* \right|} \tag{30}$$

where

$$L_{ii}^* = -2x_i^2 \overline{\Omega}_{ii}^{(2,2)} \sqrt{M_i} - \sum_{\substack{j=1 \\ j \neq i}}^{\nu} x_i x_j C_{2,ij} C_{4,ij} \overline{\Omega}_{ij}^{(1,1)} \tag{31}$$

$$L_{ij}^* = x_i x_j C_{2,ij} C_{5,ij} \overline{\Omega}_{ij}^{(1,1)} \qquad (i \neq j) \tag{32}$$

The constants C_2, C_4, and C_5 are defined by equations (B11), (B24), and (B25).

The first- and second-order approximations to equation (30) are

$$\lambda_{t,I}^* = -4 \sum_{i=1}^{\nu} \frac{x_i^2}{L_{ii}^*} \tag{33}$$

[2]Two definitions are commonly used for translational conductivity. The present form applies when the energy flux is expressed in terms of the temperature gradient and the diffusion velocities.

and

$$\lambda^*_{t,II} = -4 \sum_{i=1}^{\nu} \frac{x_i^2}{L^*_{ii}} + 4 \sum_{i=1}^{\nu} \sum_{\substack{j=1 \\ j \neq i}}^{\nu} \frac{x_i x_j L^*_{ij}}{L^*_{ii} L^*_{jj}} \tag{34}$$

The discussion, given previously in connection with viscosity, concerning the appearance and disappearance of chemical species as temperature and/or pressure change also applies to the evaluation of equation (30). Equation (30) was initially formulated to include all nine species. For a mixture containing less than nine species, the correct form was obtained by first deleting appropriate rows and columns in the numerator and denominator determinants and then shifting the remaining rows and columns to fill the gaps.

The internal contribution to the conductivity was computed from Hirschfelder's approximation (ref. 12)

$$\lambda_{int} = \sum_{i=1}^{\nu} \frac{x_i(\lambda_i - \lambda_{t,i})}{\sum_{j=1}^{\nu} x_j \frac{D_{ii}}{D_{ij}}} \tag{35}$$

together with his generalized Eucken expression (ref. 10),

$$\lambda_i = \lambda_{t,i} + \frac{D_{ii} p}{T}\left(\frac{c_{p,i}}{R} - \frac{5}{2}\right) \tag{36}$$

For computational convenience, these equations were combined and the resulting expression was written in nondimensional form as

$$\lambda^*_{int} = \frac{16}{25} \sum_{i=1}^{\nu} \frac{x_i\left(c^*_{p,i} - \frac{5}{2}\right)}{\sum_{j=1}^{\nu} x_j \overline{\Omega}^{(1,1)} C_{3,ij}} \tag{37}$$

The reactive contribution to the conductivity arises from the energy transport due to the combined effects of diffusion and chemical reactions. In regions of high temperature, dissociation occurs and then the species diffuse down the resulting concentration gradient to cooler regions where recombination occurs. Simultaneously, there is a flux

of recombined species from lower to higher temperature. The net effect is a transport of chemical enthalpy from regions of high temperature to regions of lower temperature.

The reactive contribution was computed from the original results of Butler and Brokaw (ref. 11).[3] Their formulation requires that the chemical reactions needed to account for the species present in the mixture be expressed in a special way. From the total of ν species present, t is chosen as independent. Then a system of t reactions is constructed such that each independent species occurs on the left-hand side of one, and only one, reaction and has -1 as its stoichiometric coefficient. Furthermore, the right-hand sides of the reactions contain dependent species only; that is, if n_{ij} denotes the stoichiometric coefficient of species j in the ith reaction and if $[X]_j$ denotes the chemical symbol of species j, the system of reactions takes the form

$$[X]_i = \sum_{j=t+1}^{\nu} n_{ij}[X]_j \qquad (i = 1,2,\ldots,t) \tag{38}$$

Provided the reactions are expressed in this fashion, the nondimensional form of the reactive conductivity becomes (appendix B)

$$\lambda_r^* = -\frac{\begin{vmatrix} 0 & \Delta H_1^* & \Delta H_2^* & \cdots & \Delta H_t^* \\ \Delta H_1^* & E_{11}^* & E_{12}^* & \cdots & E_{1t}^* \\ \Delta H_2^* & E_{12}^* & E_{22}^* & \cdots & E_{2t}^* \\ \vdots & \vdots & \vdots & \vdots & \vdots \\ \Delta H_t^* & E_{1t}^* & E_{2t}^* & \cdots & E_{tt}^* \end{vmatrix}}{\left|E_{ik}^*\right|} \tag{39}$$

where

$$\Delta H_i^* = \sum_{j=1}^{\nu} n_{ij} h_j^* \tag{40}$$

[3]In reference 40, Brokaw gives a simpler formulation of this problem. However, the original formulation proved more convenient for present purposes.

$$E_{kk}^{*} = \sum_{j=t+1}^{\nu-1} \sum_{m=j+1}^{\nu} \Delta_{mj}^{*} \frac{\left(n_{kj}x_m - n_{km}x_j\right)^2}{x_j x_m} + \sum_{j=t+1}^{\nu} \sum_{\substack{p=1 \\ p\neq k}}^{t} n_{kj}^2 \Delta_{pj}^{*} \frac{x_p}{x_j} + \sum_{\substack{p=1 \\ p\neq k}}^{t} \Delta_{pk}^{*} \frac{x_p}{x_k}$$

$$+ \sum_{j=t+1}^{\nu} \Delta_{pj}^{*} \frac{\left(x_j + n_{kj}x_k\right)^2}{x_j x_k} \qquad (k = 1,2,\ldots,t) \tag{41}$$

$$E_{ik}^{*} = \sum_{j=t+1}^{\nu-1} \sum_{m=j+1}^{\nu} \Delta_{mj}^{*} \frac{\left(n_{ij}x_m - n_{im}x_j\right)\left(n_{kj}x_m - n_{km}x_j\right)}{x_j x_m} + \sum_{j=t+1}^{\nu} \sum_{p=1}^{t} n_{ij}n_{kj} \Delta_{pj}^{*} \frac{x_p}{x_j}$$

$$+ \sum_{j=t+1}^{\nu} \left(n_{kj} \Delta_{ij}^{*} + n_{ij} \Delta_{kj}^{*}\right) - \Delta_{ik}^{*} \qquad (i,k = 1,2,\ldots,t) \tag{42}$$

$$\Delta_{ij}^{*} = \frac{25}{16} \bar{\Omega}_{ij}^{(1,1)} C_{3,ij} \tag{43}$$

The first approximation to λ_r^* is given by

$$\lambda_{r,I}^{*} = \sum_{i=1}^{t} \frac{\left(\Delta H_i^*\right)^2}{E_{ii}} \tag{44}$$

This approximation corresponds to setting $E_{ik}^{*}(i \neq k)$ equal to 0 in equation (39). Thus, the approximation neglects coupling among the reactions in the sense that E_{ik}^{*} truly vanishes only when reactions i and k share no common dependent species. One could easily derive a second approximation to include coupling effects; however, since the approximations are used herein to aid in explaining deviations of present results from those of other investigators and since these investigators use equation (44), a second approximation to λ_r^* was not considered.

For the mixtures considered, accuracy problems were occasionally encountered in the evaluation of equation (39) when a single set of chemical reactions was used to describe the compositional changes throughout the entire ranges of temperature and pressure. This difficulty arises because some of the elements in both the numerator and denominator determinants become extremely large whenever one or more of the mole fractions approach 0. Under these circumstances, the compositional changes should be described by a different system of reactions. Thus, several different sets of reactions are needed to evaluate λ_r^* over the entire ranges of temperature and pressure. The

technique used to automatically select appropriate reactions is discussed in the following paragraphs.

When all nine species were present in significant quantity, the following set of reactions was used:

$$\left.\begin{array}{ll} (1) & CO_2 \rightleftarrows CO + O \\ (2) & O_2 \rightleftarrows 2O \\ (3) & N_2 \rightleftarrows 2N \\ (4) & NO \rightleftarrows N + O \\ (5) & C \rightleftarrows CO - O \end{array}\right\} \qquad (45)$$

The number to the left of a reaction serves to identify the reaction and the independent component involved in the reaction; that is, CO_2, O_2, N_2, NO, and C are designated as components 1, 2, 3, 4, and 5, respectively. The dependent components, CO, O, N, and Ar are labeled as 6, 7, 8, and 9, respectively.

When one of the independent components vanishes while all the dependent components are present in significant amounts, it is obvious from equation (41) that the diagonal element corresponding to the reaction involving this component becomes unbounded. (For example, $E_{11} \to \infty$ as $x_1 \to 0$.) Inspection of equations (41) and (42) reveals that all other elements assume correct values. Accordingly, the form of equation (39) appropriate to reactions (45), can be modified to give the correct form for this situation simply by deleting the row and column containing the unbounded element in each determinant and by shifting the remaining rows and columns. The process works just as well when several independent species vanish simultaneously. In this work, the deletion and shifting process was actuated by inspecting the magnitude of E_{kk}.

When one or more of the species chosen as dependent vanish, the situation cannot be handled as easily. It is not sufficient to omit reactions in equations (45); rather, completely new sets of reactions must be formulated. This is true because some species chosen as independent in equations (45) become dependent under these circumstances.

The following cases proved sufficient for the three mixtures considered:

Case I Equations (45)

Case II $CO_2 \rightleftarrows CO + O$

$O_2 \rightleftarrows 2O$

$NO \rightleftarrows \frac{1}{2} N_2 + O$

Case III $CO_2 \rightleftharpoons CO + \frac{1}{2} O_2$

$NO \rightleftharpoons \frac{1}{2} N_2 + \frac{1}{2} O_2$

Case IV No reaction

For each case, vanishing of an independent species was handled by the technique previously explained for case I. Selection of the appropriate case was based on inspection of the mole fractions.

Prandtl number.- The Prandtl number is defined by

$$N_{Pr} = \frac{\eta c_p}{M_u \lambda} \tag{46}$$

In terms of the variables used herein, this equation becomes

$$N_{Pr} = \frac{16}{25} \frac{\eta^* c_p^*}{M_u \lambda^*} \tag{47}$$

where M_u denotes the molar mass of the undissociated mixture in g/mole. The Prandtl number defined by equation (47) is frequently termed the "effective Prandtl number" to connote that both c_p^* and λ^* include reactive contributions. Two approximations to the Prandtl number $N_{Pr,I}$ and $N_{Pr,II}$ were computed for air and CO_2. These approximations are given by

$$N_{Pr,I} = \frac{16}{25} \frac{\eta_I^* c_p^*}{M_u \lambda_I^*} \tag{48}$$

$$N_{Pr,II} = \frac{16}{25} \frac{\eta_{II}^* c_p^*}{M_u \lambda_{II}^*} \tag{49}$$

where

$$\lambda_I^* = \lambda_{t,I}^* + \lambda_{int}^* + \lambda_{r,I}^* \tag{50}$$

$$\lambda_{II}^* = \lambda_{t,II}^* + \lambda_{int}^* + \lambda_{r,I}^* \tag{51}$$

RESULTS AND DISCUSSION

In this section numerical results are given, in turn, for air, carbon dioxide, and the Mars model atmosphere (43% CO_2, 25% N_2, and 32% Ar (by vol.)). For each mixture, calculations based on the full equations are presented first. Then, for air and carbon dioxide, calculations based on the full equations are compared both with those based on approximate equations and with those of other investigators. Finally, the viscosity, total conductivity, and Prandtl number of air are compared to the respective properties of carbon dioxide and the Mars model atmosphere.

Since ionization was not taken into account in the computations, the results at a given pressure are terminated at a cut-off temperature which was estimated by comparing thermodynamic properties, c_p^* in particular, computed with and without ionization taken into account. Normally, the temperature cut-off determined in this manner corresponds to an electronic mole fraction between 5×10^{-4} and 10^{-3}.

Transport Properties of Air

The full-equation computations for viscosity, frozen conductivity, reactive conductivity, total conductivity, and Prandtl number are shown in figures 21, 22, 23, 24, and 25, respectively. For a given pressure, the temperature dependence of each property can be divided roughly into three portions, corresponding to the reactions taking place. From 1000° K to the region at which the curves start to diverge, the mixture remains essentially chemically inert. Divergence can be attributed largely to the dissociation of oxygen and to the formation and subsequent dissociation of nitric oxide. The large change in properties at still higher temperature arises primarily because of nitrogen dissociation.

Figure 26 compares the viscosity from full-equation calculations at $p = 1.0$ atm with the first and second approximations and also with the calculations of Hansen (ref. 21) and Yos (ref. 22). The curve for the first approximation falls consistently below that for the full-equation calculation, reaching a maximum deviation of approximately 11.5 percent at 6500° K. The second-approximation curve lies below but much closer to the full-equation curve; in fact, the deviations never exceed 1.5 percent. Yos' results lie slightly above the full-equation values at low temperatures and slightly below at high temperatures. Throughout most of the temperature range, Yos' values agree well with the second-approximation values. This agreement was expected because he used the same collision integrals for the major interactions and Brokaw's approximate equation (ref. 38) derived from a third-order approximation to the full viscosity equation. In contrast, the agreement with Hansen's calculations is much worse, especially above 1500° K. At the higher temperatures, his results consistently deviate from the full-equation values by about 23 percent to 24 percent. The reason for this marked difference can be

attributed to the fact that he uses simple kinetic theory and rough approximations for collision cross sections.

As shown in figure 27, the same type situation exists for the frozen conductivity at p = 1.0 atm as for viscosity. The curve for the first approximation always lies below that for the full-equation calculation and has a maximum deviation of about 19 percent between 6000° K and 7000° K. The second-approximation curve is also low, but deviates by less than 6 percent. Yos' results, which were calculated from Brokaw's formula derived from a third-order approximation, are in excellent agreement with the full-equation values. On the other hand, Hansen's results are again low with maximum deviation of about 29 percent at 6500° K.

Figure 28 illustrates the danger inherent in neglecting coupling among the reactions, or equivalently, in using the first approximation, in the computation of the reactive contribution to the conductivity. Although the figure does not show it clearly, there is substantial disagreement in the full-equation and approximate values near 2000° K. This disagreement is relatively unimportant, however, because the reactive conductivity is a small portion of the total conductivity in this temperature range. On the other hand, the differences which arise from neglecting coupling due to NO dissociation between 4000° K and 6000° K are extremely significant because λ_r^* is the principal part of the total conductivity in this temperature range. The differences are even larger than they appear at first glance. For instance, the percentage deviation of the first-approximation curve reaches a maximum of 61.6 percent at 4700° K.

Also shown in the same figure are the calculations of Yos (ref. 22) and Hansen (ref. 21). Since Yos used the first approximation to the reactive conductivity and Yun and Mason's collision integrals, his result should, in principle, lie precisely on the dashed curve. To discern why the point at 5000° K does not coincide with the dashed curve, Yos' sources of thermodynamic information were investigated. Yos used mole fractions from his reference 43 for the temperature range from 1000° K to 5000° K and mole fractions from his reference 44 for temperatures above 5000° K. He also employed unpublished calculations made at AVCO Corporation for his $c_{p,i}/R$ and h_i/RT. It was found that his reference 43 values of the mole fraction for NO differed greatly from the values used herein, the largest deviation being 80 percent. As a check, the first approximation was recalculated using Yos' sources of mole fractions and the present $c_{p,i}/R$ and h_i/RT. Excellent agreement with Yos' values of λ_r^* were then obtained throughout the entire temperature range. Hansen's results agree well with the first-approximation values up to about 3000° K. His exceptionally low values between the two peaks are due primarily to his complete neglect of the reaction $NO \rightleftarrows N + O$. The lowness of Hansen's values in the vicinity of the second peak is thought to be a direct consequence of his method for obtaining collision cross sections because it has been shown that uncertainties associated with this method increase rapidly at high temperature (ref. 23).

The same general comments apply equally well to the total conductivity shown in figure 29. Yos' results should agree closely, but not exactly, with the second-approximation results, whereas Hansen's results should be in better agreement with the first-approximation results. It is especially noteworthy that the second-approximation value deviates from the full-equation value by 29.5 percent at 4700° K. Thus, the previously noted substantial divergence of the approximate reactive conductivity perpetrates into the approximate total conductivity in a somewhat weakened but still significant manner.

Since viscosity and conductivity enter directly into the Prandtl number, it is obvious that the Prandtl number can be extremely sensitive to approximate calculations. This is borne out in figure 30, which shows the full-equation Prandtl number, the first- and second-approximation Prandtl numbers, and the results of Yos (ref. 22) and Hansen (ref. 21). The striking differences in the approximate and full-equation calculations are due primarily to the reactive-conductivity approximation. The largest deviations, occurring at 4700° K, are 25.4 percent and 23 percent for the first- and second-approximation values, respectively. Comparisons with the results of Yos and Hansen are complicated by the fact that their values reflect differences in thermodynamic data. Hansen's values of c_p^* do not differ markedly from those used herein, and accordingly, most of the difference shown in the figure can be attributed to the use of different theories and to his neglect of the NO reaction. In view of the rather large disagreement noted previously for η^* and λ^*, it is indeed surprising that Hansen's Prandtl numbers agree with the full-equation values as well as they do. As noted previously, Yos employed two different sources for mixture composition and one of these sources gives NO mole fractions which differ markedly from the present ones. His calculation of the Prandtl number is inconsistent with these sources in the following sense. Yos used the composition from his reference 43 for temperatures between 1000° K and 5000° K and that from his reference 44 at higher temperatures, but he employed the c_p/R values from his reference 43 throughout the whole temperature range. In order to obtain a useful comparison with his results, the second approximation to the Prandtl number was recomputed using Yos' sources of mole fractions and c_p/R and the present $c_{p,i}/R$ and h_i/RT. Figure 31 shows that these new values are in good agreement with Yos' calculations. It is evident that the differences between Yos' Prandtl number and the second-approximation values are primarily due to the differences in the thermodynamic data.

Transport Properties of Carbon Dioxide

The results of the full-equation calculations of viscosity, frozen conductivity, reactive conductivity, total conductivity, and Prandtl number of carbon dioxide are presented in figures 32, 33, 34, 35, and 36, respectively. Just as with air, for a fixed pressure, the temperature variation of each of these properties can be split roughly into three regions

depending upon the reactions taking place. Up to the point at which the curves initially diverge, the gas consists of practically pure CO_2. As the temperature increases beyond this point, CO_2 starts to dissociate into CO and O_2, and with a small additional increase in temperature, O_2 also starts to dissociate. Thus, the initial divergence, and for some curves, the first peak, arises from the almost simultaneous dissociation of CO_2 and O_2. After these reactions essentially go to completion, CO dissociation begins. This reaction is responsible for the rapid rise in viscosity and frozen conductivity and for the second peaks in reactive conductivity, total conductivity, and Prandtl number.

For each of these properties, results of the full-equation calculations are compared with approximate computations and with the results of Thomas (ref. 23) and Van Tassell (ref. 24) in figures 37 to 41 for a pressure of 0.1 atm. Both Thomas and Van Tassell attained widely varying Prandtl numbers at this particular pressure; therefore, this pressure was chosen to ascertain why this variation was true. (Thomas also attained wide variation at lower pressures but Van Tassell did not present data for $p < 0.1$ atm.)

In figures 37 and 38, the approximations for viscosity and frozen conductivity compare with the full-equation calculations in much the same fashion as was found in the comparison for air. Van Tassell's viscosity calculations were expected to be in good agreement with either the exact values or the second approximation because he utilized Yos' method (ref. 22) which was previously found to be quite good for air. No data from Van Tassell is included in figure 38 because he does not present results for frozen conductivity. For both viscosity and frozen conductivity, Thomas' results lie considerably below even the first approximation; this too was expected since he utilized Hansen's approach (ref. 21).

Figure 39, showing the reactive-conductivity comparisons, is particularly illuminating. In the region between 1500° K and 2700° K, the approximation values are much too low; in fact, the deviation from the solid curve approaches 100 percent near 1500° K. Between 2700° K and 3500° K, the approximation yields exceptionally high predictions, with a maximum deviation of 43 percent near 3000° K. No data are shown from Van Tassell because he does not provide sufficient data to allow determination of this contribution. With the exception of the point at 3000° K, Thomas' results agree well with the exact calculation up to 5000° K. The lowness of his values in the vicinity of the peaks is thought to be due to two possible causes:

(1) As noted earlier, uncertainties involved in his method of finding collision cross sections become larger with increasing temperature.

(2) Although he used the full equation for λ_r, his equation for E_{ik} does not agree with the original source (ref. 11). It is not clear whether this inaccurate equation was actually used in his computations.

Figure 40 shows clearly that the behavior of the reactive conductivity carries over directly to the total conductivity. Only the first-approximation curve is shown because the first- and second-approximation curves are practically indistinguishable. The data point of Thomas at 4000° K seems to be in error because his tables for λ, λ_f, and λ_r are inconsistent at this temperature.

Figure 41 clearly shows that Van Tassell's high values for Prandtl number around 2000° K are directly attributable to the use of approximate equations. In particular, the exhibited behavior is directly traceable to the reactive-conductivity approximation. The large disagreement of Thomas' values at 4000° K and 5000° K with the exact values is attributable, respectively, to a tabular inconsistency and to an extremely low specific heat.

Transport Properties of the Mars Model Atmosphere

The viscosity, frozen conductivity, reactive conductivity, total conductivity, and Prandtl number, as computed with the full equations, are presented in figures 42, 43, 44, 45, and 46, respectively. Qualitatively, these properties exhibit the same type temperature variation as previously observed for air and carbon dioxide. There are, of course, distinct quantitative differences and these are treated in detail in the next section.

The initial divergence of the constant pressure curves given for these properties stems from the dissociation of CO_2. With a slight increase in temperature, O_2 dissociation also enters the picture. Thus, the lower temperature portions of the curves are influenced by the coupled dissociation of CO_2 and O_2. As these reactions tend toward completion, CO and N_2 dissociations become predominant. It is these two reactions which are largely responsible for the steep increase in viscosity and frozen conductivity and for the second set of peaks in reactive conductivity, total conductivity and Prandtl number. Although argon does not react to any appreciable extent, it does affect the quantitative character of the transport properties both through molecular interaction and through its influence on the equilibrium composition.

Although no approximate calculations are given for this mixture, it is evident from the two preceding examples that use of approximate equations would lead to serious error in the total conductivity, and hence, the Prandtl number. This observation would be especially true in the low temperature range where CO_2 and O_2 dissociate simultaneously.

To the authors' knowledge, transport properties for this mixture have not been computed previously; hence, no comparisons are possible.

Comparisons of the Transport Properties of Air, Carbon Dioxide, and the Mars Model Atmosphere

In this section, the three mixtures are compared on the basis of the full-equation calculations of viscosity, total conductivity, and Prandtl number. For convenience, air is adopted as a standard and the properties of carbon dioxide and the Mars model atmosphere are discussed in terms of their deviation from the corresponding air properties. Attention is restricted to a pressure of 1.0 atm because similar results hold for the other pressures.

Figure 47 compares the viscosities of the three mixtures. The viscosities of air and carbon dioxide are quite similar in magnitude, the viscosity of the latter never deviating from that of the former more than 6 percent. The viscosity of the Mars model atmosphere always lies above that for both air and carbon dioxide, but its deviation from that of the former is always less than 12 percent. There are, of course, distinctive features in the fine details of the temperature variations, such as the characteristic rises associated with the occurrence of chemical reactions.

The curves for air and carbon dioxide are expected to be similar after appreciable dissociation of carbon dioxide, because the collision integrals and thermodynamic properties of the remaining atoms and diatomic species are similar. The higher viscosity of the Mars model atmosphere is due mainly to the large amount of argon present in this mixture.

Figure 48 illustrates the tremendous differences in the total conductivity of the mixtures. In the temperature region between 2000° K and 4000° K, the conductivity of CO_2 deviates from that of air by as much as 180 percent and between 5000° K and 6000° K by as much as 70 percent. For the Mars model atmosphere, deviations range from about 95 percent near 2500° K to about 34 percent near 5500° K.

As shown in figure 49, these large differences in total conductivity do not influence the Prandtl numbers as much as one might expect. The reason for this, of course, is the analogous behavior of the specific heat and total conductivity of the individual mixtures. The deviation of the Prandtl number of CO_2 from that for air ranges from about 12 percent to 20 percent. The maximum deviation of the Prandtl number of the Mars model atmosphere from that of air is about 10 percent. According to Horton and Zeh (ref. 41), such difference can be significant in problems such as blunt-body stagnation-point heat transfer.

It is noteworthy that Prandtl number comparisons based on the second approximation would differ greatly from those shown in figure 49. In particular, deviations of several hundred percent would be observed.

CONCLUSIONS

On the basis of the foregoing analysis, the following conclusions are justified:

1. Neglect of coupling terms in reactive-conductivity calculations for mixtures containing CO_2 can induce order of magnitude errors in total conductivity, and hence, large errors in Prandtl number.

2. For the mixtures considered, second approximations give reasonable accuracy ($\leq$6 percent deviation from full-equation calculations) for viscosity and translational thermal conductivity.

3. There exists a definite need for accurate interaction potentials for carbon-atom and carbon-molecule interactions. The accuracy of high-temperature transport properties of mixtures containing carbon elements and/or compounds must be regarded as uncertain until such potentials become available. However, the present calculations are regarded as the best presently available.

4. Accurate mixture specific heat is essential to accurate Prandtl number calculations.

It should be emphasized that conclusions 1 and 2 are independent of conclusion 3 because carbon—other-particle interaction potentials were used consistently in all calculations.

Langley Research Center,
National Aeronautics and Space Administration,
Langley Station, Hampton, Va., July 1, 1969.

APPENDIX A

ORIENTATION-AVERAGED POTENTIALS FOR CO_2 INTERACTIONS

The purpose of this appendix is to develop high-temperature potentials for binary interactions of CO_2 with atoms, diatomic molecules, and other CO_2 molecules. The basic idea is to construct the potential for two interacting particles from known potentials for interactions of atoms comprising the particles. This leads directly to an orientation-dependent particle potential which is then averaged over all possible orientations to yield an effective potential dependent only on the center-of-mass separation of the particles. Appropriate equations for atom—diatomic-molecule and diatomic-molecule—diatomic-molecule potentials are presented in reference 19.

The procedure incorporates the following simplifying assumptions (ref. 19):

(1) Each molecule can be treated as a rigid structure with ground-state dimensions.

(2) Atomic interactions are independent and each atomic interaction potential has the form

$$\phi = Ae^{-aR} \tag{A1}$$

where R is the interatomic separation distance.

(3) All molecular orientations are equally probable.

Sketch 1 shows appropriate coordinate systems and nomenclature for the establishment of the interaction potential for the encounter of molecule AB with a symmetric, triatomic linear molecule DCD. For a particular configuration, assumption (2) implies that

$$\phi\left(r,\theta_1,\omega_1,\theta_2,\omega_2\right) = \phi_{AC} + \phi_{BC} + \phi_{AD_1} + \phi_{AD_2} + \phi_{BD_1} + \phi_{BD_2} \tag{A2}$$

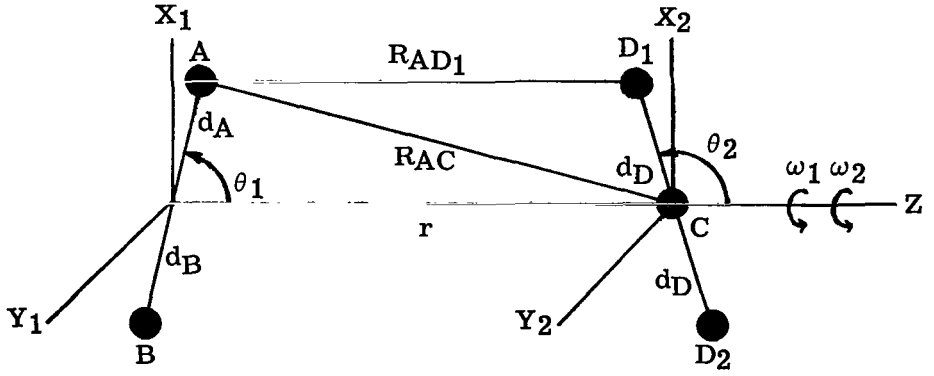

Sketch 1

where each term has the form given in equation (A1). Subscripts 1 and 2 are affixed to the D atoms because the distances from these atoms to atoms A and B generally differ, and hence, the potentials also differ; that is, in general, $\phi_{AD_1} \neq \phi_{AD_2}$ and $\phi_{BD_1} \neq \phi_{BD_2}$.

The orientation-averaged potential, $\phi(r)$ is related to $\phi\left(r,\theta_1,\omega_1,\theta_2,\omega_2\right)$ by

$$\phi(r) = \frac{1}{(4\pi)^2} \int_{\omega_2=0}^{2\pi} \int_{\omega_1=0}^{2\pi} \int_{\theta_2=0}^{\pi} \int_{\theta_1=0}^{\pi} \phi\left(r,\theta_1,\omega_1,\theta_2,\omega_2\right) \sin\theta_1 \sin\theta_2 \, d\theta_1 \, d\theta_2 \, d\omega_1 \, d\omega_2 \tag{A3}$$

Note that no Boltzmann weighting factor occurs in this equation; this is consistent with assumption (3).

When equation (A2) is substituted into equation (A3), one finds that the six resulting integrals are quite complex and difficult to integrate. However, one can easily demonstrate that the integral of ϕ_{AC} has the same form as that for ϕ_{BC} and also that the integrals of ϕ_{AD_1}, ϕ_{AD_2}, ϕ_{BD_1}, and ϕ_{BD_2} have the same form. Hence $\phi(r)$ can easily be found once the averaged potential for the A-C and A-D_1 interactions are known.

The averages of ϕ_{AC} and ϕ_{AD} must obviously be independent of the particular choice of coordinate systems. Sketch 2 shows a new coordinate system which leads to marked simplifications in the integrals. Denoting the averaged values of ϕ_{AC} and ϕ_{AD} by $\langle\phi_{AC}\rangle$ and $\langle\phi_{AD}\rangle$, respectively, one obtains

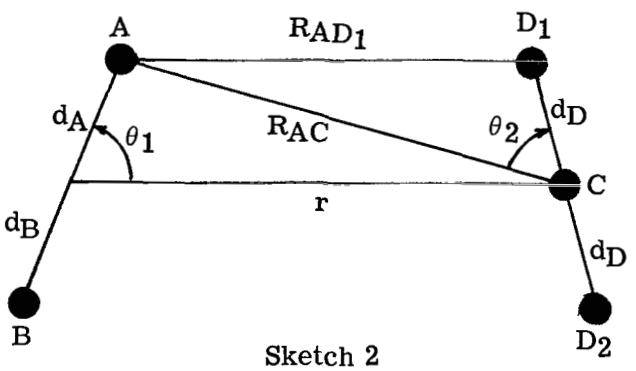

Sketch 2

$$\langle\phi_{AC}\rangle = \frac{A_{AC}}{2} \int_0^{\pi} e^{-a_{AC}R_{AC}} \sin\theta_1 \, d\theta_1 \tag{A4}$$

$$\langle\phi_{AD}\rangle = \frac{A_{AD}}{4} \int_0^{\pi} \int_0^{\pi} e^{-a_{AD}R_{AD}} \sin\theta_1 \sin\theta_2 \, d\theta_1 \, d\theta_2 \tag{A5}$$

where

$$R_{AC} = \left(r^2 - 2rd_A \cos\theta_1 + d_A^2\right)^{1/2} \tag{A6}$$

$$R_{AD} = \left(R_{AC}^2 - 2R_{AC}d_D \cos\theta_2 + d_D^2\right)^{1/2} \tag{A7}$$

Carrying out the indicated operations yields

$$\left\langle \phi_{AC} \right\rangle = \frac{A_{AC} e^{-a_{AC}r}}{a_{AC}^2 d_A r}\left[\left(a_{AC}r + 1\right)\sinh\left(a_{AC}d_A\right) - a_{AC}d_A \cosh\left(a_{AC}d_A\right)\right] \tag{A8}$$

$$\begin{aligned}\left\langle \phi_{AD} \right\rangle = \frac{A_{AD} e^{-a_{AD}r}}{a_{AD}^3 d_A d_D r}\Big[&\left(a_{AD}r + 2\right)\sinh\left(a_{AD}d_A\right)\sinh\left(a_{AD}d_D\right) \\ &- a_{AD}d_A \cosh\left(a_{AD}d_A\right)\sinh\left(a_{AD}d_D\right) \\ &- a_{AD}d_D \cosh\left(a_{AD}d_D\right)\sinh\left(a_{AD}d_A\right)\Big]\end{aligned} \tag{A9}$$

Averages for the remaining atomic potentials in equation (A2) can now be obtained by changing the subscripts appropriately in equations (A8) and (A9).

Use of these results leads directly to the following potentials for the CO_2-NO, CO_2-O_2, and CO_2-N_2 interactions:

$$\begin{aligned}\phi\left(CO_2\text{-}NO\right) = &\frac{A_{NC} e^{-a_{NC}r}}{a_{NC}^2 d_N r}\left[\left(a_{NC}r + 1\right)\sinh\left(a_{NC}d_N\right) - a_{NC}d_N \cosh\left(a_{NC}d_N\right)\right] + \frac{A_{OC} e^{-a_{OC}r}}{a_{OC}^2 d_O r}\left[\left(a_{OC}r + 1\right)\sinh\left(a_{OC}d_O\right) - A_{OC}d_O \cosh\left(a_{OC}d_O\right)\right] \\ &+ \frac{2A_{NO} e^{-a_{NO}r}}{a_{NO}^3 d_N d_D r}\left[\left(a_{NO}r + 2\right)\sinh\left(a_{NO}d_N\right)\sinh\left(a_{NO}d_D\right) - a_{NO}d_N \cosh\left(a_{NO}d_N\right)\sinh\left(a_{NO}d_D\right) - a_{NO}d_D \cosh\left(a_{NO}d_D\right)\sinh\left(a_{NO}d_N\right)\right] \\ &+ \frac{2A_{OO} e^{-a_{\infty}r}}{a_{OO}^3 d_O d_D r}\left[\left(a_{OO}r + 2\right)\sinh\left(a_{OO}d_O\right)\sinh\left(a_{OO}d_D\right) - a_{OO}d_O \cosh\left(a_{OO}d_O\right)\sinh\left(a_{OO}d_D\right) - a_{OO}d_D \cosh\left(a_{OO}d_D\right)\sinh\left(a_{OO}d_O\right)\right]\end{aligned} \tag{A10}$$

$$\begin{aligned}\phi\left(CO_2\text{-}O_2\right) = &\frac{2A_{OC} e^{-a_{OC}r}}{a_{OC}^2 d_O r}\left[\left(a_{OC}r + 1\right)\sinh\left(a_{OC}d_O\right) - a_{OC}d_O \cosh\left(a_{OC}d_O\right)\right] + \frac{4A_{OO} e^{-a_{OO}r}}{a_{OO}^3 d_O d_D r}\Big[\left(a_{OO}r + 2\right)\sinh\left(a_{OO}d_O\right)\sinh\left(a_{OO}d_D\right) \\ &- a_{OO}d_O \cosh\left(a_{OO}d_O\right)\sinh\left(a_{OO}d_D\right) - a_{OO}d_D \cosh\left(a_{OO}d_D\right)\sinh\left(a_{OO}d_O\right)\Big]\end{aligned} \tag{A11}$$

$$\phi(CO_2\text{-}N_2) = \frac{2A_{NC}e^{-a_{NC}r}}{a_{NC}^2 d_N r}\left[(a_{NC}r + 1)\sinh(a_{NC}d_N) - a_{NC}d_N\cosh(a_{NC}d_N)\right]$$

$$+\frac{4A_{NO}e^{-a_{NO}r}}{a_{NO}^3 d_N d_D r}\left[(a_{NO}r + 2)\sinh(a_{NO}d_N)\sinh(a_{NO}d_D)\right.$$

$$-a_{NO}d_N\cosh(a_{NO}d_N)\sinh(a_{NO}d_D)$$

$$\left.-a_{NO}d_D\cosh(a_{NO}d_O)\sinh(a_{NO}d_N)\right] \qquad (A12)$$

In each of these equations d_D denotes the length of the C-O bond in the CO_2 molecule. The meaning of the other d symbols depends upon the particular interaction. For example, in equation (A10) d_N denotes the distance of the N atom from the center of mass of the NO molecule whereas in equation (A12) d_N denotes the distance of the N atom from the center of mass of the N_2 molecule.

By similar analyses one can also establish the following potentials:

$$\phi(CO_2\text{-}CO_2) = A_{CC}e^{-a_{CC}r}$$

$$+\frac{4A_{OC}e^{-a_{OC}r}}{a_{OC}^2 d_D r}\left[(a_{OC}r + 1)\sinh(a_{OC}d_D) - a_{OC}d_D\cosh(a_{OC}d_D)\right]$$

$$+\frac{4A_{OO}e^{-a_{OO}r}}{a_{OO}^3 d_D^2 r}\left[(a_{OO}r + 2)\sinh(a_{OO}d_D)\sinh(a_{OO}d_D)\right.$$

$$\left.-2a_{OO}d_D\cosh(a_{OO}d_D)\sinh(a_{OO}d_D)\right] \qquad (A13)$$

$$\phi(CO_2\text{-}N) = A_{NC}e^{-a_{NC}r} + \frac{2A_{NO}e^{-a_{NO}r}}{a_{NO}^2 d_D r}\left[(a_{NO}r + 1)\sinh(a_{NO}d_D) - a_{NO}d_D\cosh(a_{NO}d_D)\right] \qquad (A14)$$

$$\phi(CO_2\text{-}O) = A_{OC}e^{-a_{OC}r} + \frac{2A_{OO}e^{-a_{OO}r}}{a_{OO}^2 d_D r}\left[\left(a_{OO}r + 1\right)\sinh\left(a_{OO}d_D\right) - a_{OO}d_D\cosh\left(a_{OO}d_D\right)\right] \tag{A15}$$

$$\phi(CO_2\text{-}Ar) = A_{ArC}e^{-a_{ArC}r} + \frac{2A_{ArO}e^{-a_{ArO}r}}{a_{ArO}^2 d_D r}\left[\left(a_{ArO}r + 1\right)\sinh\left(a_{ArO}d_D\right) - a_{ArO}d_D\cosh\left(a_{ArO}d_D\right)\right] \tag{A16}$$

APPENDIX B

ESTABLISHMENT OF EQUATIONS FOR VISCOSITY, TRANSLATIONAL CONDUCTIVITY, AND REACTIVE CONDUCTIVITY

In this appendix, the expressions for viscosity and translational thermal conductivity resulting from the first approximation of first-order Chapman-Enskog kinetic theory are cast into convenient forms for numerical computation. A convenient form for the reactive contribution to the thermal conductivity is also derived, and a first and second approximation for viscosity and translational conductivity and a first approximation for the reactive conductivity are developed.

The viscosity of a ν-component gas mixture is given by (ref. 7)

$$\eta = -\frac{\begin{vmatrix} H_{11} & H_{12} & \cdots & H_{1\nu} & x_1 \\ H_{12} & H_{22} & \cdots & H_{2\nu} & x_2 \\ \cdot & \cdot & \cdot & \cdot & \cdot \\ \cdot & \cdot & \cdot & \cdot & \cdot \\ \cdot & \cdot & \cdot & \cdot & \cdot \\ H_{1\nu} & H_{2\nu} & \cdots & H_{\nu\nu} & x_\nu \\ x_1 & x_2 & \cdots & x_\nu & 0 \end{vmatrix}}{\left|H_{ij}\right|} \tag{B1}$$

where $\left|H_{ij}\right|$ denotes the determinant of the H_{ij} elements defined by

$$H_{ii} = \frac{x_i^2}{\eta_i} + \sum_{\substack{j=1 \\ j\neq i}}^{\nu} \frac{2x_i x_j}{M_j + M_j} \frac{RT}{pD_{ij}} \left(1 + \frac{3}{5}\frac{M_j}{M_i} A_{ij}^*\right) \tag{B2}$$

$$H_{ij} = -\frac{2x_i x_j}{M_i + M_j} \frac{RT}{pD_{ij}} \left(1 - \frac{3}{5} A_{ij}^*\right) \qquad (i \neq j) \tag{B3}$$

APPENDIX B

Here η_i, the viscosity of species i, is given by

$$\eta_i = \left\{ \frac{5}{16}\left(\frac{R}{\pi N_A^2}\right)^{1/2} \times \left[10^{16}\left(\frac{\text{Å}}{\text{cm}}\right)^2 \right] \right\} \frac{\sqrt{M_i T}}{\overline{\Omega}_{ii}^{(2,2)}} \tag{B4}$$

with $\overline{\Omega}^{(2,2)}$ expressed in units of Å^2. The binary diffusion coefficient of species i and j, D_{ij}, is given by

$$D_{ij} = \left\{ \frac{3}{8}\left(\frac{R^3}{\pi N_A^2}\right)^{1/2} \times \left[10^{16}\left(\frac{\text{Å}}{\text{cm}}\right)^2 \right] \right\} \frac{1}{p\overline{\Omega}_{ij}^{(1,1)}} \sqrt{\frac{(M_i + M_j)T^3}{2M_i M_j}} \tag{B5}$$

where $\overline{\Omega}_{ij}^{(1,1)}$ is also expressed in Å^2.

It is convenient to arbitrarily define a reference viscosity η_o by

$$\eta_o = \left\{ \frac{3}{8}\left(\frac{R}{\pi N_A^2}\right)^{1/2} \times \left[10^{16}\left(\frac{g}{\text{cm}^4\text{-mole}}\right)^{1/2} \right] \right\} \sqrt{T} \tag{B6}$$

This particular choice was made solely because it leads to convenient numerical values for the dimensionless viscosity η^*. Dividing equation (B1) by equation (B6) and substituting equations (B4) and (B5) into equations (B2) and (B3) give

$$\eta^* = \frac{\eta}{\eta_o} = -\frac{\begin{vmatrix} H_{11}^* & H_{12}^* & \cdots & H_{1\nu}^* & x_1 \\ H_{12}^* & H_{22}^* & \cdots & H_{2\nu}^* & x_2 \\ \cdot & \cdot & \cdot & \cdot & \cdot \\ \cdot & \cdot & \cdot & \cdot & \cdot \\ \cdot & \cdot & \cdot & \cdot & \cdot \\ H_{1\nu}^* & H_{2\nu}^* & \cdots & H_{\nu\nu}^* & x_\nu \\ x_1 & x_2 & \cdots & x_\nu & 0 \end{vmatrix}}{\left| H_{ij}^* \right|} \tag{B7}$$

where

$$H_{ii}^{*} = \frac{1.2\overline{\Omega}_{ii}^{(2,2)} x_i^2}{\sqrt{M_i}} + 2 \sum_{\substack{j=1 \\ j \neq i}}^{\nu} x_i x_j C_{1,ij} \overline{\Omega}_{ij}^{(1,1)} \tag{B8}$$

$$H_{ij}^{*} = -2x_i x_j C_{2,ij} \overline{\Omega}_{ij}^{(1,1)} \left(1 - \frac{3}{5} A_{ij}^{*}\right) \qquad (i \neq j) \tag{B9}$$

$$C_{1,ij} = \left(1 + \frac{3}{5} \frac{M_j}{M_i} A_{ij}^{*}\right) C_{2,ij} \tag{B10}$$

$$C_{2,ij} = \frac{C_{3,ij}}{M_i + M_j} \tag{B11}$$

$$C_{3,ij} = \frac{2M_i M_j}{M_i + M_j} \tag{B12}$$

The reasons for defining C in this fashion are twofold. First, they can be computed once at the beginning of the calculations and used throughout the whole range of temperatures and pressures. (Recall that A_{ij}^{*} is taken as being constant.) Second, some of these same quantities occur naturally in conductivity equations. Although the units are not shown in equations (B8) and (B9), it is easily verified that H_{ii}^{*} $\left(= \eta_o H_{ii}\right)$ and H_{ij}^{*} $\left(= \eta_o H_{ij}\right)$ are actually nondimensional.

According to reference 7, equation (B7) can be expanded as

$$\eta^{*} = \sum_{i=1}^{\nu} \frac{x_i^2}{H_{ii}^{*}} - \sum_{i=1}^{\nu} \sum_{\substack{j=1 \\ j \neq i}}^{\nu} \frac{x_i x_j H_{ij}^{*}}{H_{ii}^{*} H_{jj}^{*}} + \cdots \tag{B13}$$

The first term in this expansion will be referred to as the first approximation η_{I}^{*} and the first two terms will be referred to as the second approximation η_{II}^{*}. Thus

$$\eta_{\mathrm{I}}^{*} = \sum_{i=1}^{\nu} \frac{x_i^2}{H_{ii}^{*}} \tag{B14}$$

APPENDIX B

$$\eta_{II}^{*} = \sum_{i=1}^{\nu} \frac{x_i^2}{H_{ii}^{*}} - \sum_{i=1}^{\nu} \sum_{\substack{j=1 \\ j \neq i}}^{\nu} \frac{x_i x_j H_{ij}^{*}}{H_{ii}^{*} H_{jj}^{*}} \tag{B15}$$

The translational thermal conductivity can be treated in a completely analogous fashion. According to Muckenfuss and Curtiss (ref. 13), the governing equation is

$$\lambda_t = 4 \frac{\begin{vmatrix} L_{11} & L_{12} & \cdots & L_{1\nu} & x_1 \\ L_{12} & L_{22} & \cdots & L_{2\nu} & x_2 \\ \cdot & \cdot & \cdot & \cdot & \cdot \\ \cdot & \cdot & \cdot & \cdot & \cdot \\ \cdot & \cdot & \cdot & \cdot & \cdot \\ L_{1\nu} & L_{2\nu} & \cdots & L_{\nu\nu} & x_\nu \\ x_1 & x_2 & \cdots & x_\nu & 0 \end{vmatrix}}{\left| L_{ij} \right|} \tag{B16}$$

where

$$L_{ii} = -\frac{4x_i^2}{\lambda_i} - \frac{16T}{25p} \sum_{\substack{j=1 \\ j \neq i}}^{\nu} \frac{x_i x_j}{\left(M_i + M_j\right)^2 D_{ij}} \left(\frac{15}{2} M_i^2 + \frac{25}{4} M_j^2 - 3M_j^2 B_{ij}^{*} + 4M_i M_j A_{ij}^{*} \right) \tag{B17}$$

$$L_{ij} = \frac{16T}{25p} \frac{x_i x_j}{\left(M_i + M_j\right)^2} \frac{M_i M_j}{D_{ij}} \left(\frac{55}{4} - 3B_{ij}^{*} - 4A_{ij}^{*} \right) \qquad (i \neq j) \tag{B18}$$

In equation (B17), λ_i, the thermal conductivity of pure component i, is defined by

$$\lambda_i = \left\{ \frac{75}{64} \left(\frac{R^3}{\pi N_A^2} \right)^{1/2} \times \left[10^{16} \left(\frac{\text{Å}}{\text{cm}} \right)^2 \right] \right\} \frac{\sqrt{T/M_i}}{\overline{\Omega}_{ii}^{(2,2)}} \tag{B19}$$

where $\overline{\Omega}_{ii}^{(2,2)}$ is expressed in Å^2.

APPENDIX B

After nondimensionalizing λ_t with a reference conductivity defined by

$$\lambda_o = \left\{ \frac{75}{128} \left(\frac{R^3}{\pi N_A^2} \right)^{1/2} \times \left[10^{16} \left(\frac{\text{mole}}{\text{g-cm}^4} \right)^{1/2} \right] \right\} \sqrt{T} \tag{B20}$$

and using equation (B5) to eliminate D_{ij}, equation (B16) can be expressed as

$$\lambda_t^* = \frac{\lambda_t}{\lambda_o} = 4 \frac{\begin{vmatrix} L_{11}^* & L_{12}^* & \cdots & L_{1\nu}^* & x_1 \\ L_{12}^* & L_{22}^* & \cdots & L_{2\nu}^* & x_2 \\ \cdot & \cdot & \cdot & & \cdot \\ \cdot & \cdot & \cdot & \cdot & \cdot \\ \cdot & \cdot & \cdot & \cdot & \cdot \\ L_{1\nu}^* & L_{2\nu}^* & \cdots & L_{\nu\nu}^* & x_\nu \\ x_1 & x_2 & \cdots & x_\nu & 0 \end{vmatrix}}{\left| L_{ij}^* \right|} \tag{B21}$$

where

$$L_{ii}^* = -2x_i^2 \bar{\Omega}_{ii}^{(2,2)} \sqrt{M_i} - \sum_{\substack{j=1 \\ j \neq i}}^{\nu} x_i x_j C_{2,ij} C_{4,ij} \bar{\Omega}_{ij}^{(1,1)} \tag{B22}$$

$$L_{ij}^* = x_i x_j C_{2,ij} C_{5,ij} \bar{\Omega}_{ij}^{(1,1)} \qquad (i \neq j) \tag{B23}$$

$$C_{4,ij} = \frac{\frac{15}{2} M_i^2 + \frac{25}{4} M_j^2 - 3M_j^2 B_{ij}^* + 4M_i M_j A_{ij}^*}{M_i + M_j} \tag{B24}$$

$$C_{5,ij} = \frac{M_i M_j \left(\frac{55}{4} - 3B_{ij}^* - 4A_{ij}^* \right)}{M_i + M_j} \tag{B25}$$

With the assumed constancy of A_{ij}^* and B_{ij}^*, this formulation proves especially convenient for numerical evaluation.

APPENDIX B

Equation (B21) can be expanded as

$$\lambda_t^* = -4 \sum_{i=1}^{\nu} \frac{x_i^2}{L_{ii}^*} + 4 \sum_{i=1}^{\nu} \sum_{\substack{j=1 \\ j \neq i}}^{\nu} \frac{x_i x_j L_{ij}^*}{L_{ii}^* L_{jj}^*} + \cdots \tag{B26}$$

The first approximation is defined as

$$\lambda_{t,I}^* = -4 \sum_{i=1}^{\nu} \frac{x_i^2}{L_{ii}^*} \tag{B27}$$

and the second approximation as

$$\lambda_{t,II}^* = -4 \sum_{i=1}^{\nu} \frac{x_i^2}{L_{ii}^*} + 4 \sum_{i=1}^{\nu} \sum_{\substack{j=1 \\ j \neq i}}^{\nu} \frac{x_i x_j L_{ij}^*}{L_{ii}^* L_{jj}^*} \tag{B28}$$

According to Butler and Brokaw (ref. 11), the reactive contribution to the conductivity of a ν-component system whose equilibrium composition is described by t independent chemical reactions has the form

$$\lambda_r = -\frac{1}{RT^2} \frac{\begin{vmatrix} 0 & \Delta H_1 & \Delta H_2 & \cdots & \Delta H_t \\ \Delta H_1 & E_{11} & E_{12} & \cdots & E_{1t} \\ \Delta H_2 & E_{12} & E_{22} & \cdots & E_{2t} \\ \vdots & \vdots & \vdots & \cdots & \vdots \\ \Delta H_t & E_{1t} & E_{2t} & \cdots & E_{tt} \end{vmatrix}}{\left| E_{ik} \right|} \tag{B29}$$

where ΔH_i is the enthalpy of reaction of the ith independent reaction and

APPENDIX B

$$E_{kk} = \sum_{j=t+1}^{\nu-1} \sum_{m=j+1}^{\nu} \Delta_{mj} \frac{\left(n_{kj}x_m - n_{km}x_j\right)^2}{x_j x_m} + \sum_{j=t+1}^{\nu} \sum_{\substack{p=1 \\ p\neq k}}^{t} n_{kj}^2 \Delta_{pj} \frac{x_p}{x_j}$$

$$+ \sum_{\substack{p=1 \\ p\neq k}}^{t} \Delta_{pk} \frac{x_p}{x_k} + \sum_{j=t+1}^{\nu} \Delta_{kj} \frac{\left(x_j + n_{kj}x_k\right)^2}{x_j x_k} \qquad (k = 1,2,\ldots,t) \qquad \text{(B30)}$$

$$E_{ik} = \sum_{j=t+1}^{\nu-1} \sum_{m=j+1}^{\nu} \Delta_{mj} \frac{\left(n_{ij}x_m - n_{im}x_j\right)\left(n_{kj}x_m - n_{km}x_j\right)}{x_j x_m} + \sum_{j=t+1}^{\nu} \sum_{p=1}^{t} n_{ij}n_{kj} \Delta_{pj} \frac{x_p}{x_j}$$

$$+ \sum_{j=t+1}^{\nu} \left(n_{kj} \Delta_{ij} + n_{ij} \Delta_{kj}\right) - \Delta_{ik} \qquad (i,k = 1,2,\ldots,t) \qquad \text{(B31)}$$

$$\Delta_{ij} = \frac{RT}{pD_{ij}} \qquad \text{(B32)}$$

Dividing equation (B29) by λ_o and introducting equation (B5) for D_{ij} yield

$$\lambda_r^* = \frac{\lambda_r}{\lambda_o} = -\frac{\begin{vmatrix} 0 & \Delta H_1^* & \Delta H_2^* & \cdots & \Delta H_t^* \\ \Delta H_1^* & E_{11}^* & E_{12}^* & \cdots & E_{1t}^* \\ \Delta H_2^* & E_{12}^* & E_{22}^* & \cdots & E_{2t}^* \\ \cdot & \cdot & \cdot & \cdots & \cdot \\ \cdot & \cdot & \cdot & \cdots & \cdot \\ \cdot & \cdot & \cdot & \cdots & \cdot \\ \Delta H_t^* & E_{1t}^* & E_{2t}^* & \cdots & E_{tt}^* \end{vmatrix}}{\left|E_{ik}^*\right|} \qquad \text{(B33)}$$

where

$$\Delta H_i^* = \sum_{j=1}^{\nu} n_{ij} h_j^* \qquad \text{(B34)}$$

APPENDIX B

$$E^*_{kk} = \sum_{j=t+1}^{\nu-1} \sum_{m=j+1}^{\nu} \Delta^*_{mj} \frac{\left(n_{kj}x_m - n_{km}x_j\right)^2}{x_j x_m} + \sum_{j=t+1}^{\nu} \sum_{\substack{p=1 \\ p\neq k}}^{t} n^2_{kj} \Delta^*_{pj} \frac{x_p}{x_j}$$

$$+ \sum_{\substack{p=1 \\ p\neq k}}^{t} \Delta^*_{pk} \frac{x_p}{x_k} + \sum_{j=t+1}^{\nu} \Delta^*_{kj} \frac{\left(x_j + n_{kj}x_k\right)^2}{x_j x_k} \qquad (k = 1,2,\ldots,t) \tag{B35}$$

$$E^*_{ik} = \sum_{j=t+1}^{\nu-1} \sum_{m=j+1}^{\nu} \Delta^*_{mj} \frac{\left(n_{ij}x_m - n_{im}x_j\right)\left(n_{kj}x_m - n_{km}x_j\right)}{x_j x_m} + \sum_{j=t+1}^{\nu} \sum_{p=1}^{t} n_{ij}n_{kj} \Delta^*_{pj} \frac{x_p}{x_j}$$

$$+ \sum_{j=t+1}^{\nu} \left(n_{kj} \Delta^*_{ij} + n_{ij} \Delta^*_{kj}\right) - \Delta^*_{ik} \qquad (i,k = 1,2,\ldots,t) \tag{B36}$$

$$\Delta^*_{ij} = \frac{25}{16} \overline{\Omega}^{(1,1)}_{ij} C_{3,ij} \tag{B37}$$

When equation (B33) is expanded, the first approximation is

$$\lambda^*_{r,I} = \sum_{i=1}^{t} \frac{\left(\Delta H^*_i\right)^2}{E^*_{ii}} \tag{B38}$$

REFERENCES

1. Bailey, Harry E.: Equilibrium Thermodynamic Properties of Three Engineering Models of the Martian Atmosphere. NASA SP-3021, 1965.

2. Allison, Dennis O.: Calculation of Thermodynamic Properties of Gas Mixtures at High Temperatures. M.S. Thesis, Virginia Polytech. Inst., 1965.

3. Allison, Dennis O.: Calculation of Thermodynamic Properties of Arbitrary Gas Mixtures With Modified Vibrational-Rotational Corrections. NASA TN D-3538, 1966.

4. Newman, Perry A.; and Allison, Dennis O.: Direct Calculation of Specific Heats and Related Thermodynamic Properties of Arbitrary Gas Mixtures With Tabulated Results. NASA TN D-3540, 1966.

5. Kennard, Earle H.: Kinetic Theory of Gases. McGraw-Hill Book Co., Inc., 1938.

6. Chapman, Sydney; and Cowling, T. G.: The Mathematical Theory of Non-Uniform Gases. Second ed., Cambridge Univ. Press, London, 1952.

7. Hirschfelder, Joseph O.; Curtiss, Charles F.; and Bird, R. Bryon: Molecular Theory of Gases and Liquids. John Wiley & Sons, Inc., c.1954. (Reprinted with corrections 1964.)

8. Mason, Edward A.; Vanderslice, Joseph T.; and Yos, Jerrold M.: Transport Properties of High-Temperature Multicomponent Gas Mixtures. Phys. Fluids, vol. 2, no. 6, Nov.-Dec. 1959, pp. 688-694.

9. Monchick, L.; Yun, K. S.; and Mason, E. A.: Formal Kinetic Theory of Transport Phenomena in Polyatomic Gas Mixtures. J. Chem. Phys., vol. 39, no. 3, Aug. 1, 1963, pp. 654-669.

10. Hirschfelder, Joseph O.: Heat Conductivity in Polyatomic or Electronically Excited Gases. II. J. Chem. Phys., vol. 26, no. 2, Feb. 1957, pp. 282-285.

11. Butler, James N.; and Brokaw, Richard S.: Thermal Conductivity of Gas Mixtures in Chemical Equilibrium. J. Chem. Phys., vol. 26, no. 6, June 1957, pp. 1636-1643.

12. Hirschfelder, Joseph O.: Heat Conductivity in Polyatomic, Electronically Excited, or Chemically Reacting Mixtures. III. Sixth Symposium (International) on Combustion, Reinhold Pub. Corp., c.1957, pp. 351-366.

13. Muckenfuss, Charles; and Curtiss, C. F.: Thermal Conductivity of Multicomponent Gas Mixtures. J. Chem. Phys., vol. 29, no. 6, Dec. 1958, pp. 1273-1277.

14. Brokaw, R. S.: Energy Transport in High Temperature and Reacting Gases. Planetary Space Sci., vol. 3, Feb. 1961, pp.238-252.

15. Vanderslice, Joseph T.; Mason, Edward A.; and Lippincott, Ellis R.: Interactions Between Ground-State Nitrogen Atoms and Molecules. The N-N, N-N_2, and N_2-N_2 Interactions. J. Chem. Phys., vol. 30, no. 1, Jan. 1959, pp. 129-136.

16. Vanderslice, Joseph T.; Mason, Edward A.; and Maisch, William G.: Interactions Between Oxygen and Nitrogen: O-N, O-N_2, and O_2-N_2. J. Chem. Phys., vol. 31, no. 3, Sept. 1959, pp. 738-746.

17. Vanderslice, Joseph T.; Mason, Edward A.; and Maisch, William G.: Interactions Between Ground State Oxygen Atoms and Molecules: O-O and O_2-O_2. J. Chem. Phys., vol. 32, no. 2, Feb. 1960, pp. 515-524.

18. Meador, Willard E., Jr.: The Interactions Between Nitrogen and Oxygen Molecules. NASA TR R-68, 1960.

19. Yun, K. S.; and Mason, E. A.: Collision Integrals for the Transport Properties of Dissociating Air at High Temperatures. Phys. Fluids, vol. 5, no. 4, Apr. 1962, pp. 380-386.

20. Amdur, I.; and Mason, E. A.: Properties of Gases at Very High Temperatures. Phys. Fluids, vol. 1, no. 5, Sept.-Oct. 1958, pp. 370-383.

21. Hansen, C. Frederick: Approximations for the Thermodynamic and Transport Properties of High-Temperature Air. NASA TR R-50, 1959. (Supersedes NACA TN 4150.)

22. Yos, Jerrold M.: Transport Properties of Nitrogen, Hydrogen, Oxygen, and Air to 30,000° K. Tech. Mem. RAD-TM-63-7 (Contract AF33(616)-7578), AVCO Corp., Mar. 22, 1963.

23. Thomas, M.: The High Temperature Transport Properties of Carbon Dioxide. Rep. No. SM-37790, Douglas Aircraft Co., Inc., July 1960.

24. Van Tassell, W.: Convective Heating in Planetary Atmospheres. Tech. Mem. RAD-TM-63-72, AVCO Corp., Oct. 18, 1963.

25. Mason, Edward A.; and Rice, William E.: The Intermolecular Potentials for Some Simple Nonpolar Molecules. J. Chem. Phys., vol. 22, no. 5, May 1954, pp. 843-851.

26. Amdur, I.; and Mason, E. A.: Scattering of High Velocity Neutral Particles. VIII. H-He. J. Chem. Phys., vol. 25, no. 4, Oct. 1956, pp. 630-632.

27. Amdur, I.; and Mason, E. A.: Scattering of High Velocity Neutral Particles. IX. Ne-A; A-Ne. J. Chem. Phys., vol. 25, no. 4, Oct. 1956, pp. 632-634.

28. Amdur, I.; Mason, E. A.; and Jordan, J. E.: Scattering of High Velocity Neutral Particles. X. He-N_2; A-N_2. The N_2-N_2 Interaction. J. Chem. Phys., vol. 27, no. 2, Aug. 1957, pp. 527-531.

29. Amdur, I.; and Jordan, J. E.: Elastic Scattering of High-Energy Beams: Repulsive Forces. Molecular Beams, John Ross, ed., Interscience Publ., c.1966, pp. 29-73.

30. Herzberg, Gerhard: Molecular Spectra and Molecular Structure. I. Spectra of Diatomic Molecules. Second ed., D. Van Nostrand Co., Inc., c.1950.

31. Walker, R. E.; Monchick, L.; Westenberg, A. A.; and Favin, S.: High Temperature Gaseous Diffusion Experiments and Intermolecular Potential Energy Functions. Planetary Space Sci., vol. 3, Feb. 1961, pp. 221-227.

32. Ember, G.; Ferron, J. R.; and Wohl, K.: Self-Diffusion Coefficients of Carbon Dioxide at 1180°-1680° K. J. Chem. Phys., vol. 37, no. 4, Aug. 15, 1962, pp. 891-897.

33. Pakurar, Thomas A.; and Ferron, John R.: Self-Diffusion Coefficient of Carbon Dioxide. J. Chem. Phys. (Lett. Ed.), vol. 43, no. 8, Oct. 15, 1965, pp. 2917-2918.

34. Vukalovich, M. P.; Altunin, V. V.; and Blinov, V. V.: Thermophysical Properties of Carbon Dioxide – 2. Transport Coefficients at Atmospheric Pressure and Temperature 200-1700° K. High Temp. (USSR), vol. 1, no. 3, Nov.-Dec. 1963, pp. 319-330.

35. Hirschfelder, Joseph O.; and Eliason, Morton A.: The Estimation of the Transport Properties for Electronically Excited Atoms and Molecules. Unstable Chemical Species: Free Radicals, Ions, and Excited Molecules, Henry C. Thacher, Jr., ed., WADC Tech. Rep. 57-217, DDC Doc. No. AD 118181, U.S. Air Force, May 24, 1957, pp. 1-11.

36. Kihara, Taro; Taylor, Marion H.; and Hirschfelder, Joseph O.: Transport Properties for Gases Assuming Inverse Power Intermolecular Potentials. Phys. Fluids, vol. 3, no. 5, Sept.-Oct. 1960, pp. 715-720.

37. Monchick, Louis: Collision Integrals for the Exponential Repulsive Potential. Phys. Fluids, vol. 2, no. 6, Nov.-Dec. 1959, pp. 695-700.

38. Brokaw, Richard S.: Approximate Formulas for the Viscosity and Thermal Conductivity of Gas Mixtures. J. Chem. Phys., vol. 29, no. 2, Aug. 1958, pp. 391-397.

39. Brokaw, Richard S.: Approximate Formulas for the Viscosity and Thermal Conductivity of Gas Mixtures. II. J. Chem. Phys., vol. 42, no. 4, Feb. 1965, pp. 1140-1146. (Also available as NASA TN D-2502.)

40. Brokaw, Richard S.: Thermal Conductivity of Gas Mixtures in Chemical Equilibrium. II. J. Chem. Phys., vol. 32, no. 4, Apr. 1960, pp. 1005-1006.

41. Horton, Thomas E.; and Zeh, Dale W.: Effect of Uncertainties in Transport Properties on Prediction of Stagnation-Point Heat Transfer. AIAA J. (Tech. Notes), vol. 5, no. 8, Aug. 1967, pp. 1497-1498.

TABLE 1

BINARY INTERACTIONS FOR DISSOCIATING CO_2-N_2-Ar MIXTURES WITHOUT IONIZATION

CO_2-CO_2	CO_2-O_2	CO_2-N_2	CO_2-NO	CO_2-CO	CO_2-O	[CO_2-N]	[CO_2-C]	CO_2-Ar
	(O_2-O_2)	(O_2-N_2)	O_2-NO	O_2-CO	(O_2-O)	[O_2-N]	[O_2-C]	O_2-Ar
		(N_2-N_2)	(N_2-NO)	N_2-CO	(N_2-O)	(N_2-N)	N_2-C	N_2-Ar
			(NO-NO)	NO-CO	(NO-O)	NO-N	NO-C	NO-Ar
				CO-CO	CO-O	CO-N	CO-C	CO-Ar
					(O-O)	(O-N)	O-C	O-Ar
						(N-N)	N-C	N-Ar
							C-C	C-Ar
								Ar-Ar

Parentheses around a pair designate that its interaction potential has been considered previously and that the corresponding collision integrals can be obtained from reference 19.

Brackets around a pair mean that an accurate interaction potential is not critical because one or both of the mole fractions are always small.

TABLE 2

INTERACTION POTENTIALS FOR DISSOCIATING CO_2-N_2-O_2-Ar MIXTURES

Interaction	Potential (r in Å)	Temperature range	Reference	Comments
Interactions enclosed by parentheses in table 1	See reference 19		19	Averages of tabulated values were used for minor interactions
CO-atom or molecule	Use N_2-atom or molecule potentials			See section "Carbon monoxide interactions"
Ar-O_2	Exp-6: $\alpha = 15.5$, $\epsilon/k = 127.5^{\circ}$ K, $r_m = 3.796$ Å	Low	19, 25	Obtained from viscosity data and combination rules
	$\frac{1360}{r^{8.34}}$ eV	High	29	Scattering potential
Ar-N_2	Exp-6: $\alpha = 15.5$, $\epsilon/k = 111.6^{\circ}$ K, $r_m = 3.938$ Å	Low	25	Obtained from viscosity data and combination rules
	$\frac{760}{r^{7.78}}$ eV	High	28	Scattering potential
Ar-NO	$2382e^{-3.205r}$ eV	All	18, 19, 20	See section "Argon interactions"
Ar-O	$1025e^{-3.330r}$ eV	All	18, 20	Obtained from equations (10) and (11) by combination rule
Ar-N	$\frac{142.4}{r^{7.10}}$ eV	All	28	Obtained indirectly from scattering data
Ar-Ar	Exp-6: $\alpha = 14$, $\epsilon/k = 123.2^{\circ}$ K, $r_m = 3.866$ Å	Low	25	
	$32\,300e^{-4.46r}$ eV	High	20	Obtained from scattering data
CO_2-CO_2	6-12: $\sigma = 3.897$ Å, $\epsilon/k = 213^{\circ}$ K	Low	32	Obtained from viscosity data
	$678.4e^{-2.166r}$ eV	High	Appendix A	Obtained by averaging
CO_2-O_2	Exp-6: $\alpha = 17$, $\epsilon/k = 255^{\circ}$ K, $r_m = 3.616$ Å	Low	31	Obtained from diffusion data
	$320.8e^{-2.153r}$ eV	High	Appendix A	Obtained by averaging; equation (11) used for ϕ(O-O)
CO_2-N_2	Exp-6: $\alpha = 17$, $\epsilon/k = 184^{\circ}$ K, $r_m = 3.782$ Å	Low	31	Obtained from diffusion data
	$674.5e^{-2.416r}$ eV	High	Appendix A	Obtained by averaging; equations (14) and (15) used for ϕ(N-N) and ϕ(N-O)
CO_2-NO	6-12: $\sigma = 3.748$ Å, $\epsilon/k = 139.2^{\circ}$ K	Low	7	Obtained from viscosity data and combination rules
	$473.4e^{-2289r}$ eV	High	Appendix A	Obtained by averaging; equations (11), (14), and (15) used for ϕ(O-O), ϕ(N-N), and ϕ(N-O)
CO_2-Ar	6-12: $\sigma = 3.681$ Å, $\epsilon/k = 157.2^{\circ}$ K	Low	7	Obtained from viscosity data and combination rules
	$5401.7e^{-3.130r}$ eV	High	Appendix A	Obtained by averaging
CO_2-O	$151.3e^{-2.198r}$ eV	All	Appendix A	Obtained by averaging; equation (11) used for ϕ(O-O)
N-NO	$253.1e^{-2.647r}$ eV	All	18, 19	Obtained by averaging; equations (14) and (15) used for ϕ(N-N) and ϕ(N-O)
C-NO	$262.2e^{-2.670r}$ eV	All	18	Obtained by averaging; equation (14) used for ϕ(N-C) and ϕ(O-C)
C-O	Use N-N potential	All		See section "Carbon interactions"
Remaining C-Interactions	Use N-interactions			See sections "Carbon interactions" and "Carbon dioxide interactions"

Potentials for CO_2-N, CO_2-C, O_2-N, and O_2-C are not included because either one or both of the species involved in these interactions are always small. Transport-property calculations were made with various potentials for these interactions and absolutely no change in the results occurred.

TABLE 3

COLLISION INTEGRALS

T, °K	Ar-Ar		Ar-O$_2$		Ar-N$_2$		Ar-O		Ar-N		Ar-NO		CO$_2$-O$_2$	
	$\bar{\Omega}^{(1,1)}$, Å^2	$\bar{\Omega}^{(2,2)}$, Å^2	$\bar{\Omega}^{(1,1)}$, Å^2	$\bar{\Omega}^{(2,2)}$, Å^2	$\bar{\Omega}^{(1,1)}$, Å^2	$\bar{\Omega}^{(2,2)}$, Å^2	$\bar{\Omega}^{(1,1)}$, Å^2	$\bar{\Omega}^{(2,2)}$, Å^2	$\bar{\Omega}^{(1,1)}$, Å^2	$\bar{\Omega}^{(2,2)}$, Å^2	$\bar{\Omega}^{(1,1)}$, Å^2	$\bar{\Omega}^{(2,2)}$, Å^2	$\bar{\Omega}^{(1,1)}$, Å^2	$\bar{\Omega}^{(2,2)}$, Å^2
1000	8.73	9.91	8.94	9.95	9.40	10.49	6.98	8.23	6.90	8.39	9.03	10.54	9.60	10.56
1500	7.50	8.55	8.22	9.33	8.56	9.66	6.35	7.54	6.16	7.48	8.29	9.72	8.94	9.80
2000	6.92	7.95	7.61	8.84	7.80	9.00	5.93	7.06	5.67	6.89	7.78	9.17	8.50	9.38
2500	6.48	7.60	7.13	8.41	7.18	8.48	5.61	6.70	5.33	6.48	7.41	8.74	8.20	9.07
3000	6.20	7.29	6.78	8.04	6.75	8.08	5.36	6.42	5.08	6.18	7.10	8.41	7.98	8.86
3500	6.04	7.03	6.54	7.75	6.48	7.78	5.15	6.18	4.83	5.88	6.85	8.12	7.80	8.68
4000	5.88	6.82	6.35	7.52	6.27	7.53	4.97	5.98	4.67	5.68	6.63	7.88	7.65	8.52
4500	5.76	6.65	6.17	7.31	6.08	7.30	4.82	5.80	4.51	5.49	6.45	7.68	7.51	8.38
5000	5.65	6.53	6.02	7.13	5.92	7.10	4.68	5.65	4.38	5.32	6.28	7.49	7.38	8.24
5500	5.55	6.42	5.88	6.97	5.78	6.94	4.56	5.52	4.27	5.19	6.14	7.33	7.26	8.13
6000	5.46	6.32	5.76	6.82	5.65	6.78	4.45	5.39	4.16	5.06	6.01	7.18	7.14	8.03
6500	5.38	6.23	5.64	6.69	5.54	6.65	4.35	5.27	4.06	4.94	5.89	7.04	7.02	7.96
7000	5.31	6.15	5.55	6.58	5.44	6.52	4.26	5.17	3.99	4.85	5.78	6.92	6.91	7.87
7500	5.23	6.07	5.45	6.46	5.34	6.40	4.17	5.07	3.92	4.77	5.68	6.81	6.80	7.80
8000	5.17	6.01	5.36	6.36	5.25	6.29	4.09	4.98	3.83	4.66	5.58	6.70	6.70	7.73

T, °K	CO$_2$-N$_2$		CO$_2$-O		CO$_2$-Ar		CO$_2$-NO		CO$_2$-CO$_2$		NO-N		NO-C	
	$\bar{\Omega}^{(1,1)}$, Å^2	$\bar{\Omega}^{(2,2)}$, Å^2	$\bar{\Omega}^{(1,1)}$, Å^2	$\bar{\Omega}^{(2,2)}$, Å^2	$\bar{\Omega}^{(1,1)}$, Å^2	$\bar{\Omega}^{(2,2)}$, Å^2	$\bar{\Omega}^{(1,1)}$, Å^2	$\bar{\Omega}^{(2,2)}$, Å^2	$\bar{\Omega}^{(1,1)}$, Å^2	$\bar{\Omega}^{(2,2)}$, Å^2	$\bar{\Omega}^{(1,1)}$, Å^2	$\bar{\Omega}^{(2,2)}$, Å^2	$\bar{\Omega}^{(1,1)}$, Å^2	$\bar{\Omega}^{(2,2)}$, Å^2
1000	9.94	10.84	9.72	11.71	10.90	12.03	11.05	12.21	13.08	14.40	7.84	9.44	7.78	9.36
1500	9.26	10.23	8.75	10.71	10.14	11.25	10.30	11.44	12.10	13.38	7.02	8.50	6.96	8.43
2000	8.84	9.80	8.01	9.85	9.68	10.79	9.88	10.99	11.50	12.78	6.46	7.87	6.41	7.81
2500	8.54	9.50	7.46	9.21	9.28	10.43	9.51	10.62	11.13	12.40	6.05	7.39	6.00	7.34
3000	8.30	9.28	7.02	8.70	8.93	10.15	9.14	10.31	10.83	12.05	5.72	7.01	5.68	6.97
3500	8.10	9.08	6.65	8.28	8.64	9.89	8.78	10.07	10.55	11.78	5.45	6.70	5.41	6.66
4000	7.94	8.90	6.35	7.93	8.39	9.68	8.46	9.86	10.30	11.52	5.22	6.44	5.19	6.40
4500	7.79	8.76	6.09	7.62	8.18	9.51	8.18	9.67	10.04	11.30	5.02	6.21	4.99	6.17
5000	7.65	8.63	5.86	7.35	7.99	9.35	7.93	9.48	9.80	11.15	4.85	6.01	4.82	5.97
5500	7.51	8.51	5.67	7.11	7.82	9.20	7.69	9.30	9.56	10.98	4.69	5.83	4.67	5.79
6000	7.37	8.41	5.46	6.90	7.67	9.05	7.49	9.11	9.34	10.88	4.55	5.67	4.53	5.63
6500	7.24	8.31	5.31	6.70	7.53	8.90	7.30	8.94	9.12	10.75	4.43	5.52	4.40	5.49
7000	7.11	8.22	5.16	6.52	7.40	8.76	7.13	8.77	8.92	10.66	4.31	5.39	4.29	5.36
7500	6.98	8.16	5.02	6.36	7.29	8.64	6.97	8.61	8.73	10.53	4.21	5.26	4.19	5.23
8000	6.85	8.08	4.89	6.21	7.17	8.51	6.83	8.44	8.56	10.43	4.11	5.15	4.09	5.12

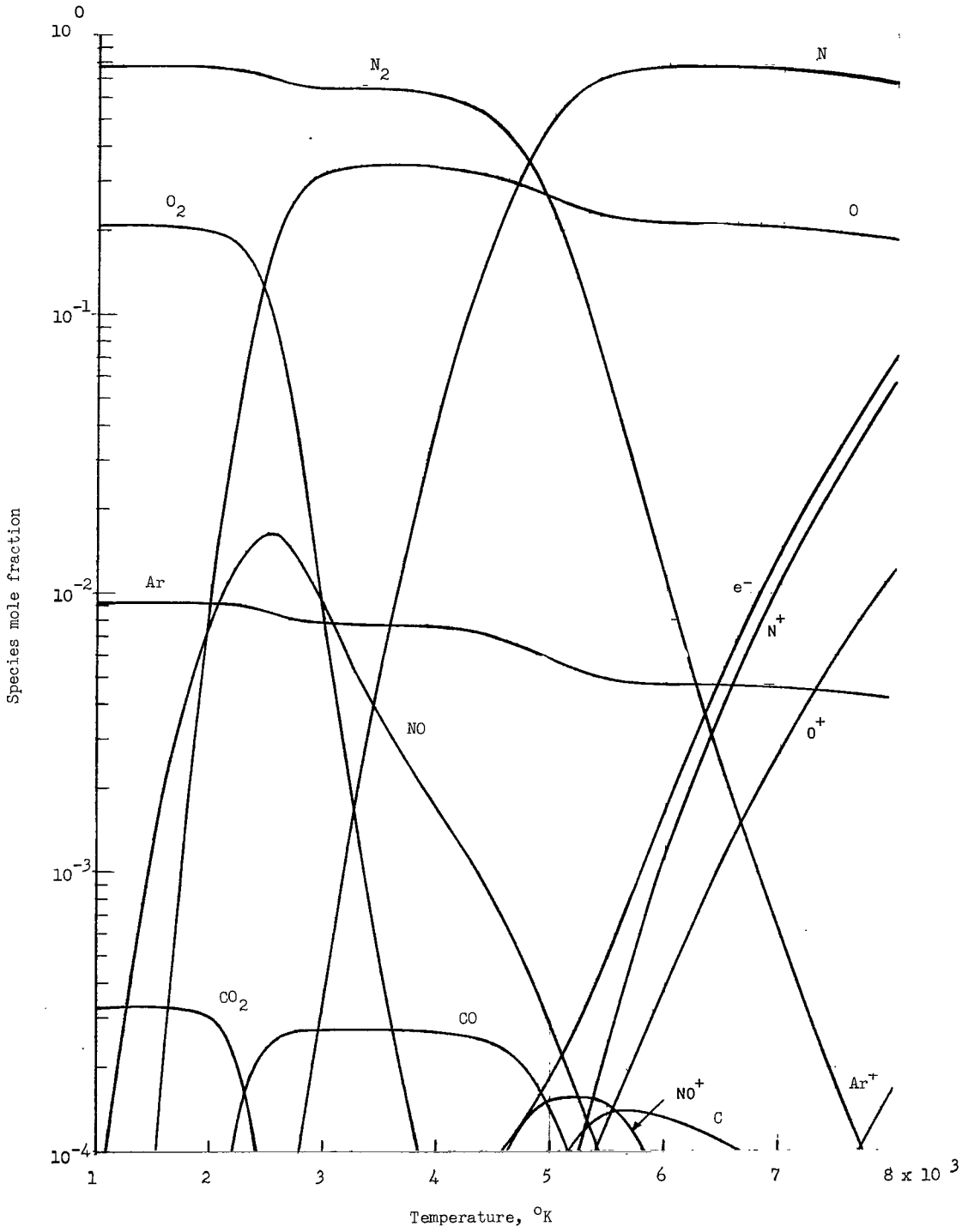

(a) p = 0.001 atm.

Figure 1.- Equilibrium mole fractions of high-temperature air for several pressures.

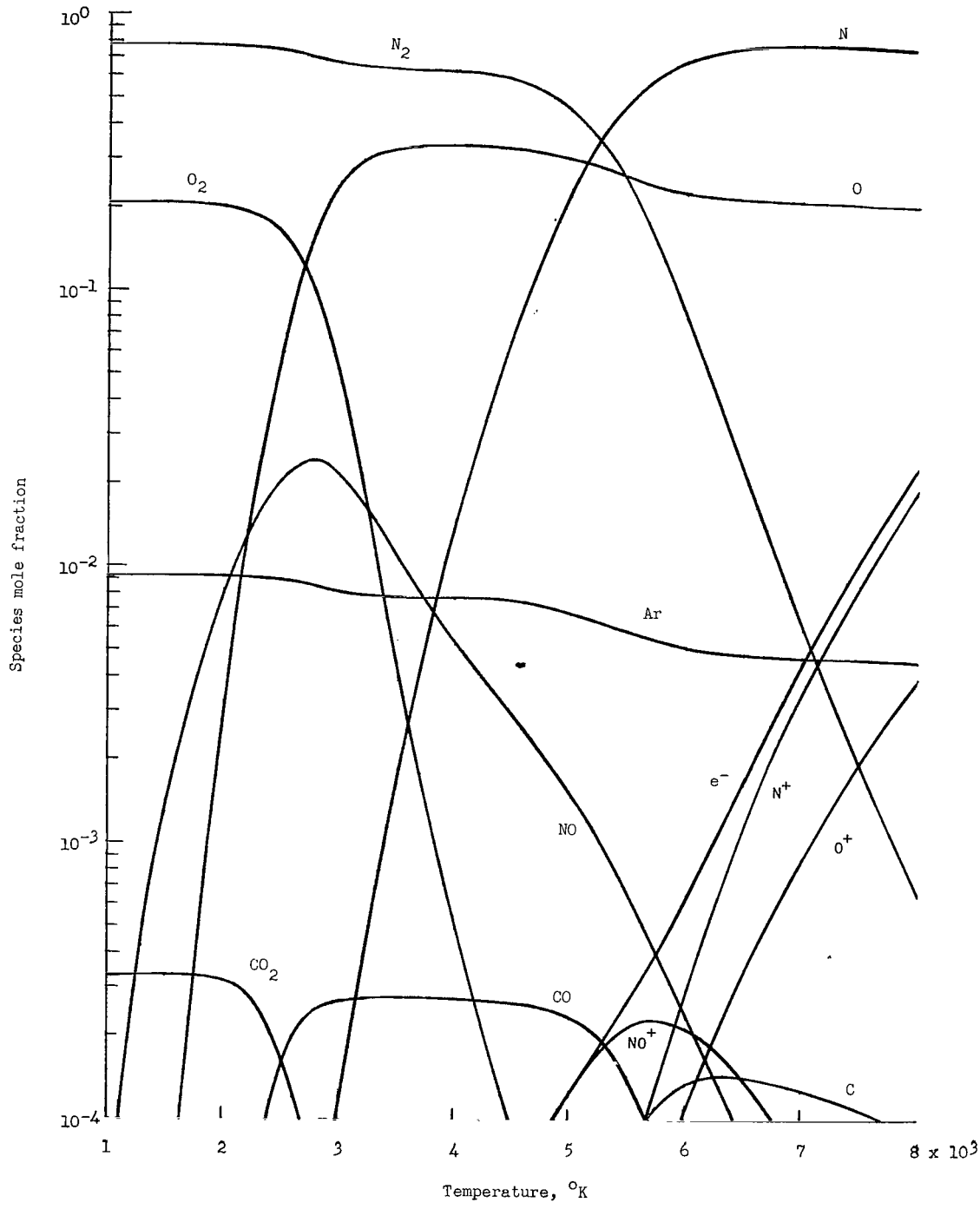

(b) p = 0.01 atm.

Figure 1.- Continued.

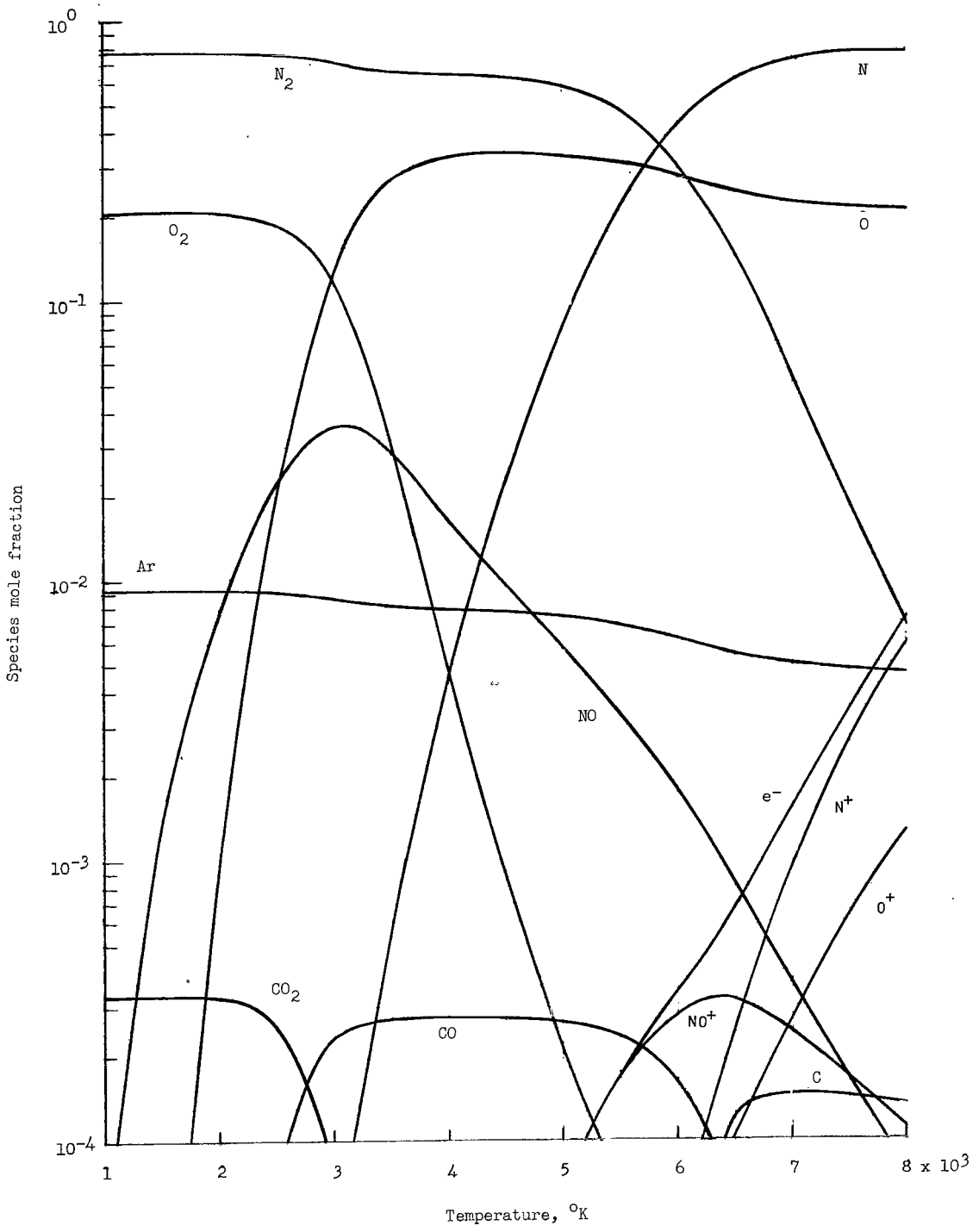

(c) p = 0.1 atm.

Figure 1.- Continued.

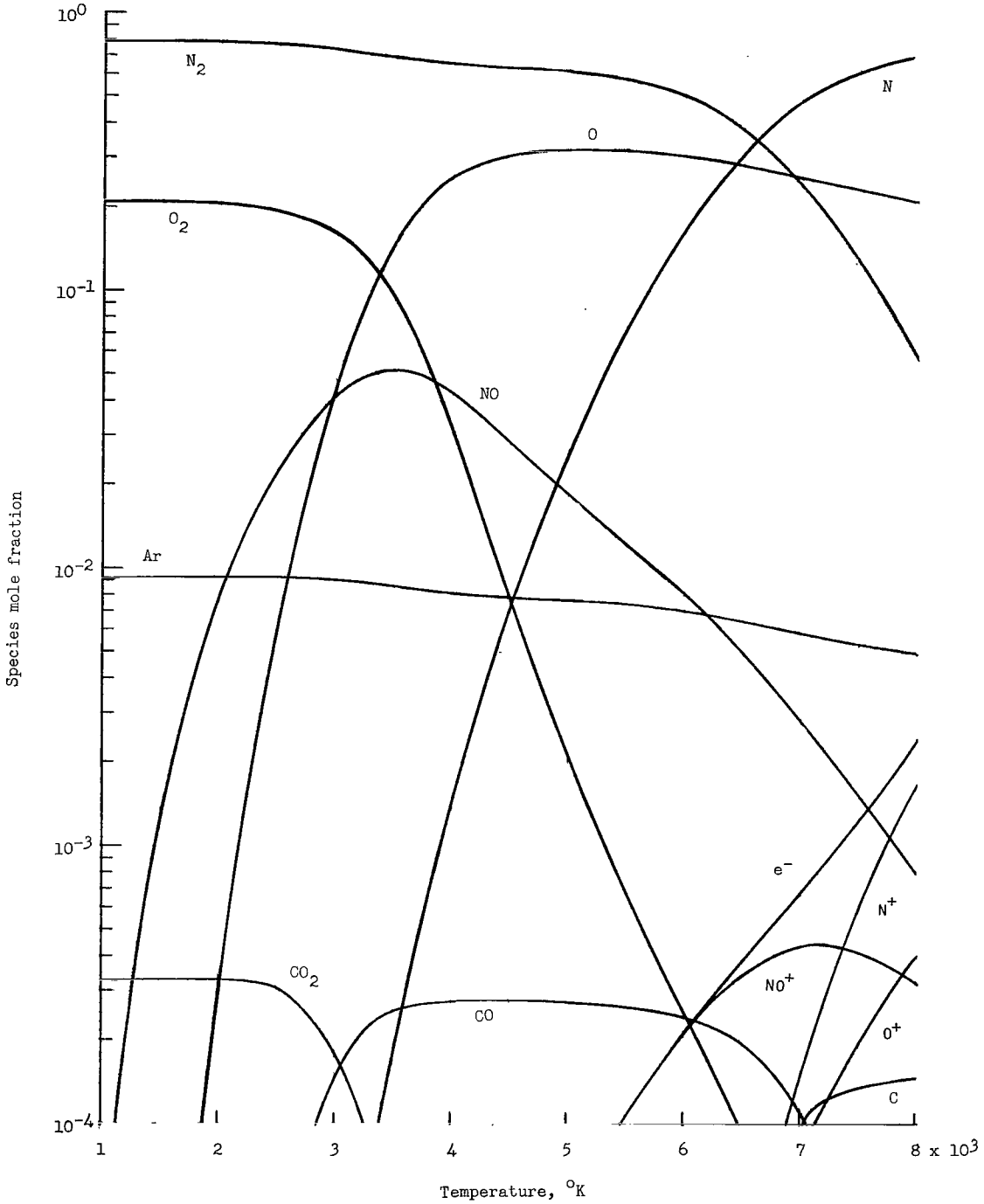

(d) p = 1 atm.

Figure 1.- Continued.

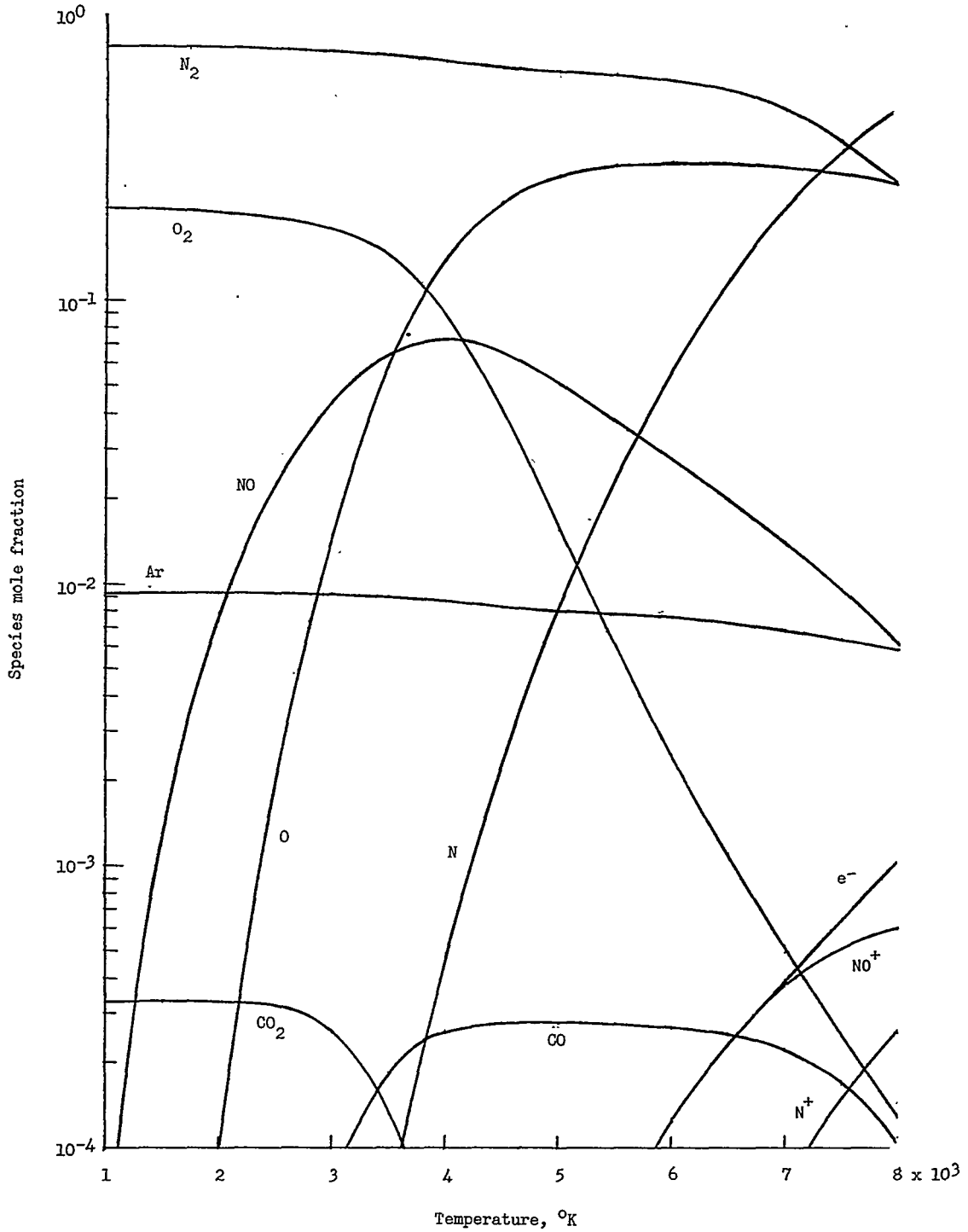

(e) p = 10 atm.

Figure 1.- Concluded.

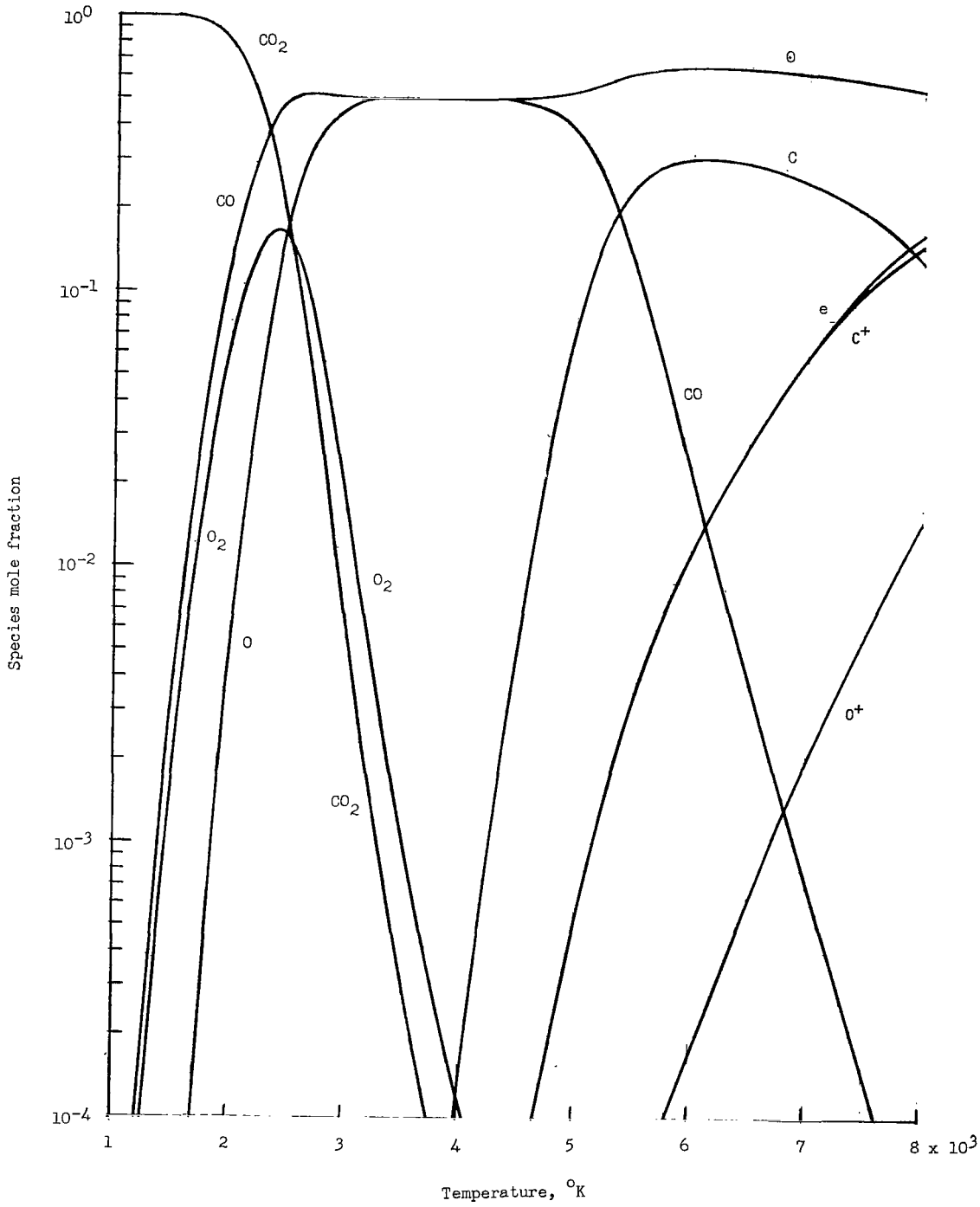

(a) p = 0.001 atm.

Figure 2.- Equilibrium mole fractions of high-temperature CO_2 for several pressures.

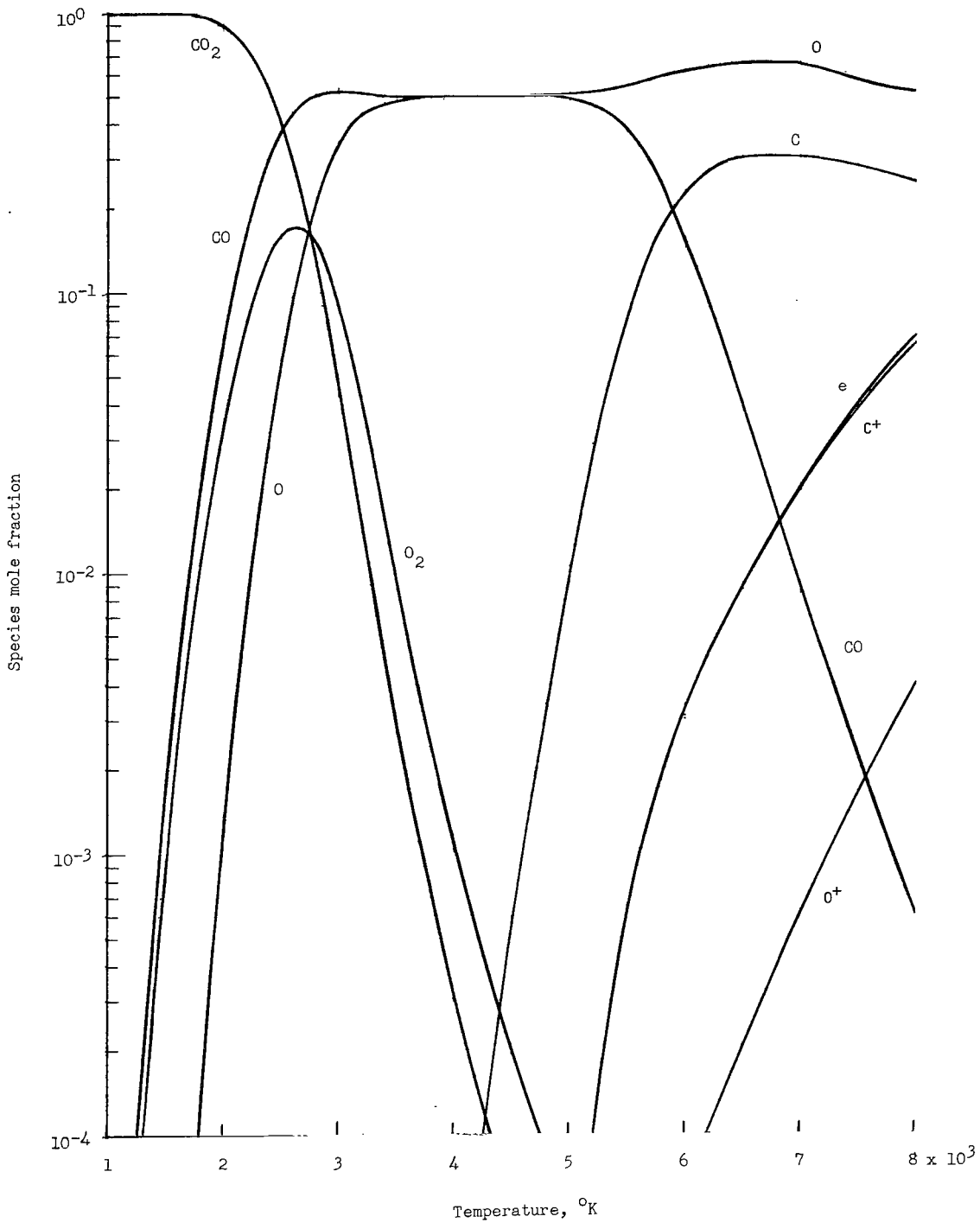

(b) p = 0.01 atm.

Figure 2.- Continued.

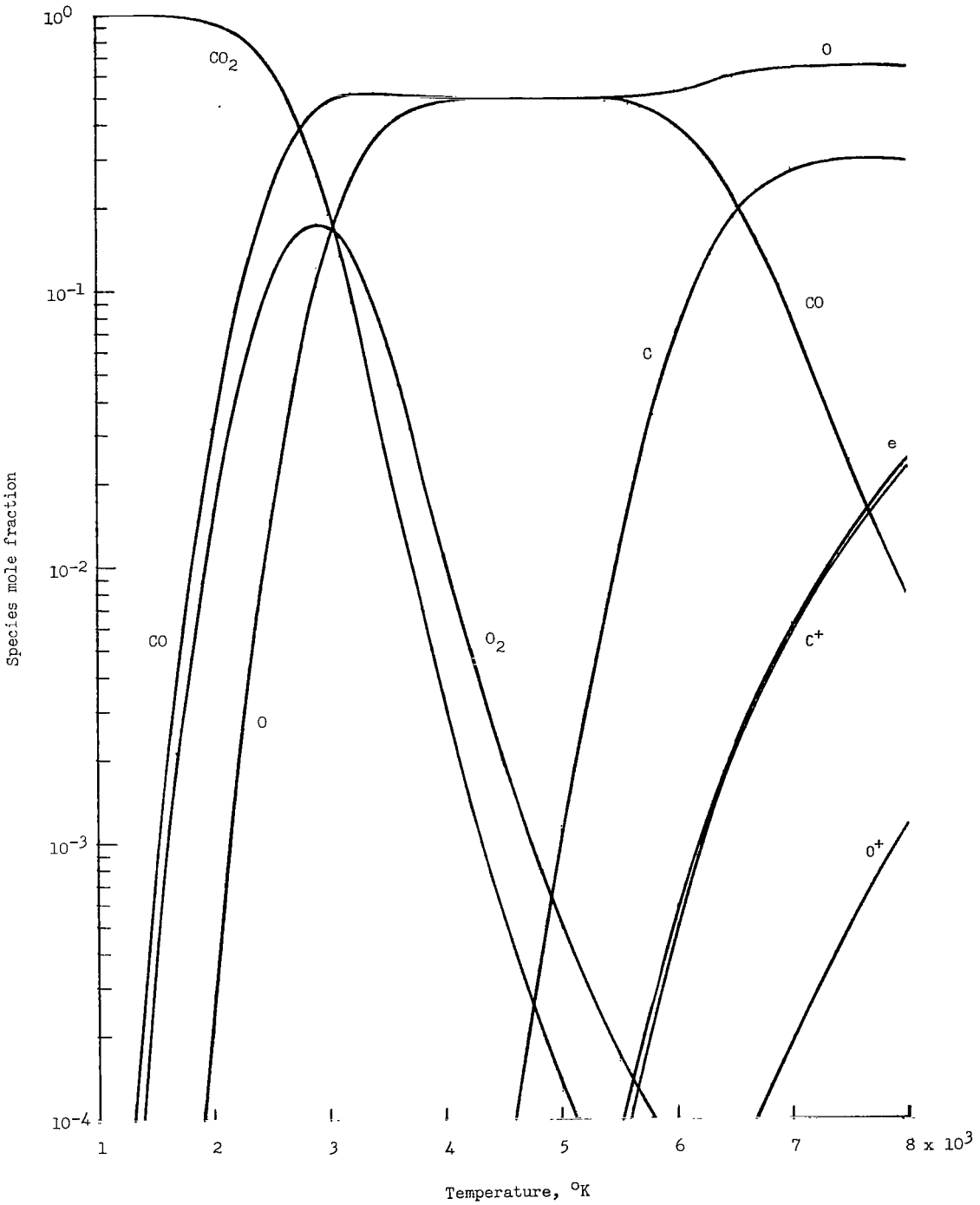

(c) p = 0.1 atm.

Figure 2.- Continued.

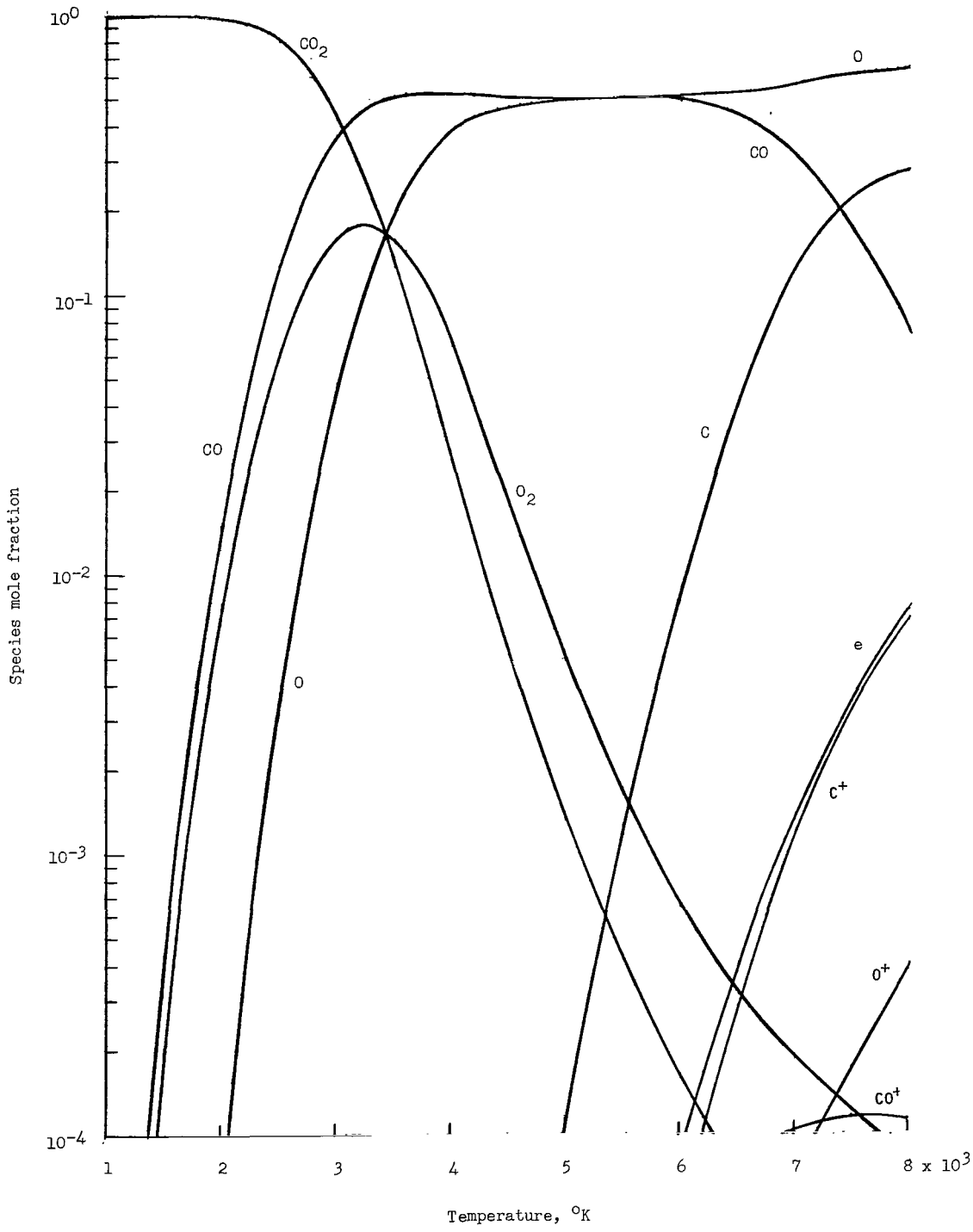

(d) p = 1 atm.

Figure 2.- Continued.

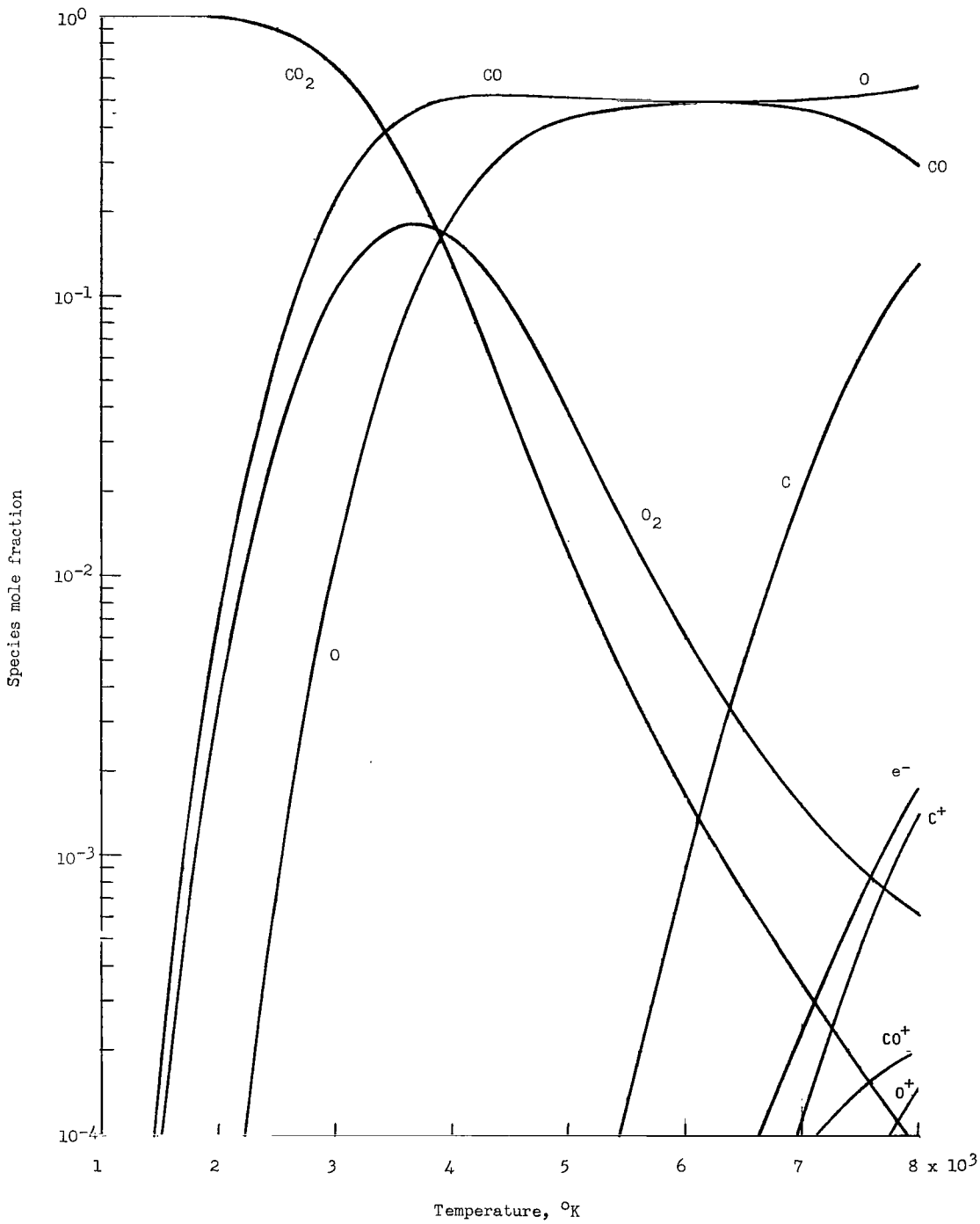

(e) p = 10 atm.

Figure 2.- Concluded.

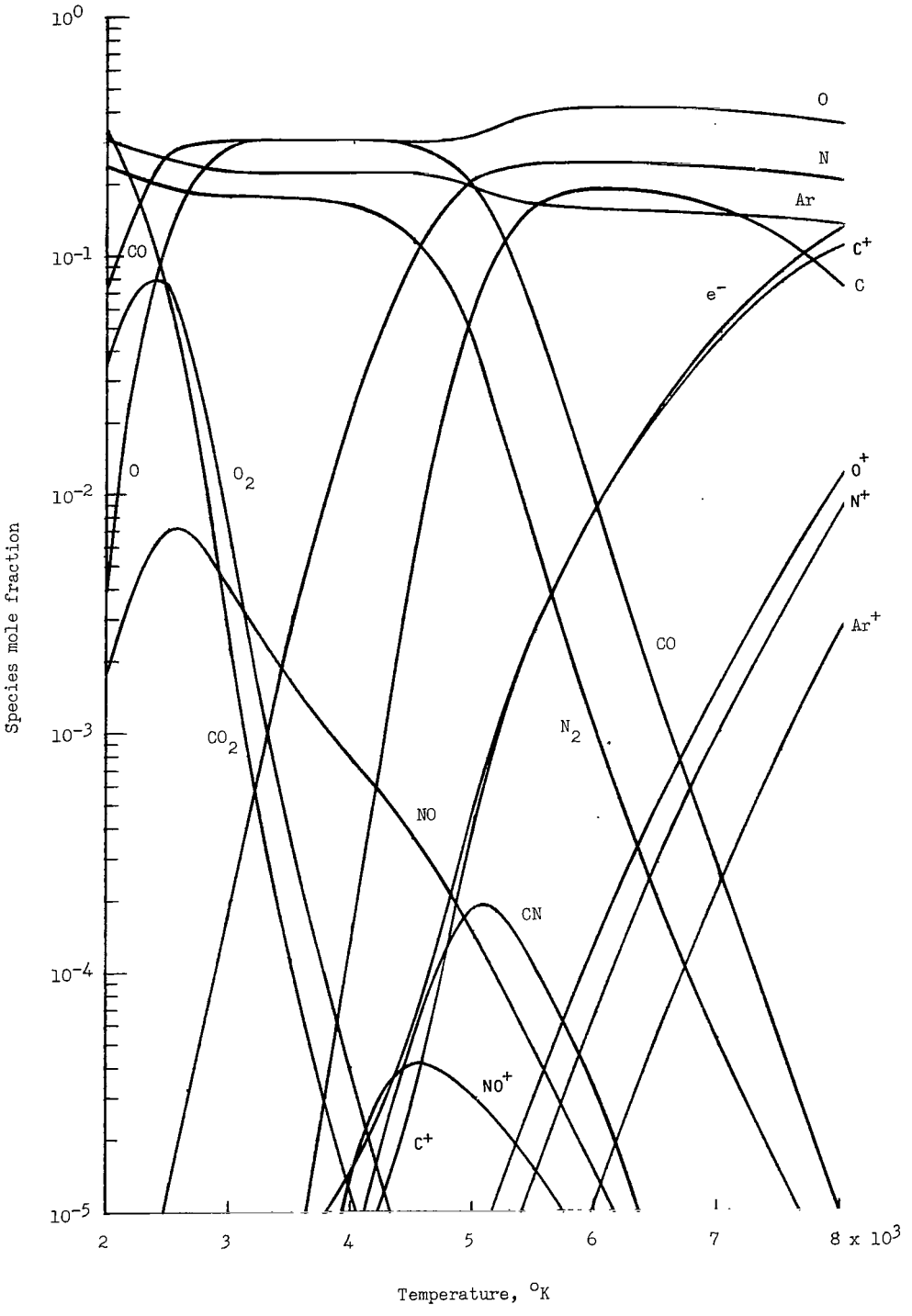

(a) p = 0.001 atm.

Figure 3.- Equilibrium mole fractions of Mars model atmosphere (43% CO_2, 25% N_2, 32% Ar (by vol.)) for several pressures.

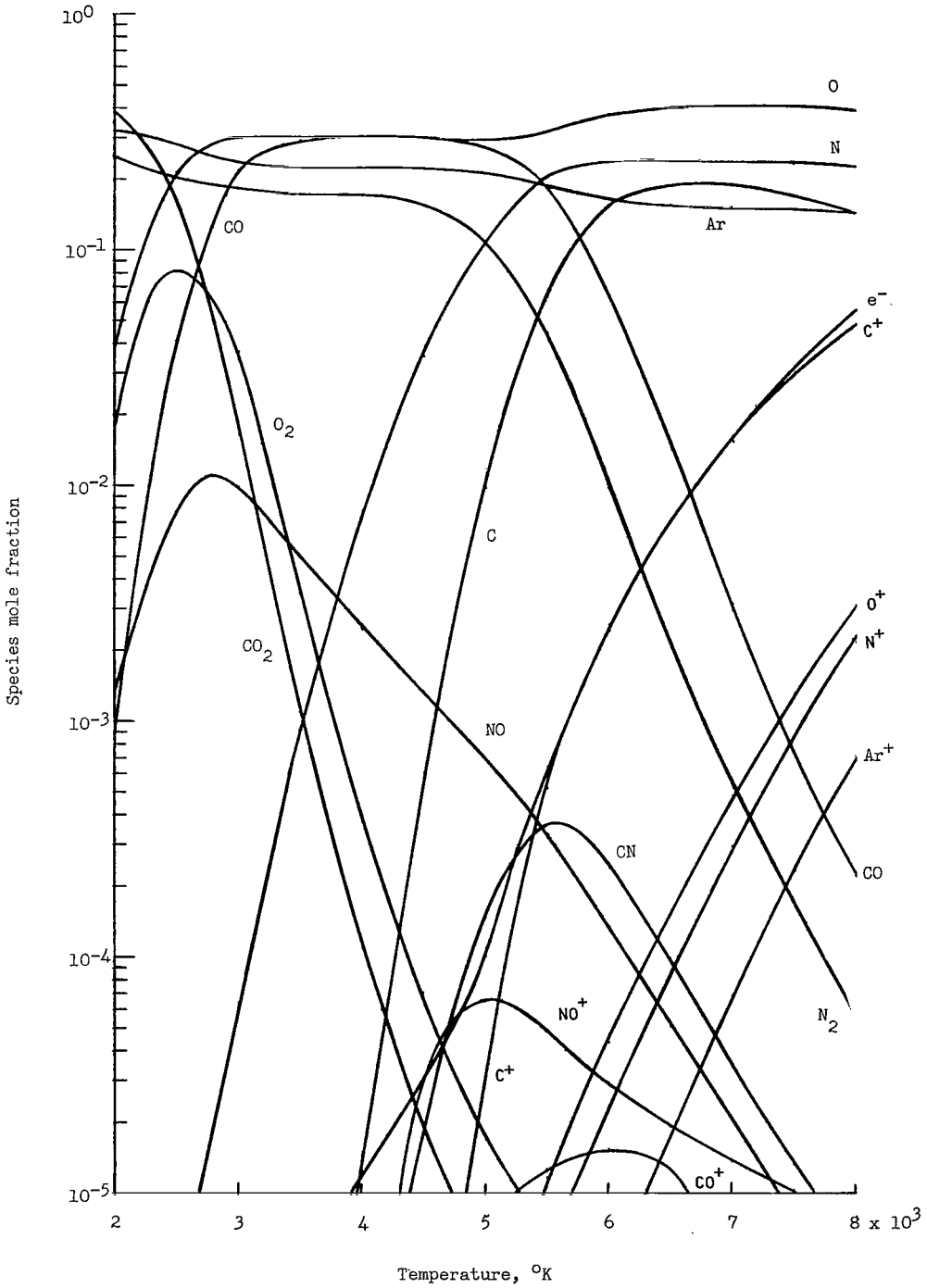

(b) p = 0.01 atm.

Figure 3.- Continued.

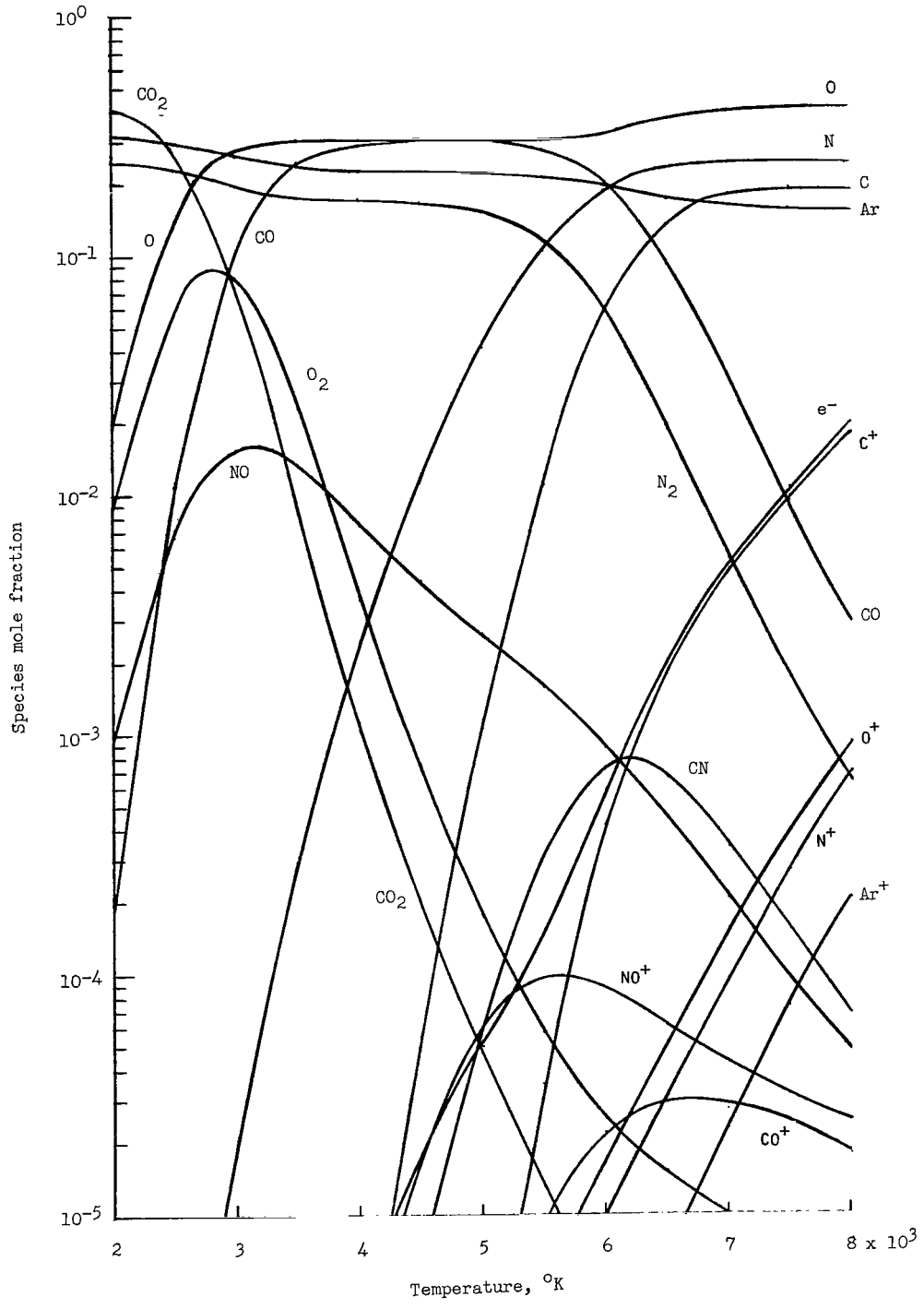

(c) p = 0.1 atm.

Figure 3.- Continued.

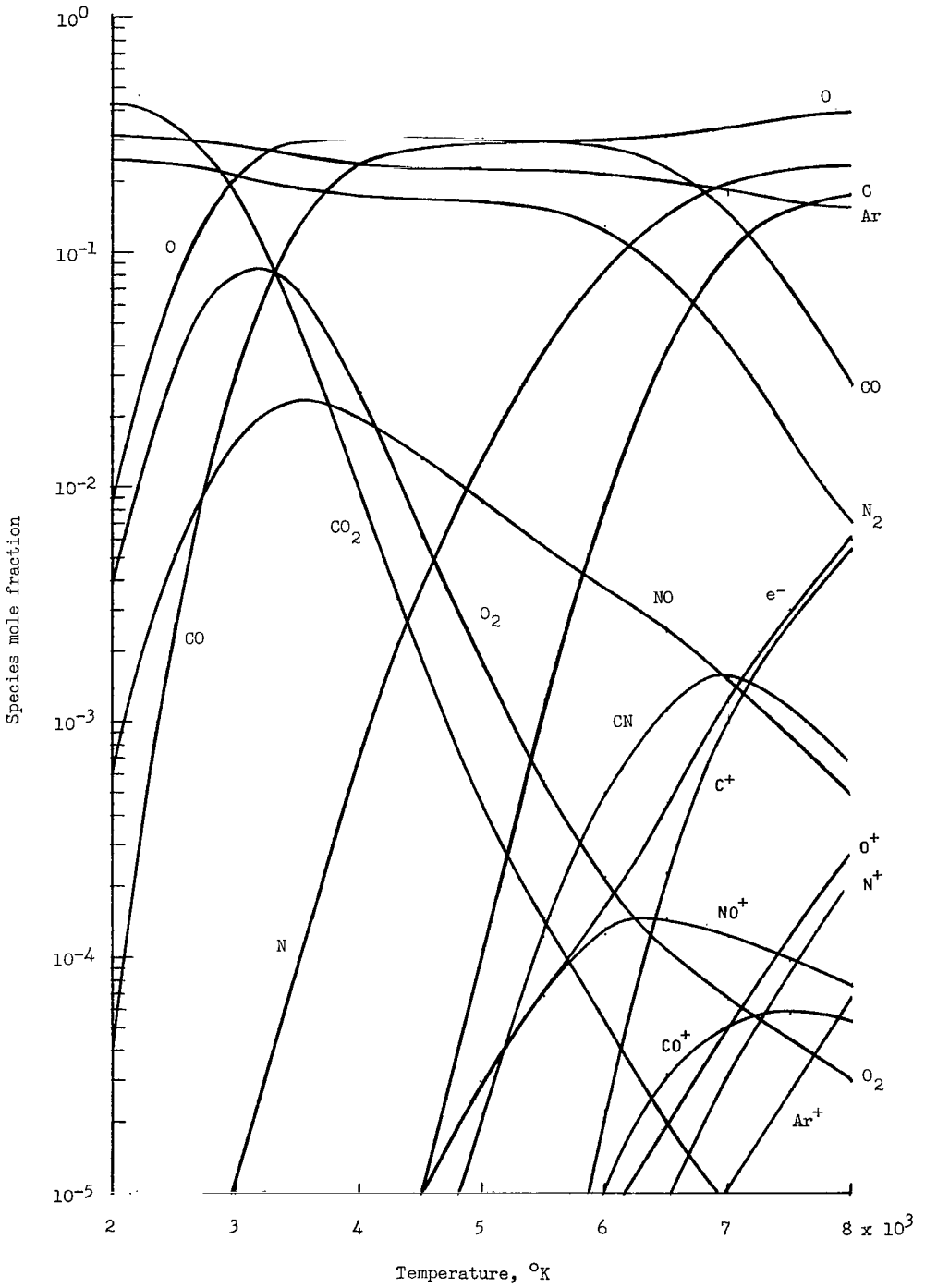

(d) p = 1 atm.

Figure 3.- Continued.

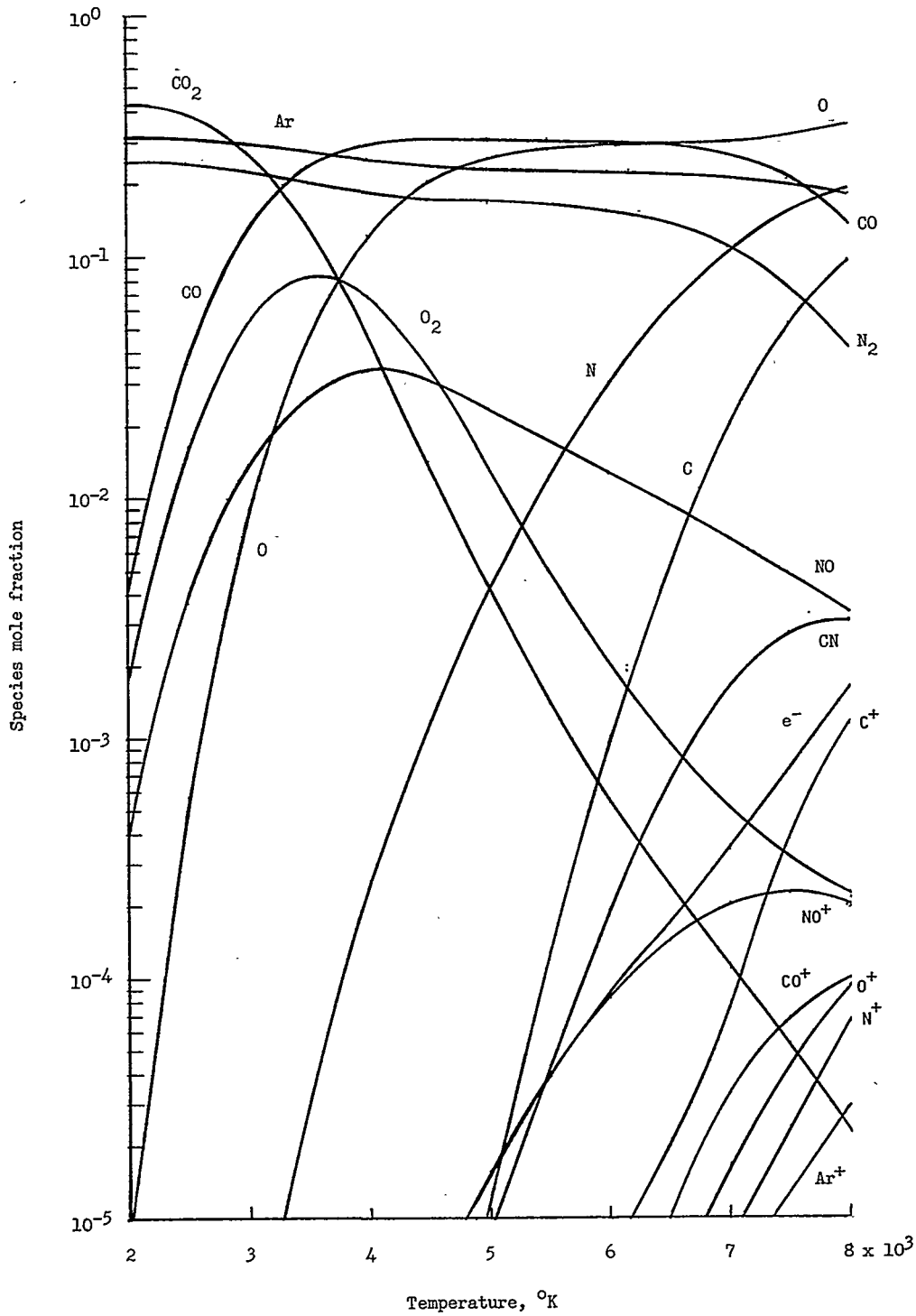

(e) p = 10 atm.

Figure 3.- Concluded.

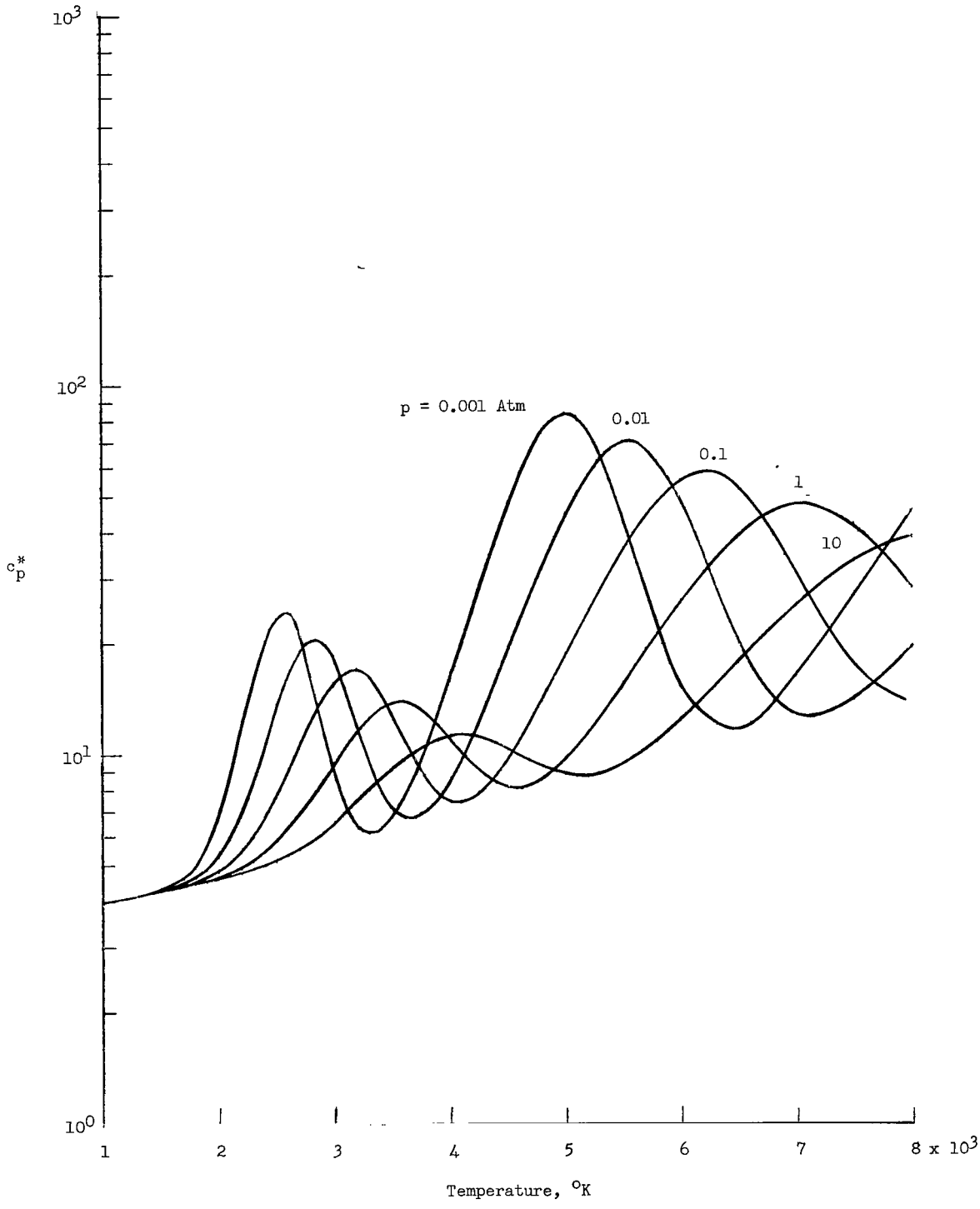

Figure 4.- Variation of nondimensional mixture specific heat of air with temperature.

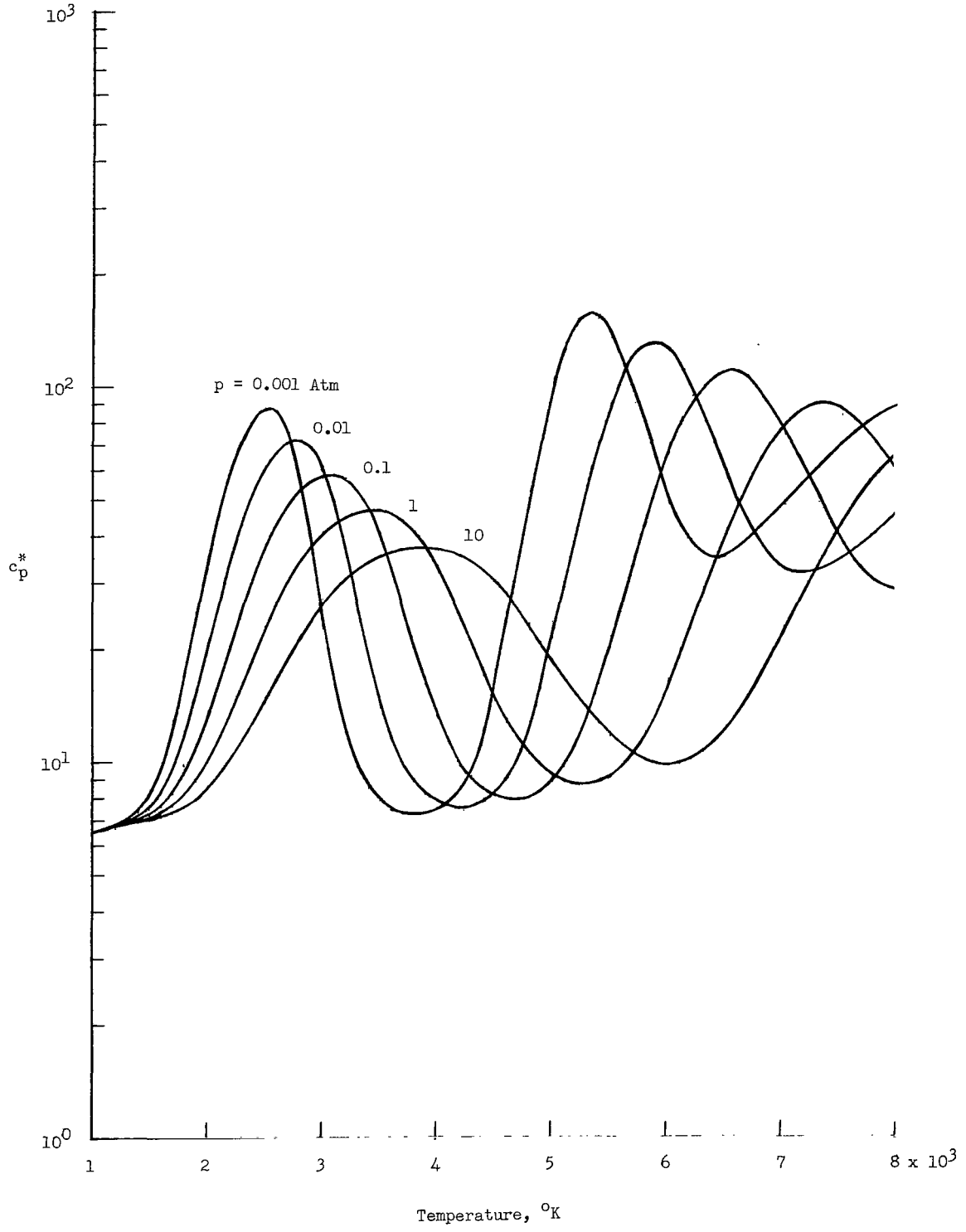

Figure 5.- Variation of nondimensional mixture specific heat of CO_2 with temperature.

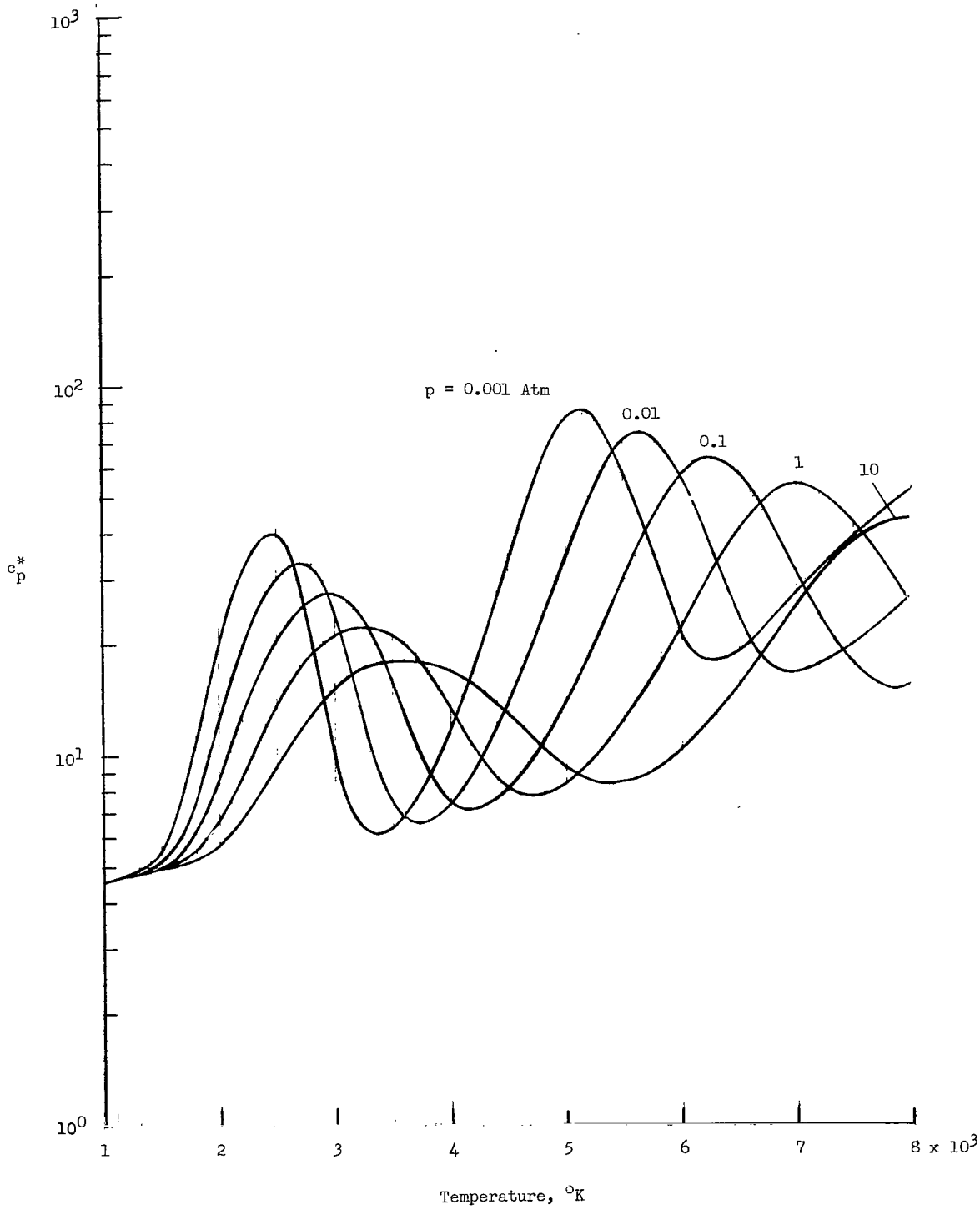

Figure 6.- Variation of nondimensional mixture specific heat of Mars model atmosphere with temperature.

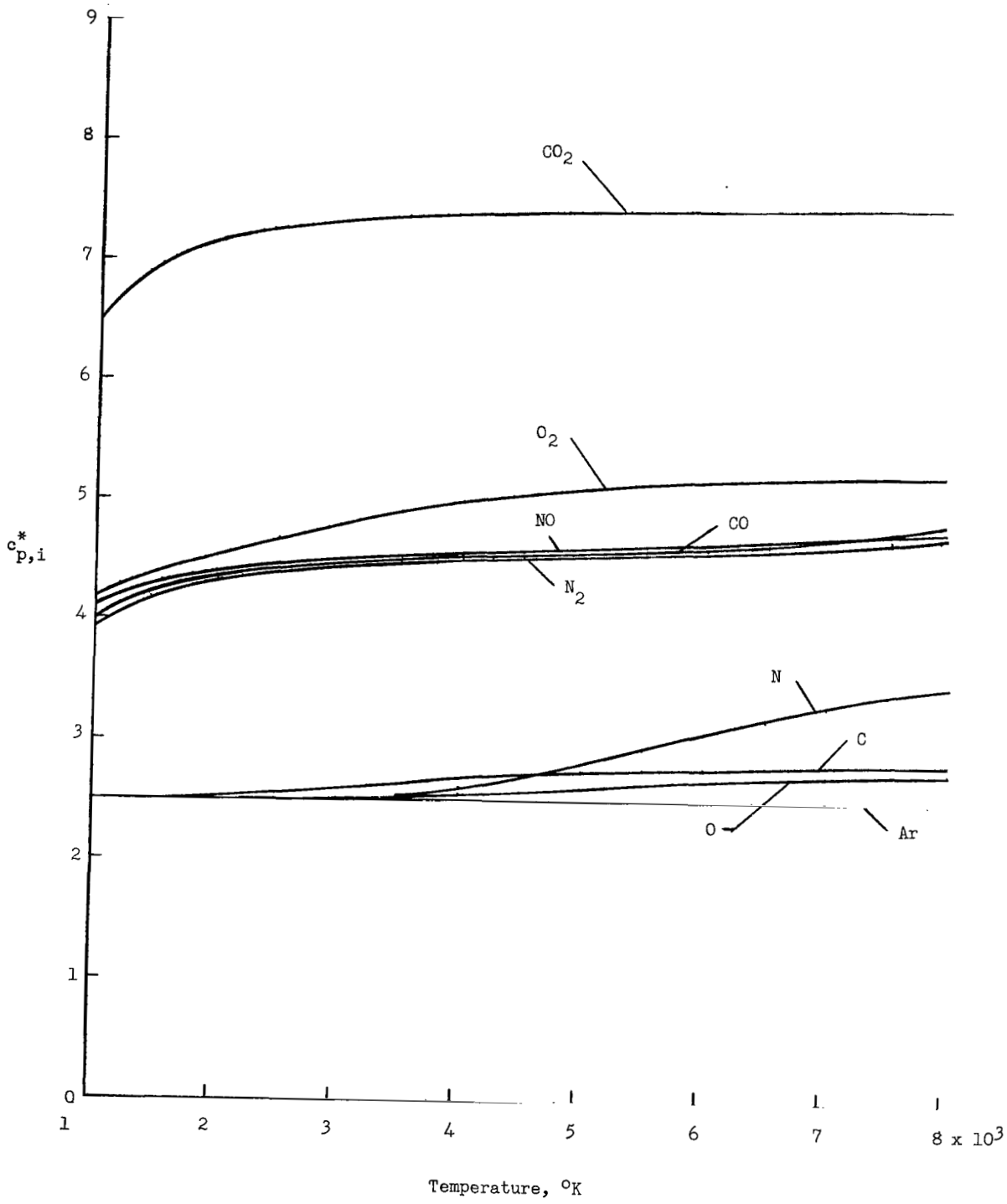

Figure 7.- Variation of nondimensional species specific heat with temperature.

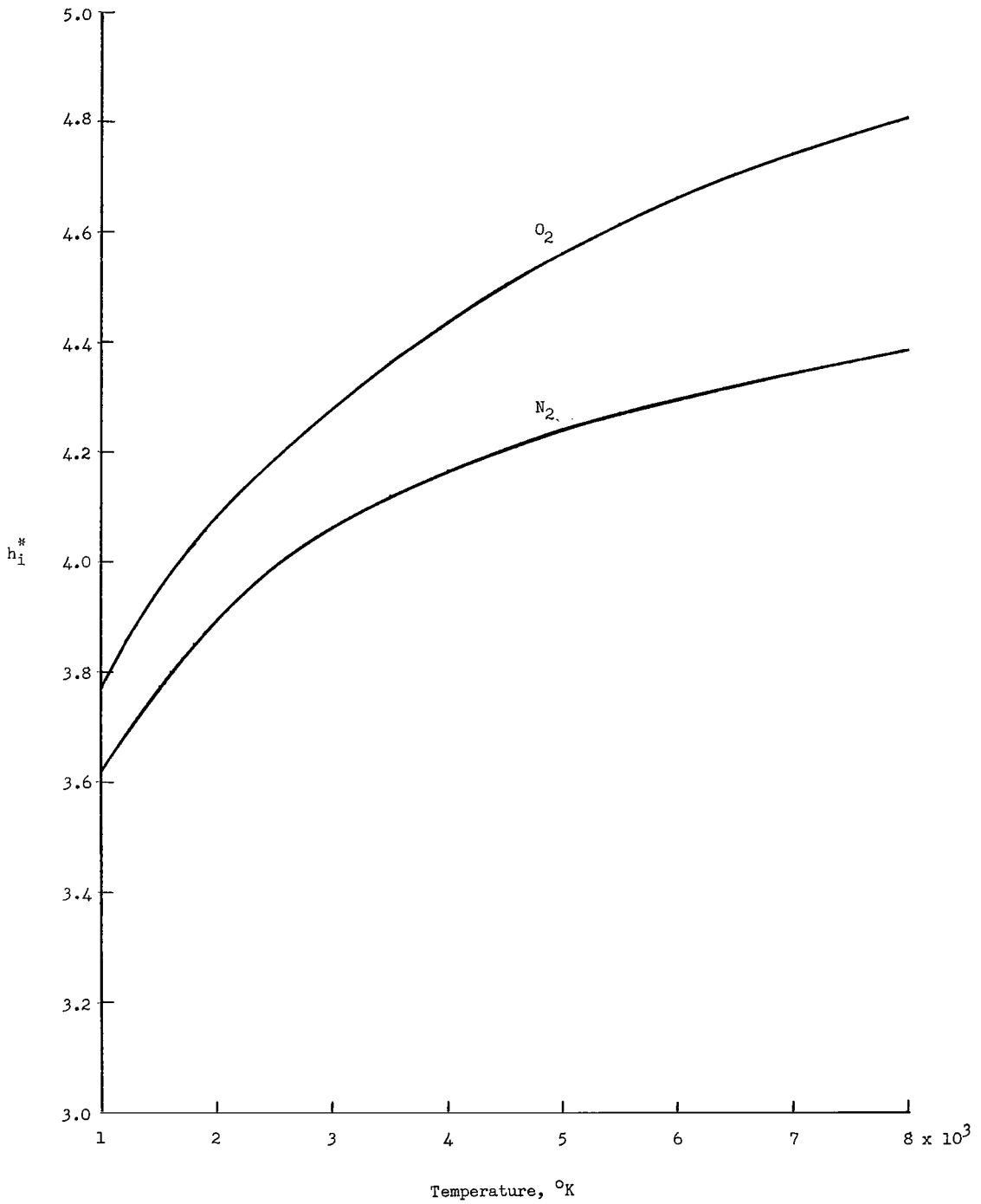

(a) O_2 and N_2.

Figure 8.- Variation of nondimensional species enthalpy with temperature.

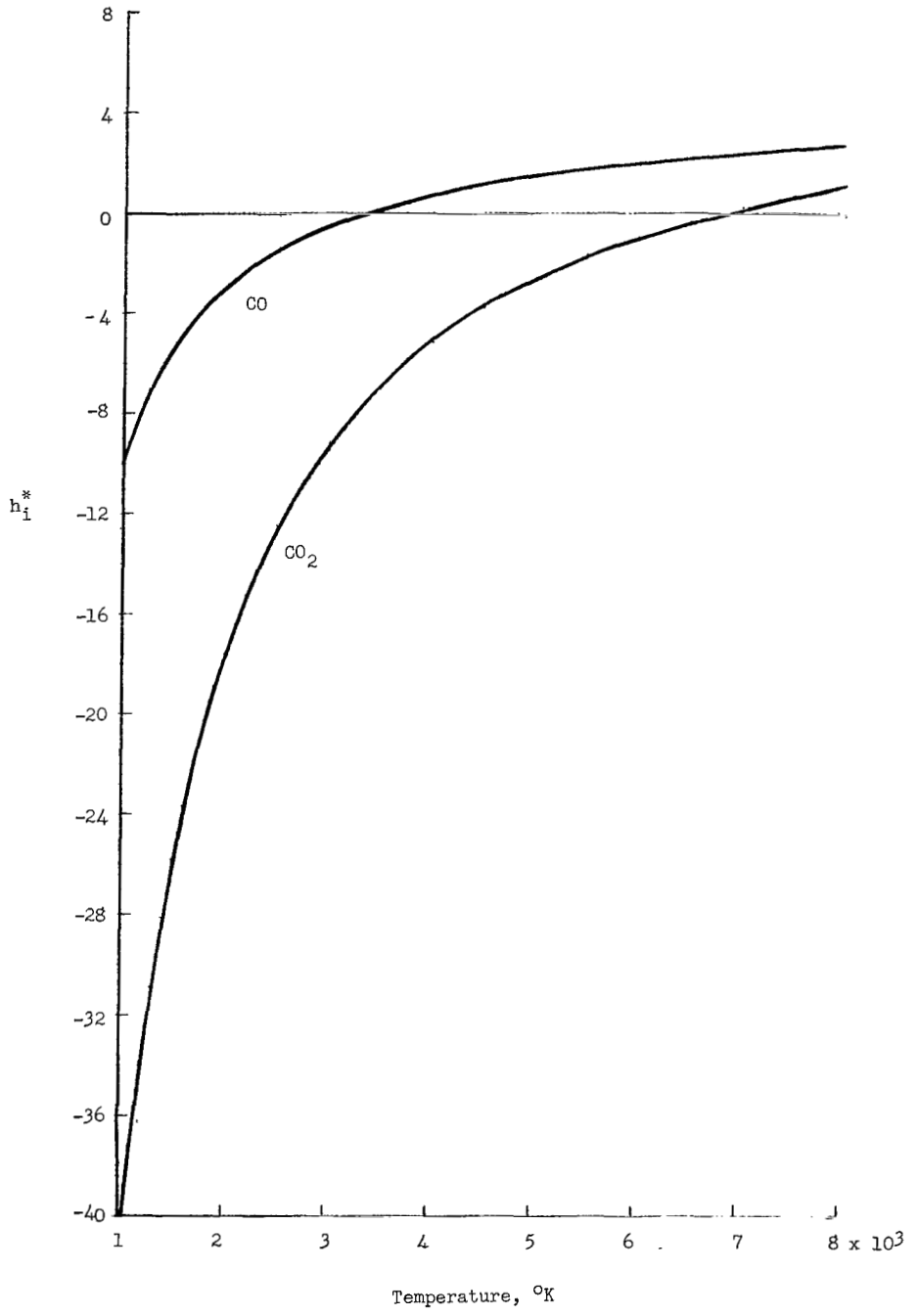

(b) CO and CO_2.

Figure 8.- Continued.

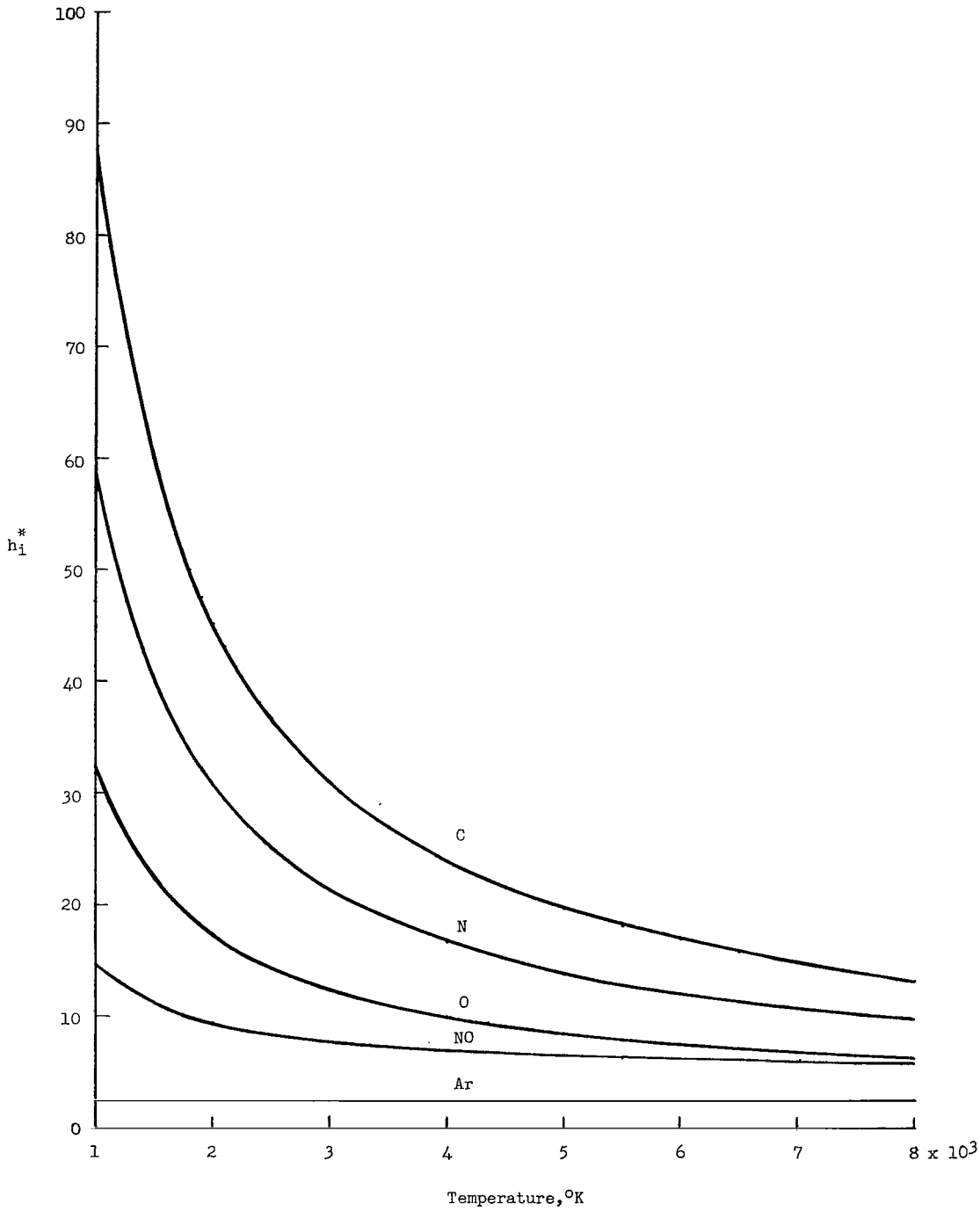

(c) C, N, O, NO, and Ar.

Figure 8.- Concluded.

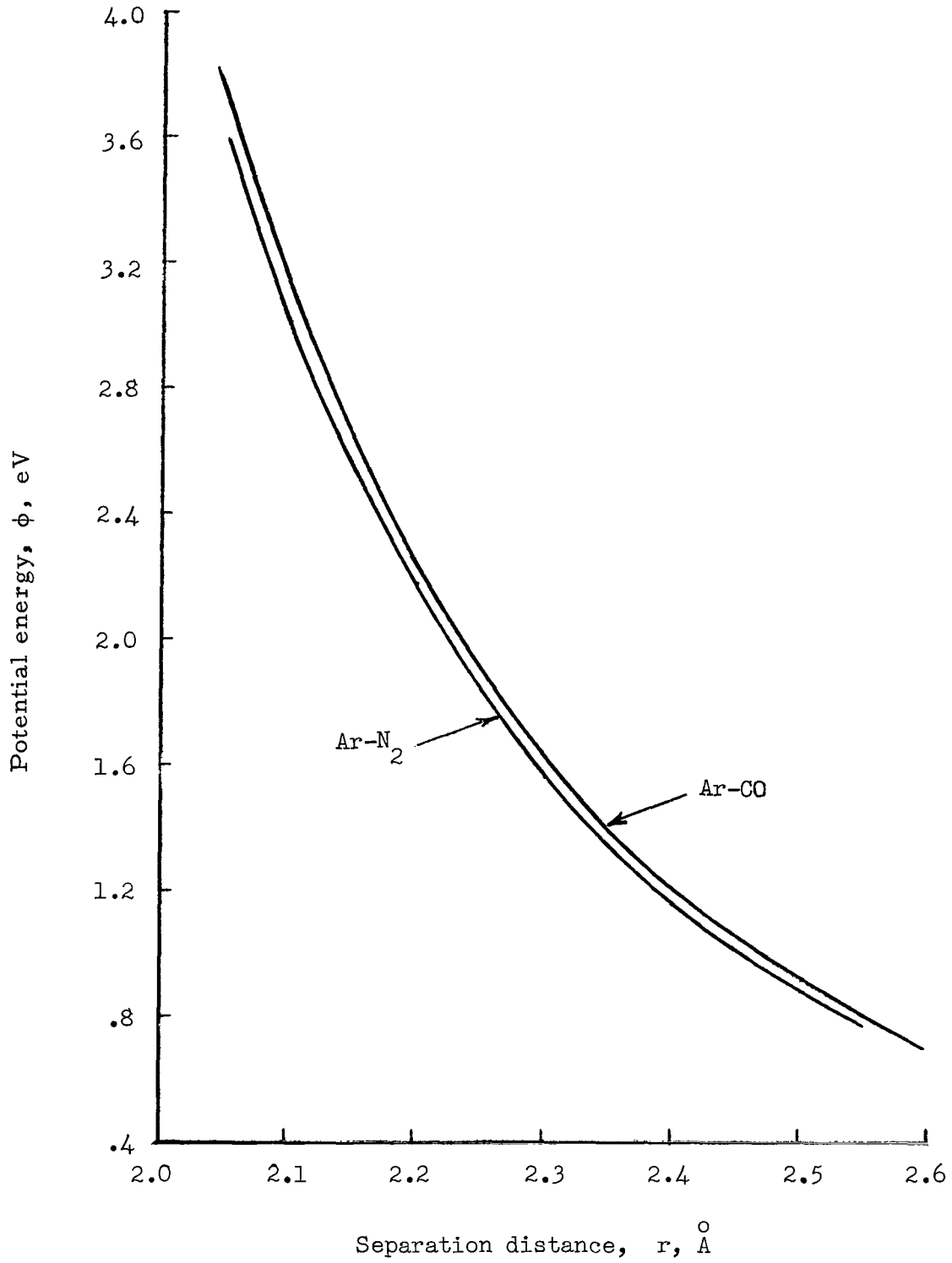

Figure 9.- Comparison of high-temperature potentials for Ar-N_2 and Ar-CO interactions.

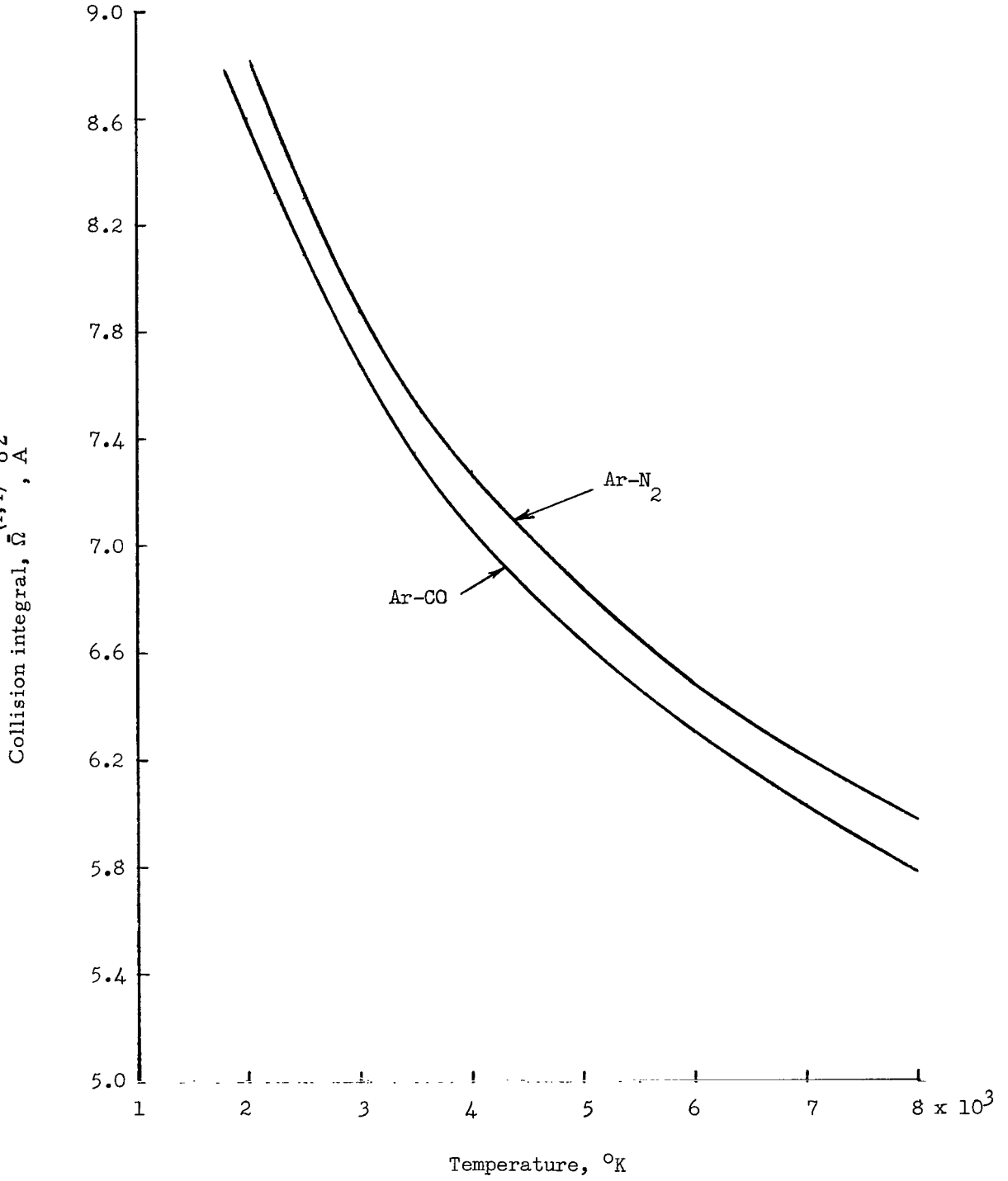

Figure 10.- Comparison of $\bar{\Omega}^{(1,1)}$ computed from high-temperature Ar-N_2 and Ar-CO potentials.

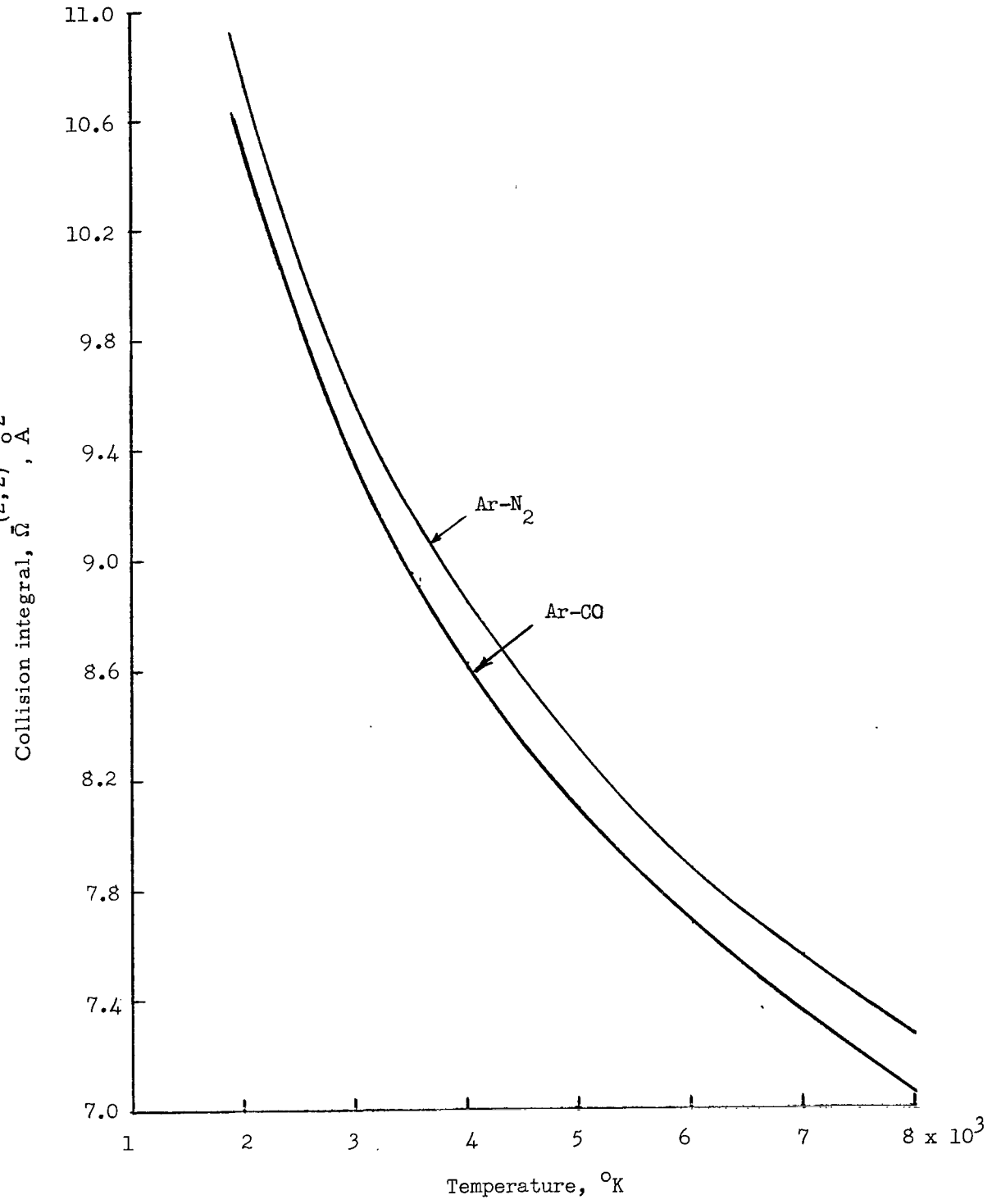

Figure 11.- Comparison of $\bar{\Omega}^{(2,2)}$ computed from high-temperature Ar-N_2 and Ar-CO potentials.

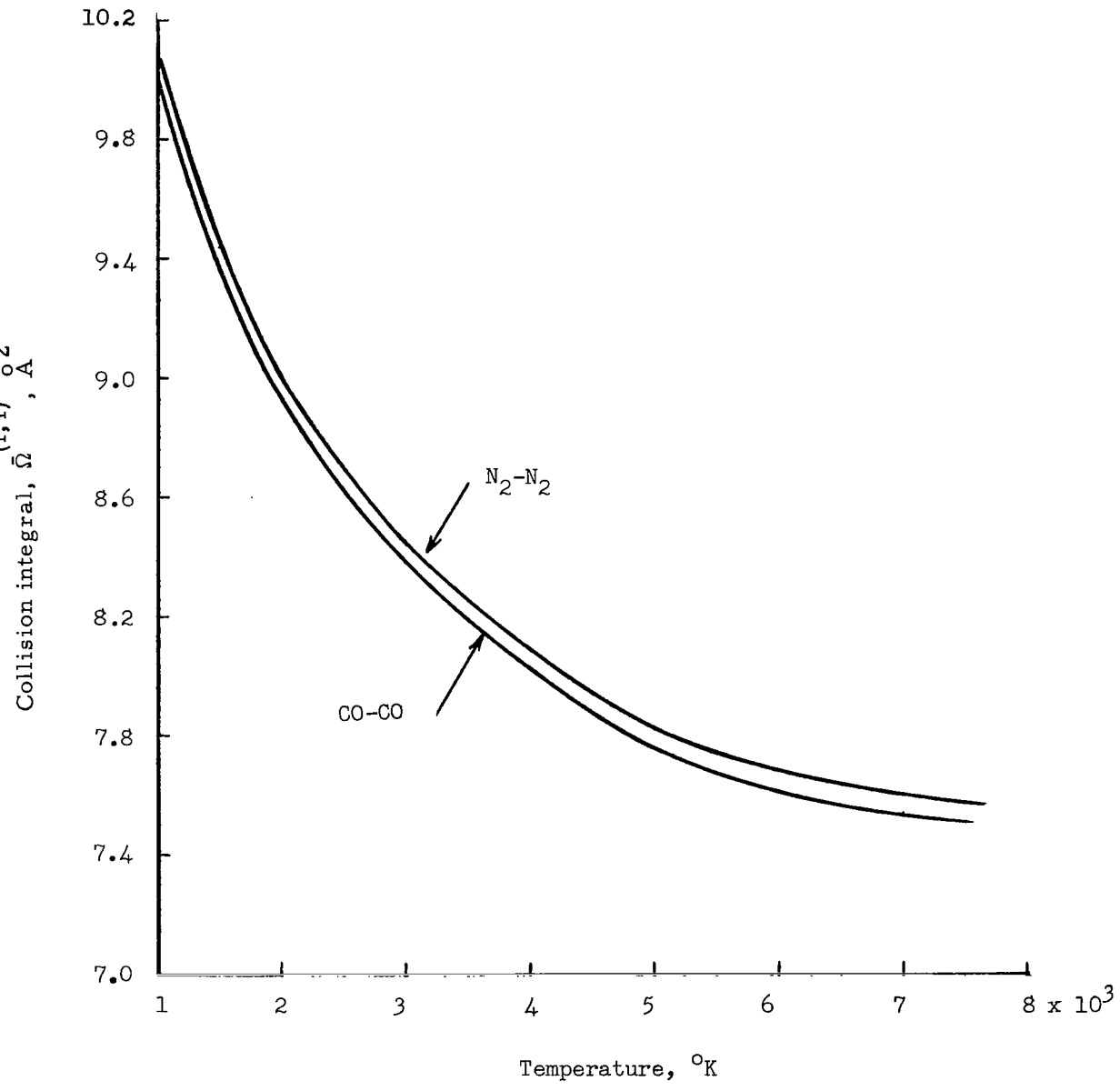

Figure 12.- Comparison of $\bar{\Omega}^{(1,1)}$ computed from low-temperature CO-CO and N_2-N_2 potentials.

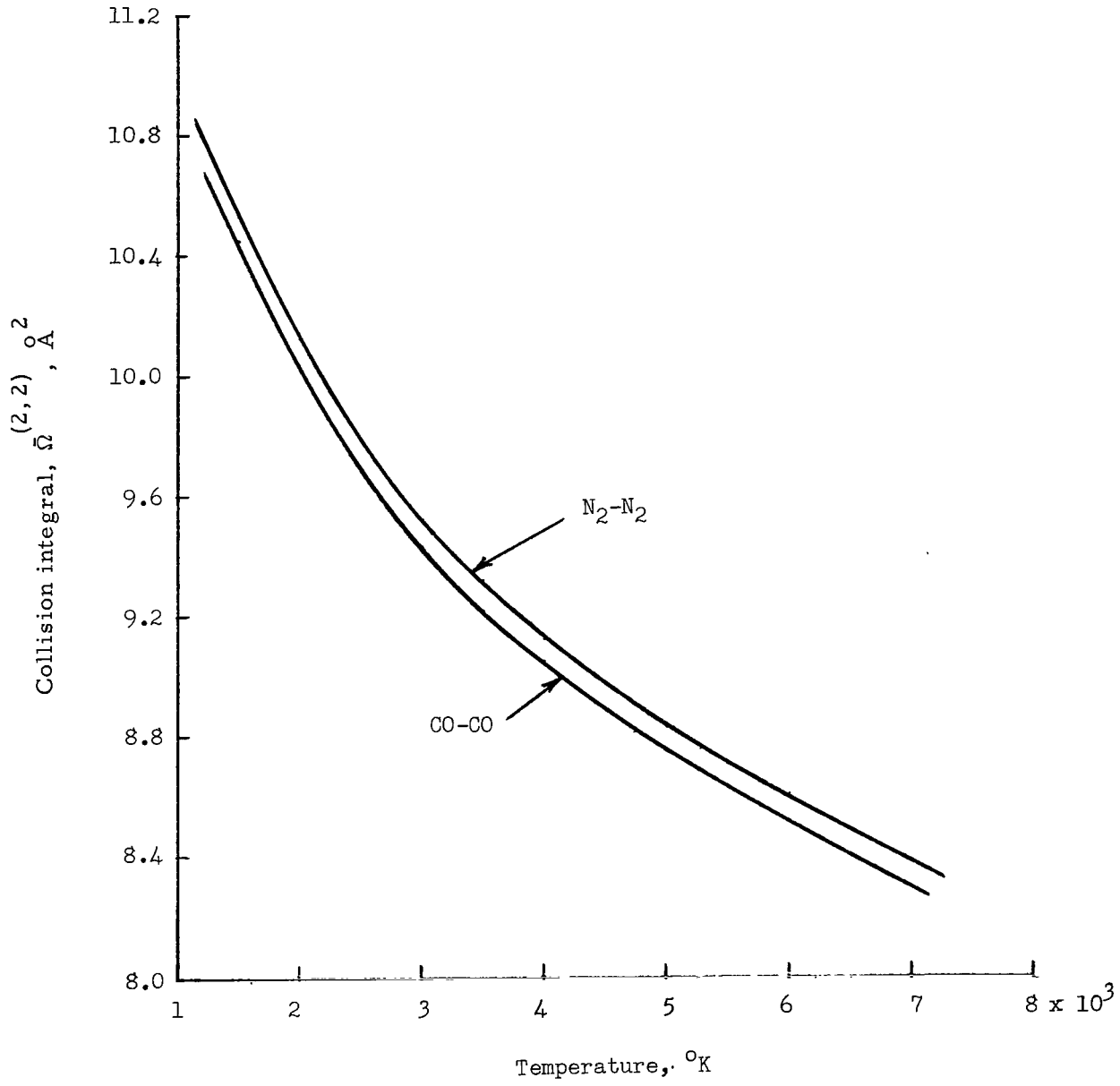

Figure 13.- Comparison of $\bar{\Omega}^{(2,2)}$ computed from low-temperature CO-CO and N_2-N_2 potentials.

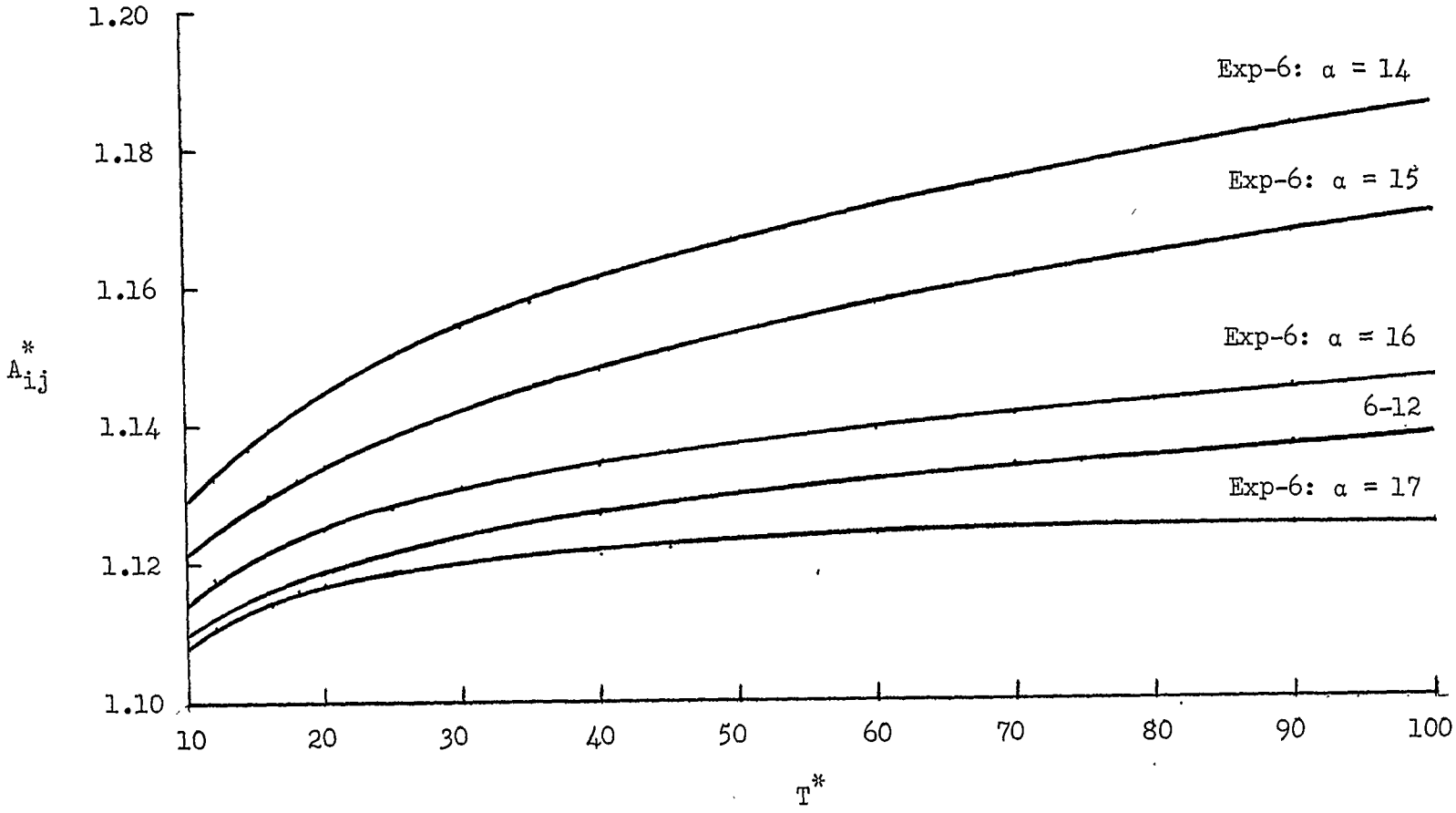

Figure 14.- Collision integral ratio A^*_{ij} for Lennard-Jones 6-12 and modified Buckingham exp-6 potentials.

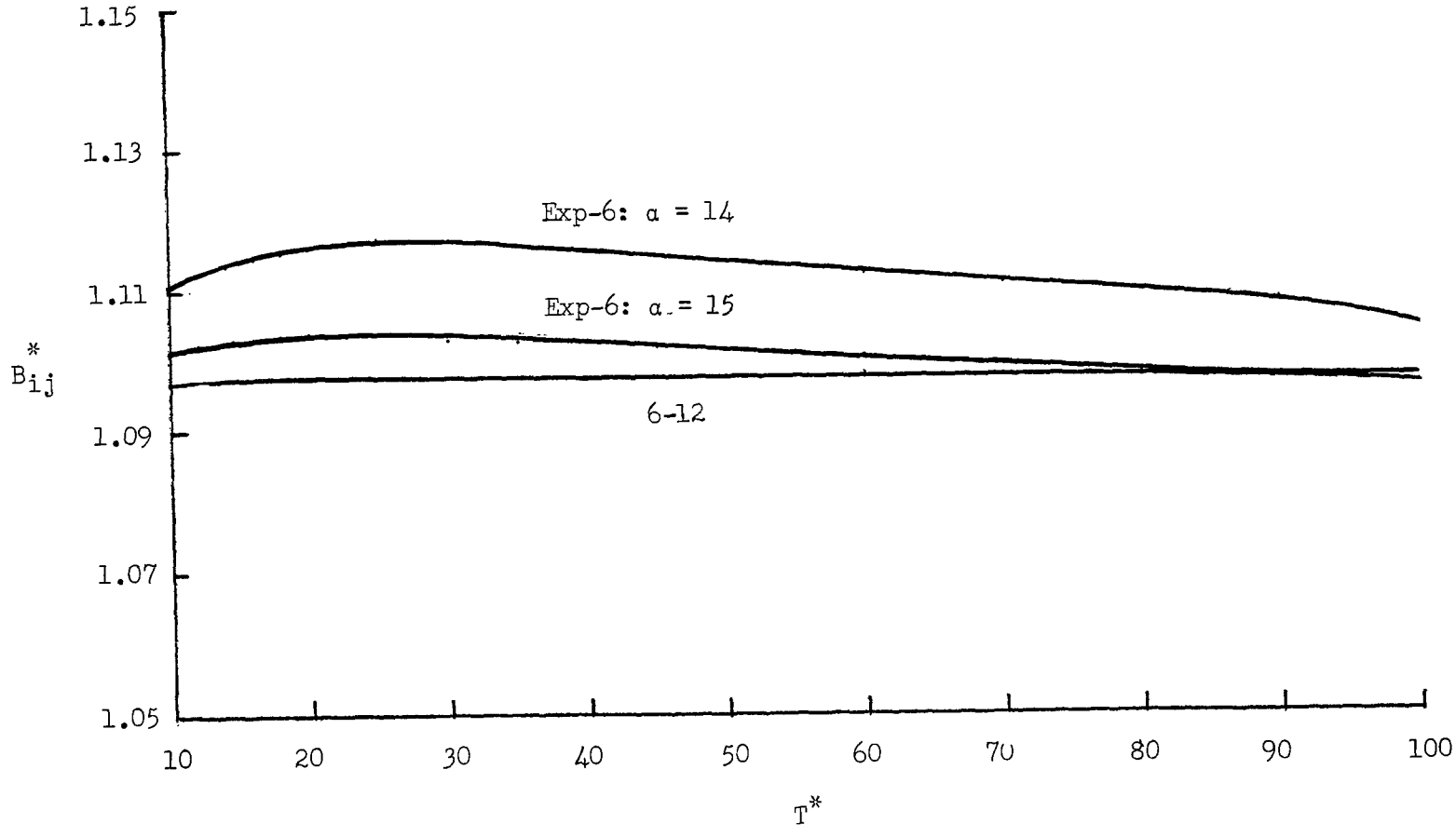

Figure 15.- Collision integral ratio B^*_{ij} for Lennard-Jones 6-12 and modified Buckingham exp-6 potentials.

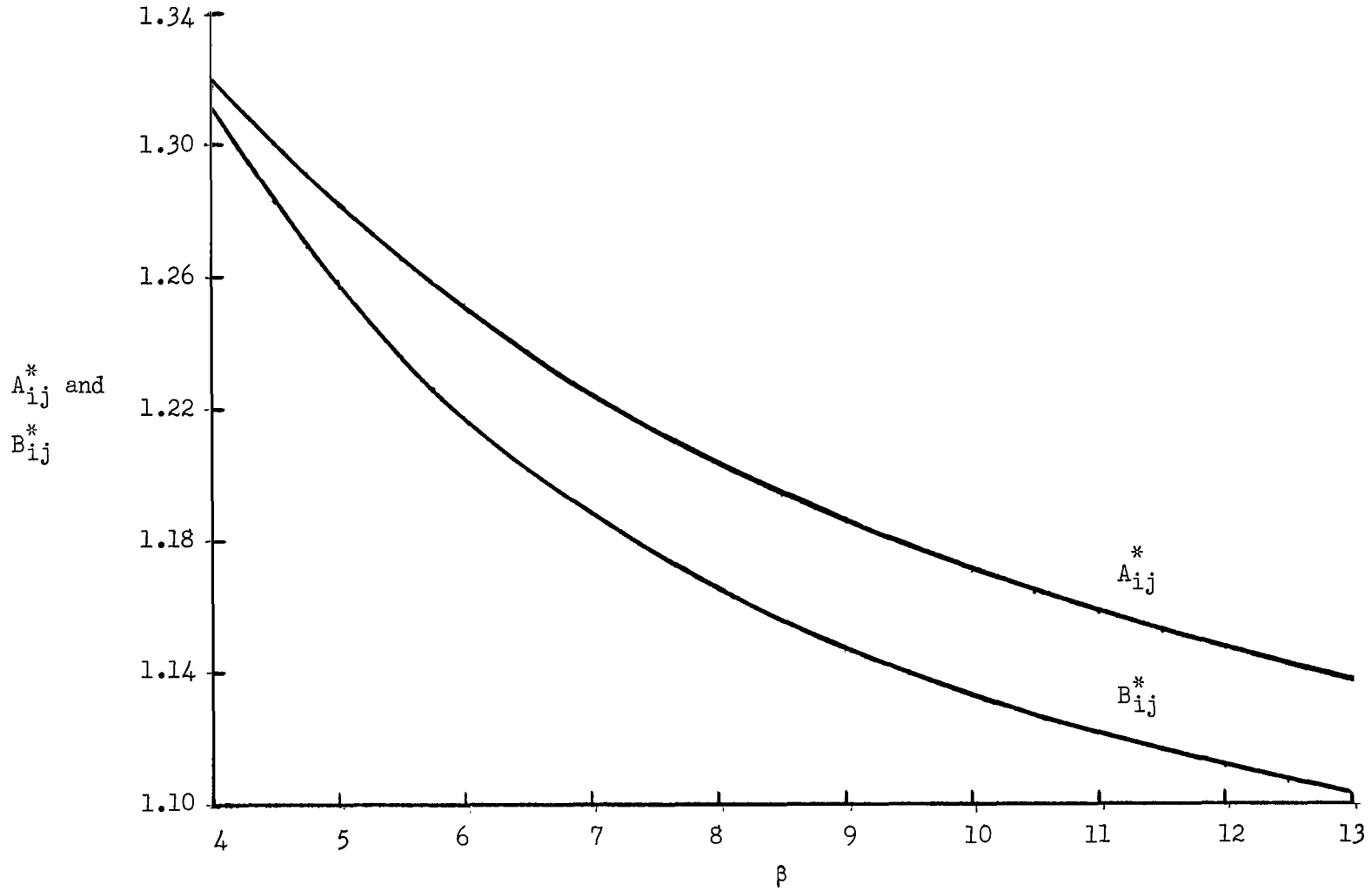

Figure 16.- Collision integral ratios for the exponential repulsive potential.

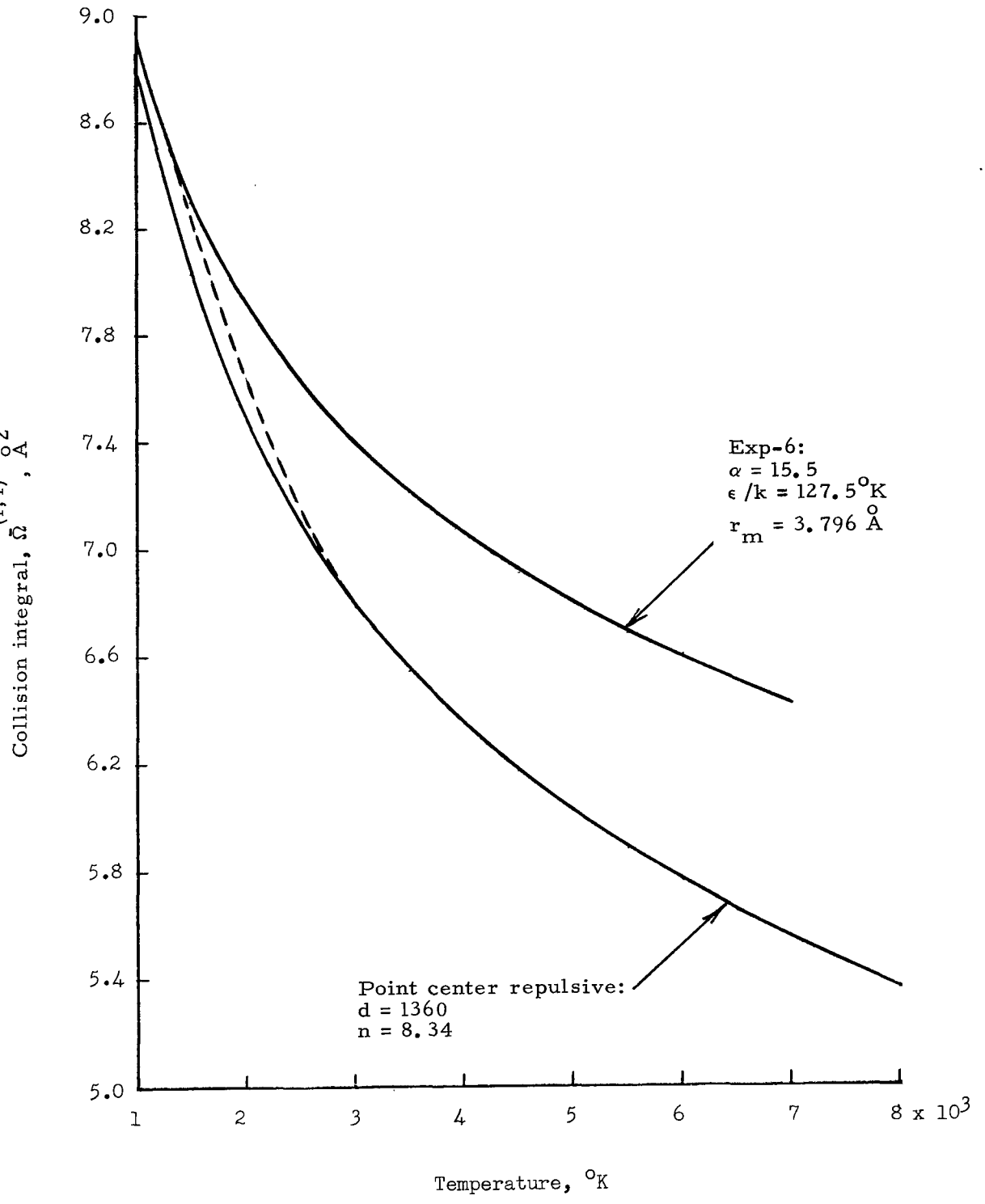

Figure 17.- Illustration of graphical method of finding $\bar{\Omega}^{(1,1)}$ for Ar-O_2 interaction.

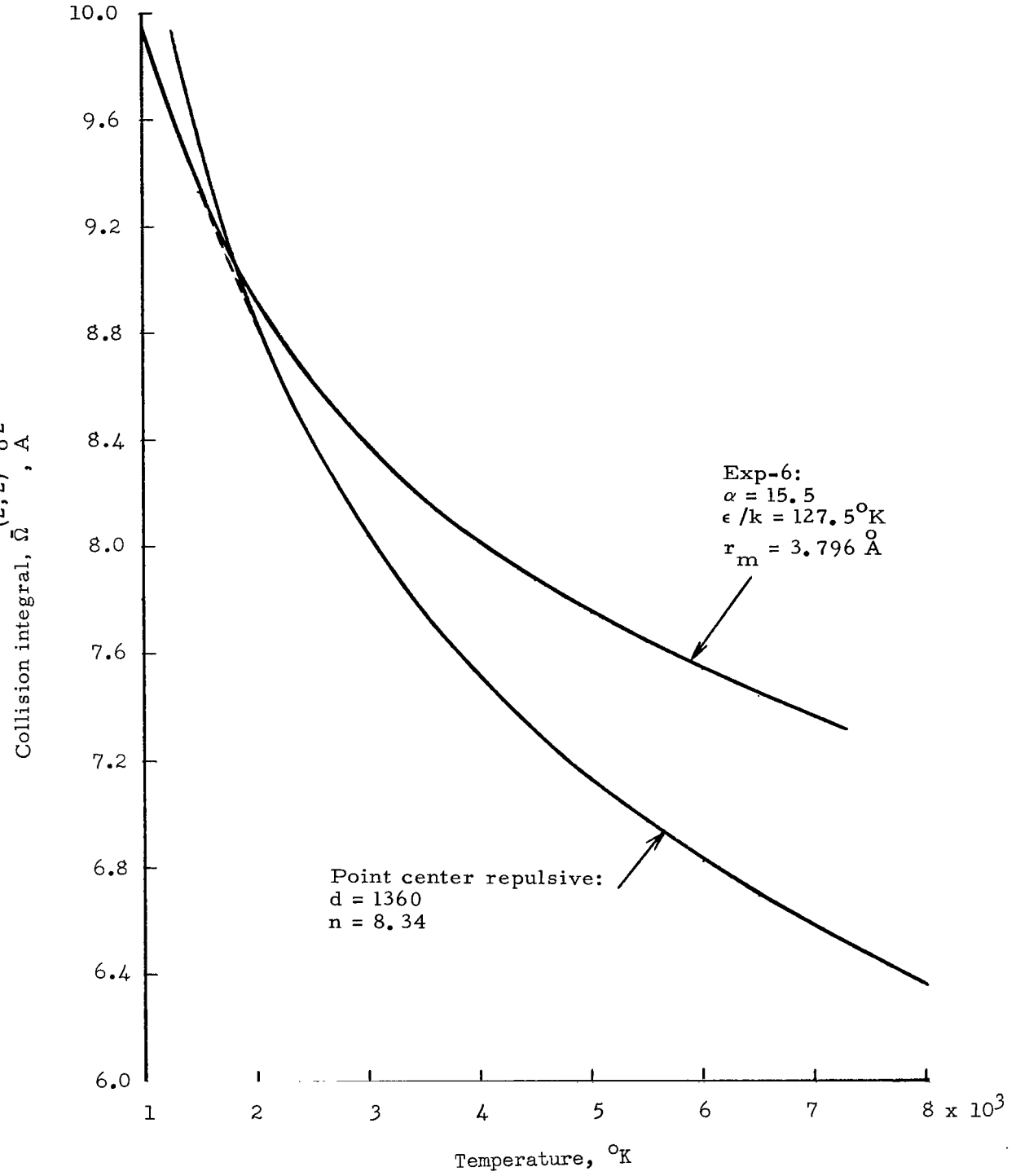

Figure 18.- Illustration of graphical method of finding $\bar{\Omega}^{(2,2)}$ for Ar-O_2 interaction.

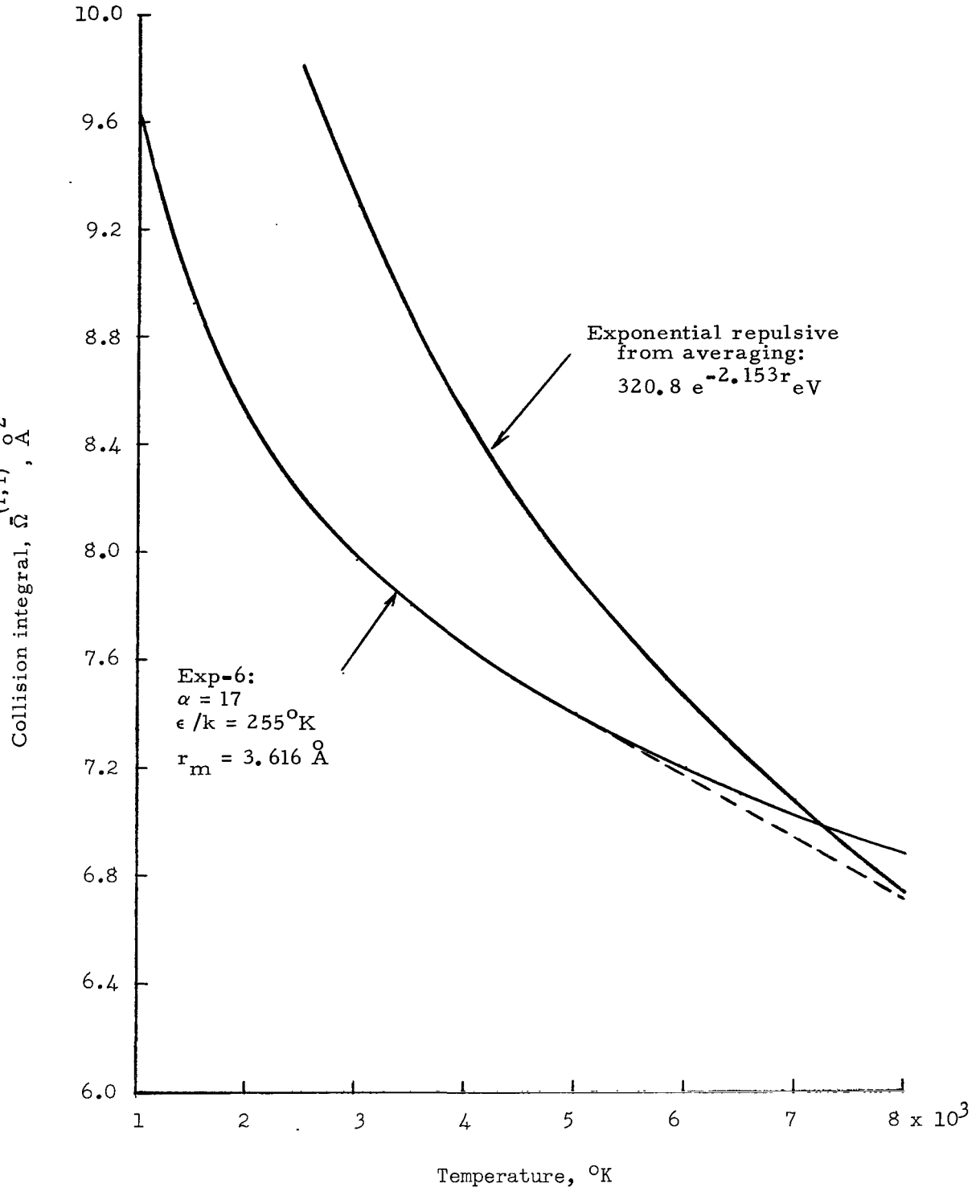

Figure 19.- Illustration of graphical method of finding $\bar{\Omega}^{(1,1)}$ for CO_2-O_2 interaction.

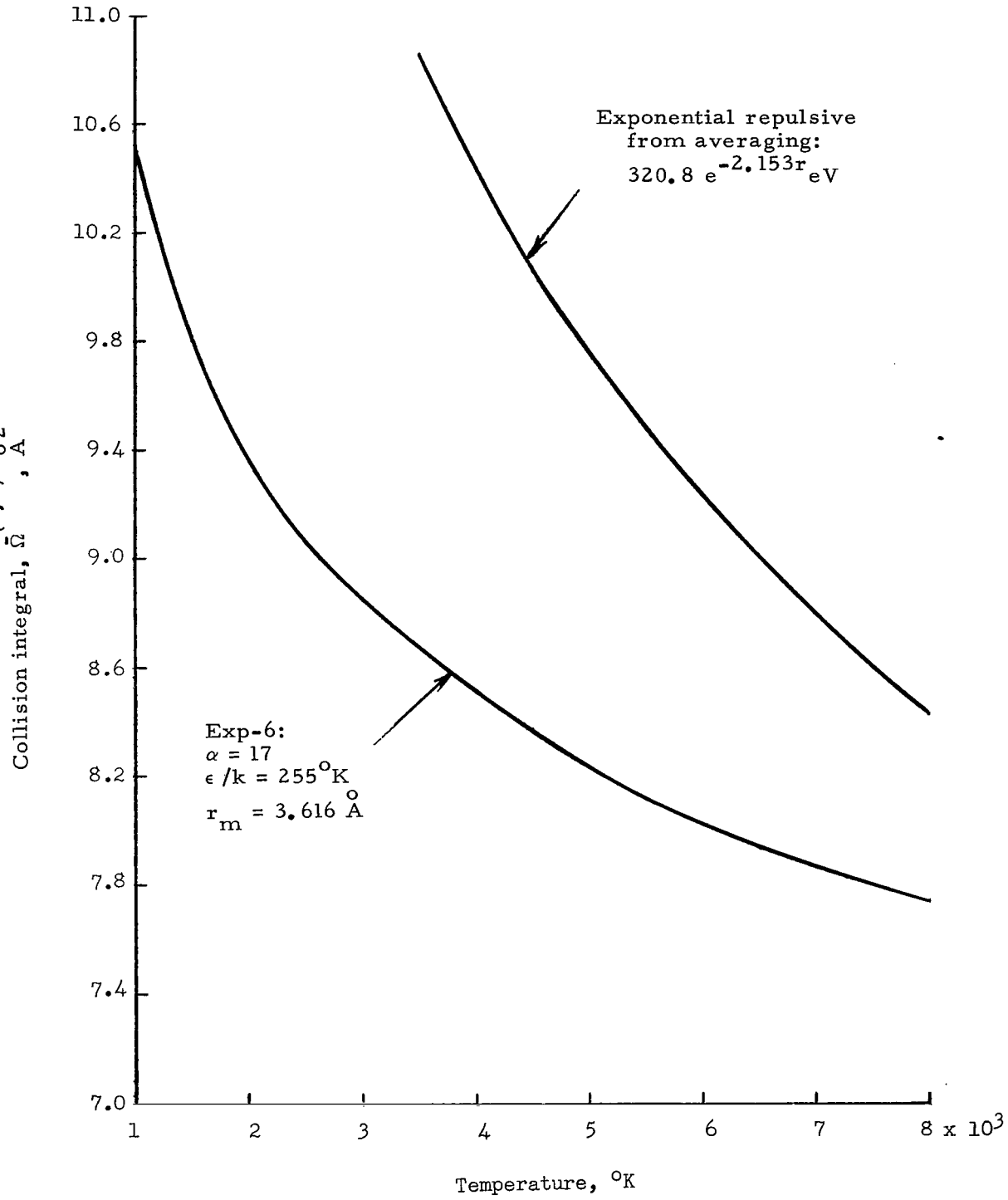

Figure 20.- Illustration of graphical method of finding $\bar{\Omega}^{(2,2)}$ for CO_2-O_2 interaction.

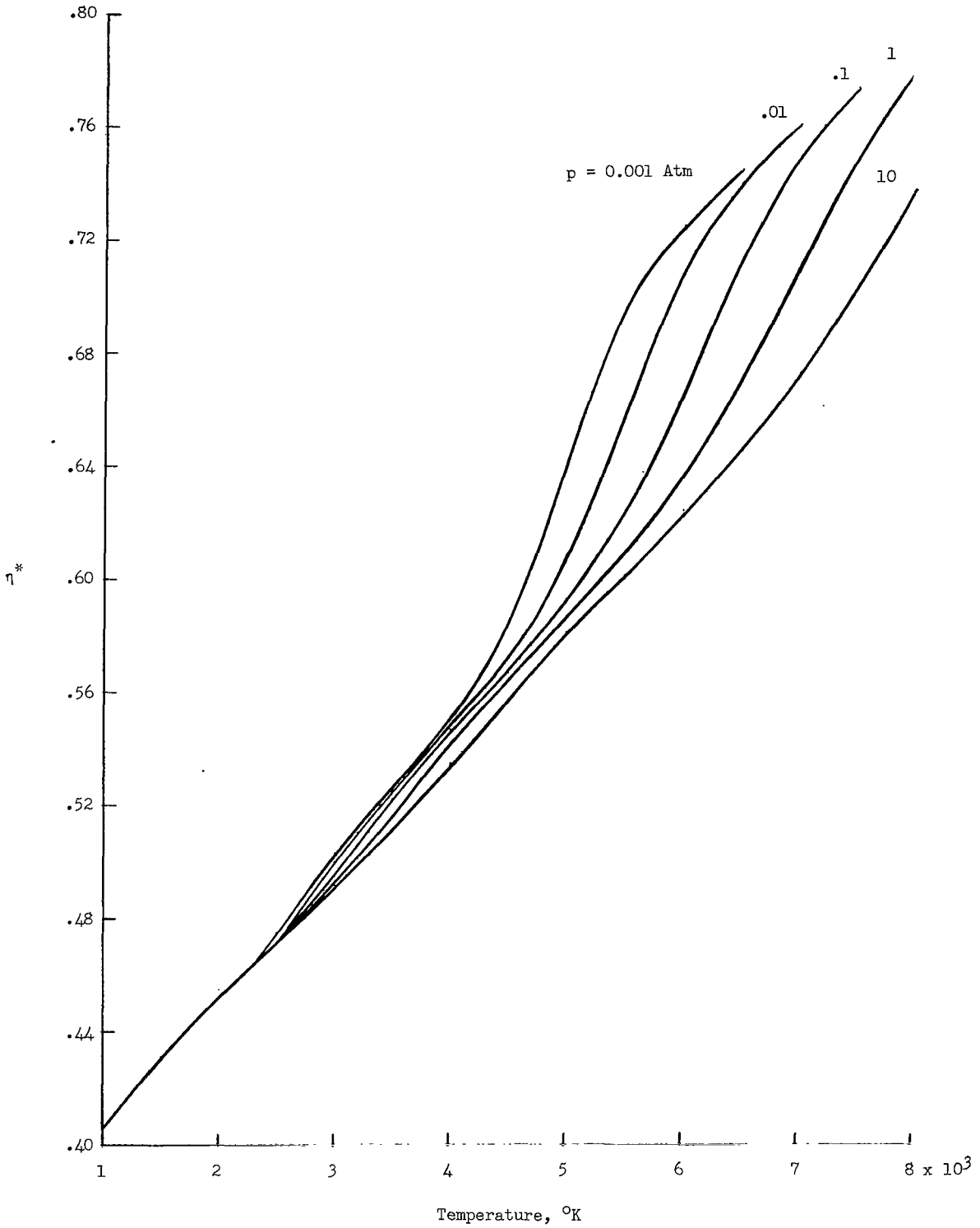

Figure 21.- Variation of nondimensional viscosity of air with temperature.

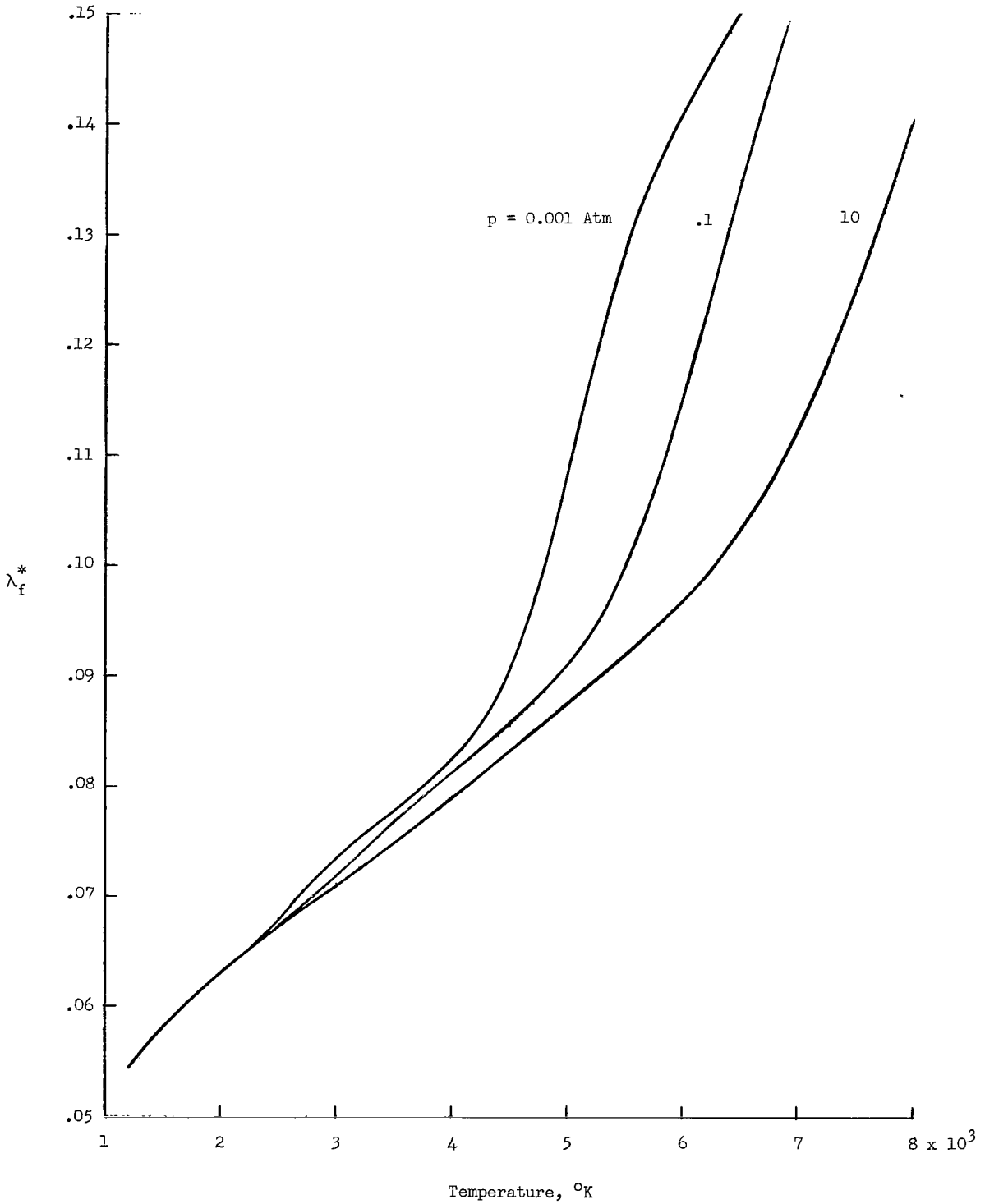

Figure 22.- Variation of nondimensional frozen conductivity of air with temperature.

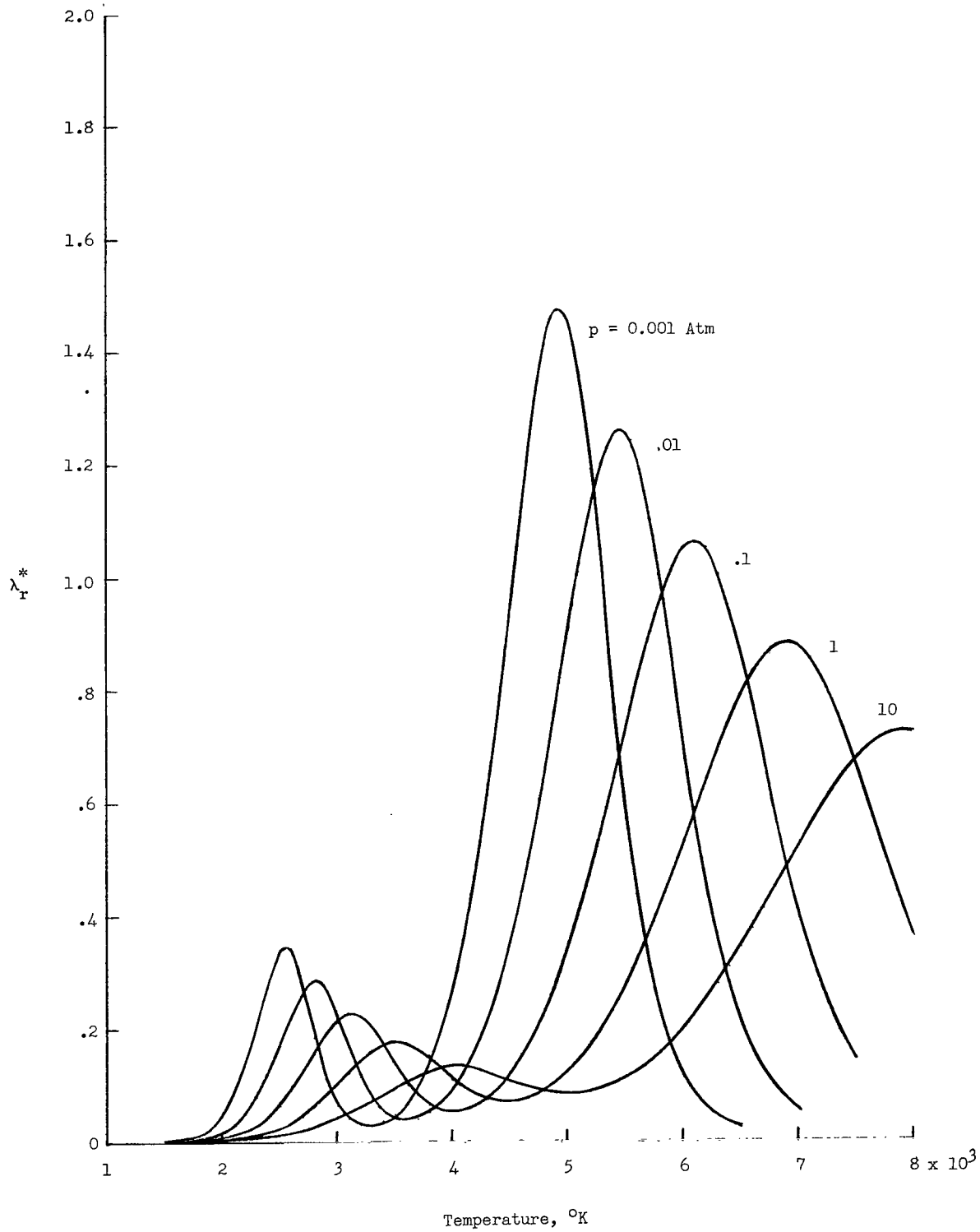

Figure 23.- Variation of nondimensional reactive conductivity of air with temperature.

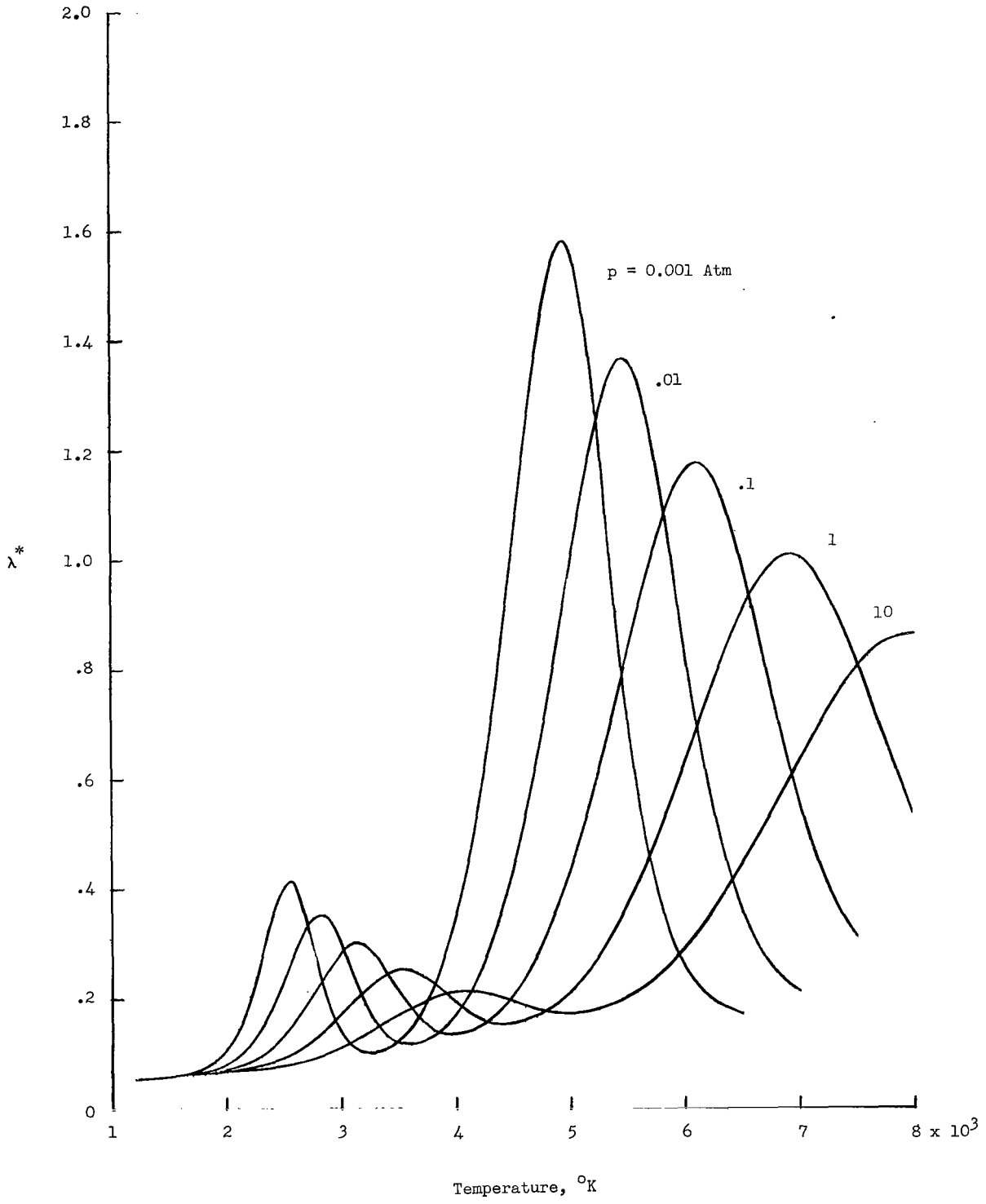

Figure 24.- Variation of nondimensional total conductivity of air with temperature.

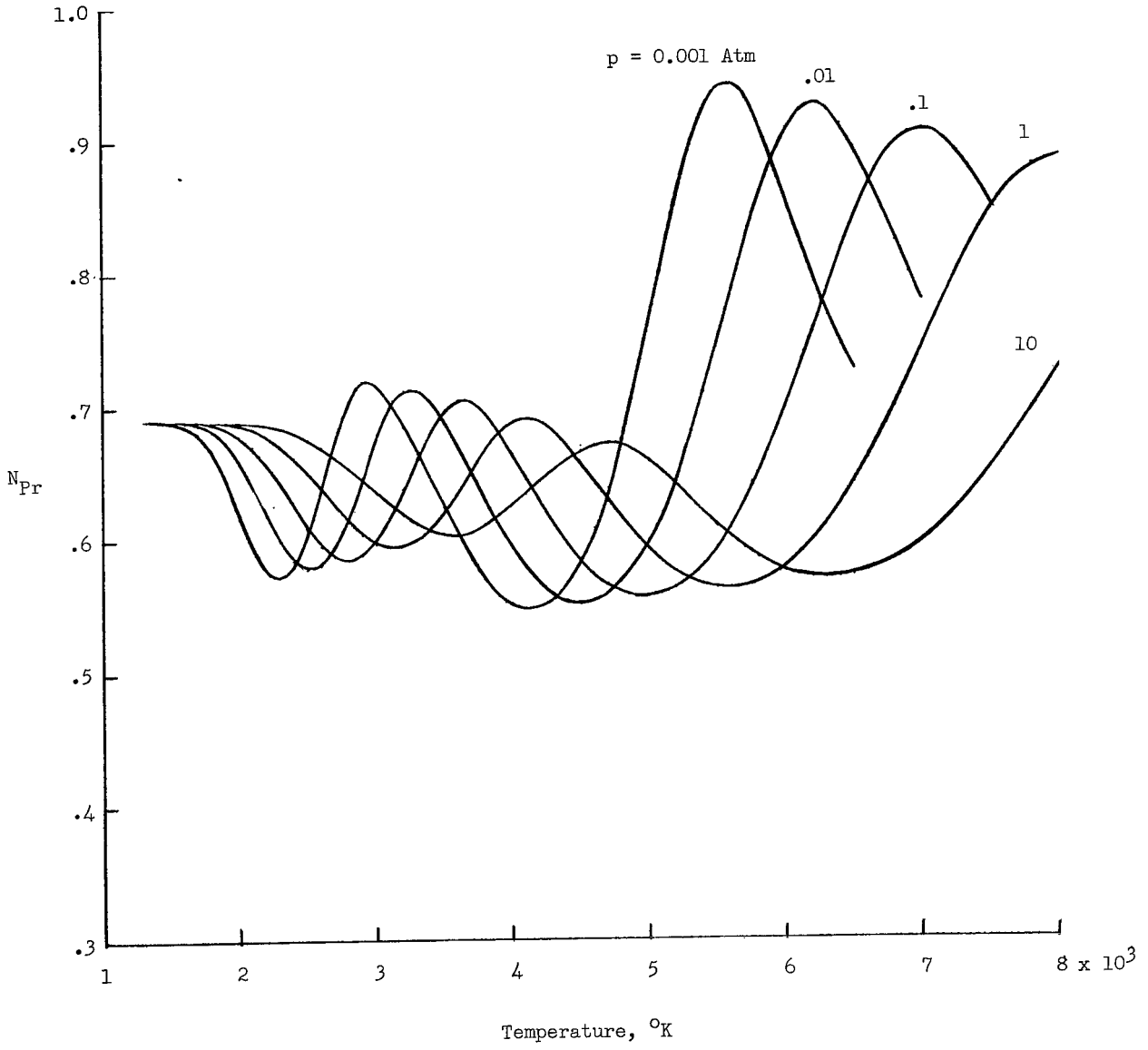

Figure 25.- Variation of Prandtl number of air with temperature.

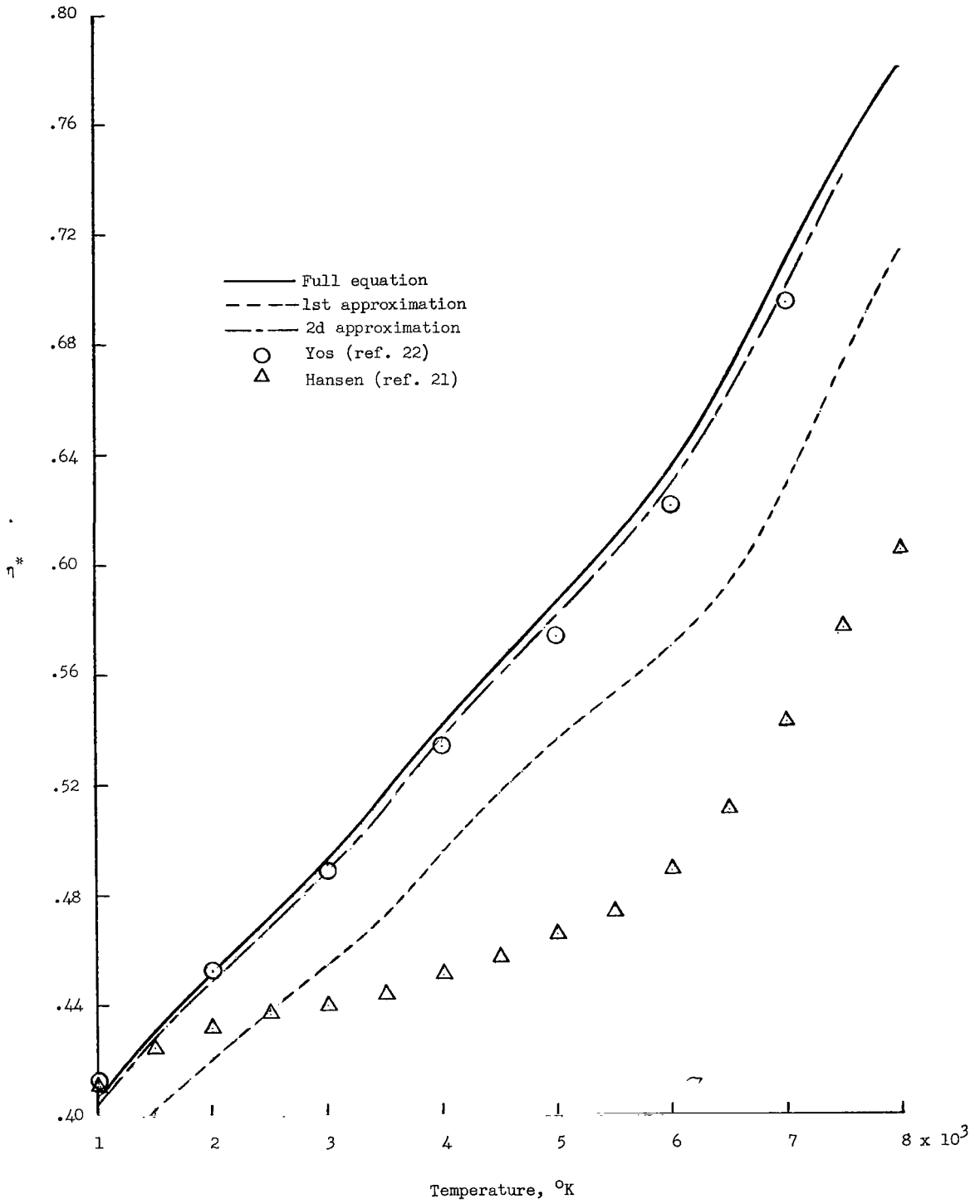

Figure 26.- Comparison of full-equation calculation of nondimensional viscosity of air with approximate calculations and previous results for p = 1 atm.

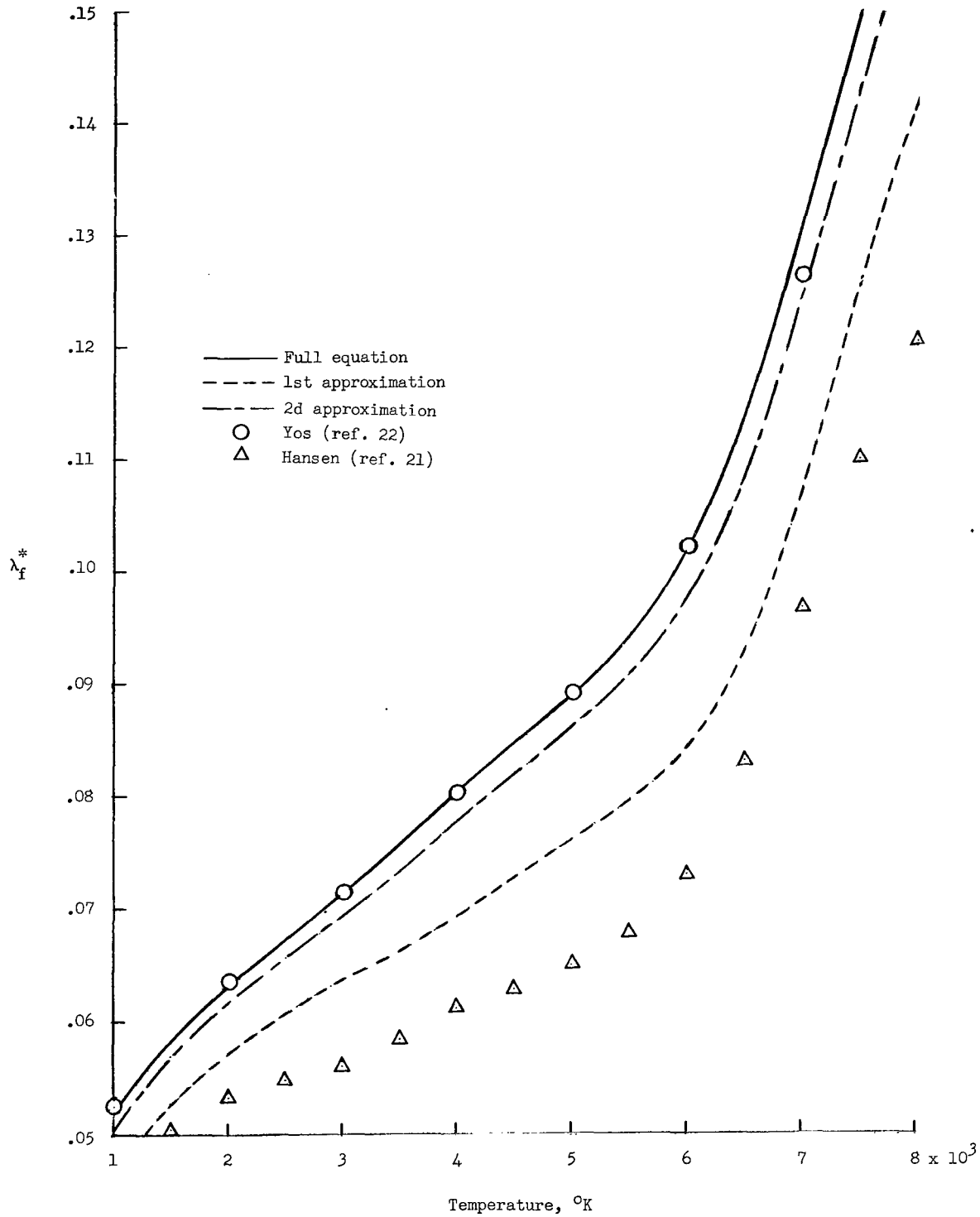

Figure 27.- Comparison of full-equation calculation of nondimensional frozen conductivity of air with approximate calculations and previous results for p = 1 atm.

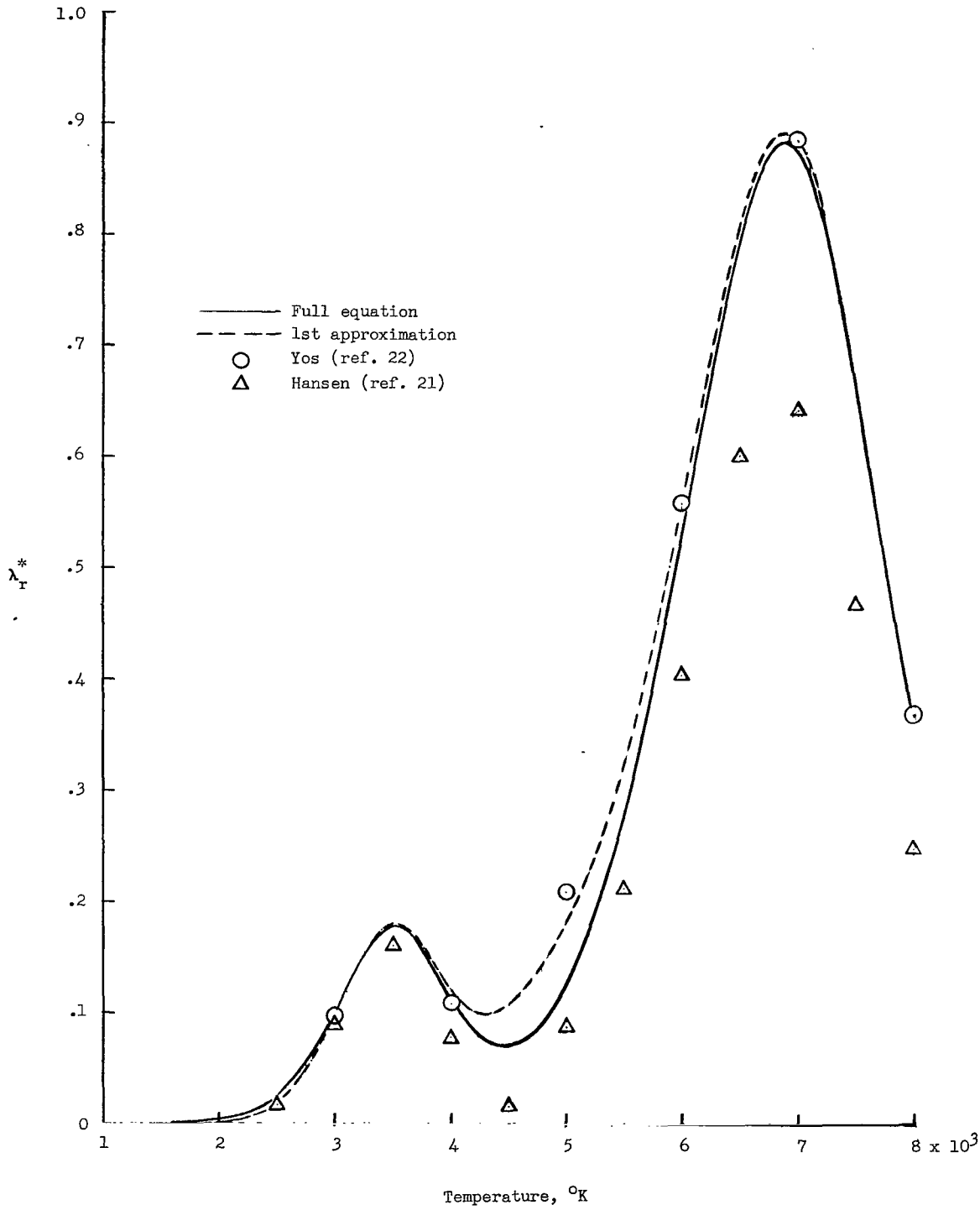

Figure 28.- Comparison of full-equation calculation of nondimensional reactive conductivity of air with approximate calculations and previous results for p = 1 atm.

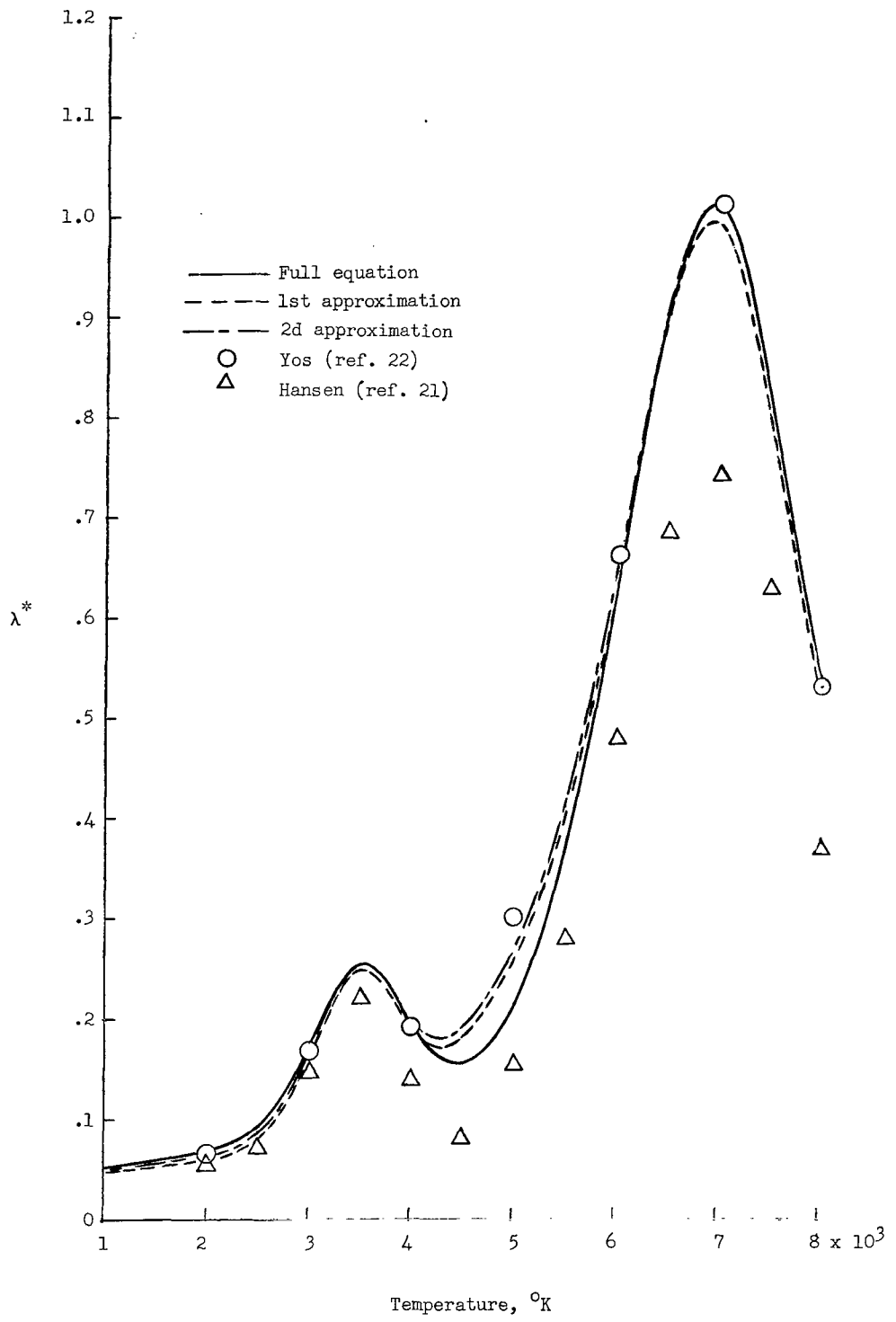

Figure 29.- Comparison of full-equation calculation of nondimensional total conductivity of air with approximate calculations and previous results for p = 1 atm.

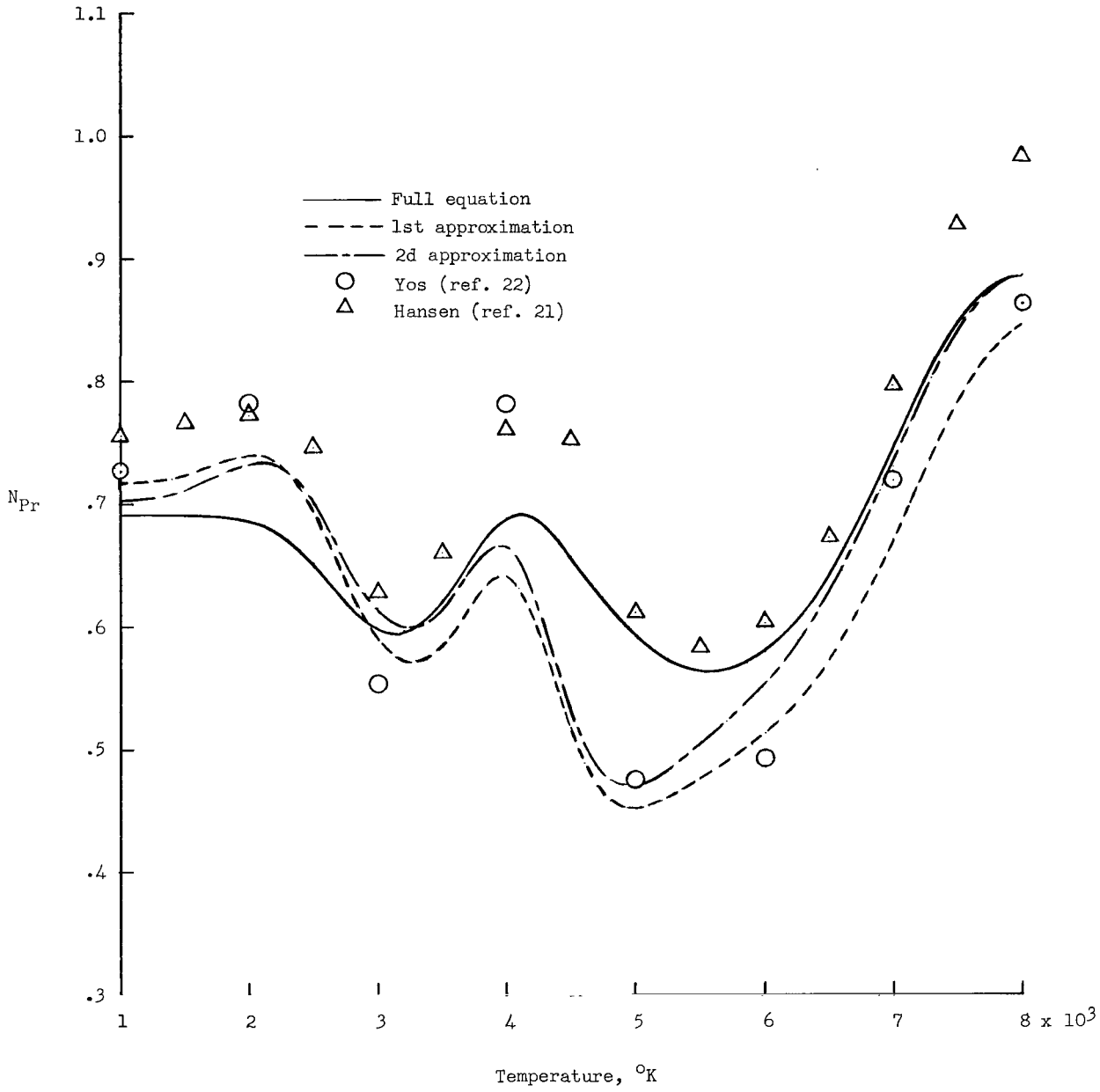

Figure 30.- Comparison of full-equation calculation of Prandtl number of air with approximate calculations and previous results for p = 1 atm.

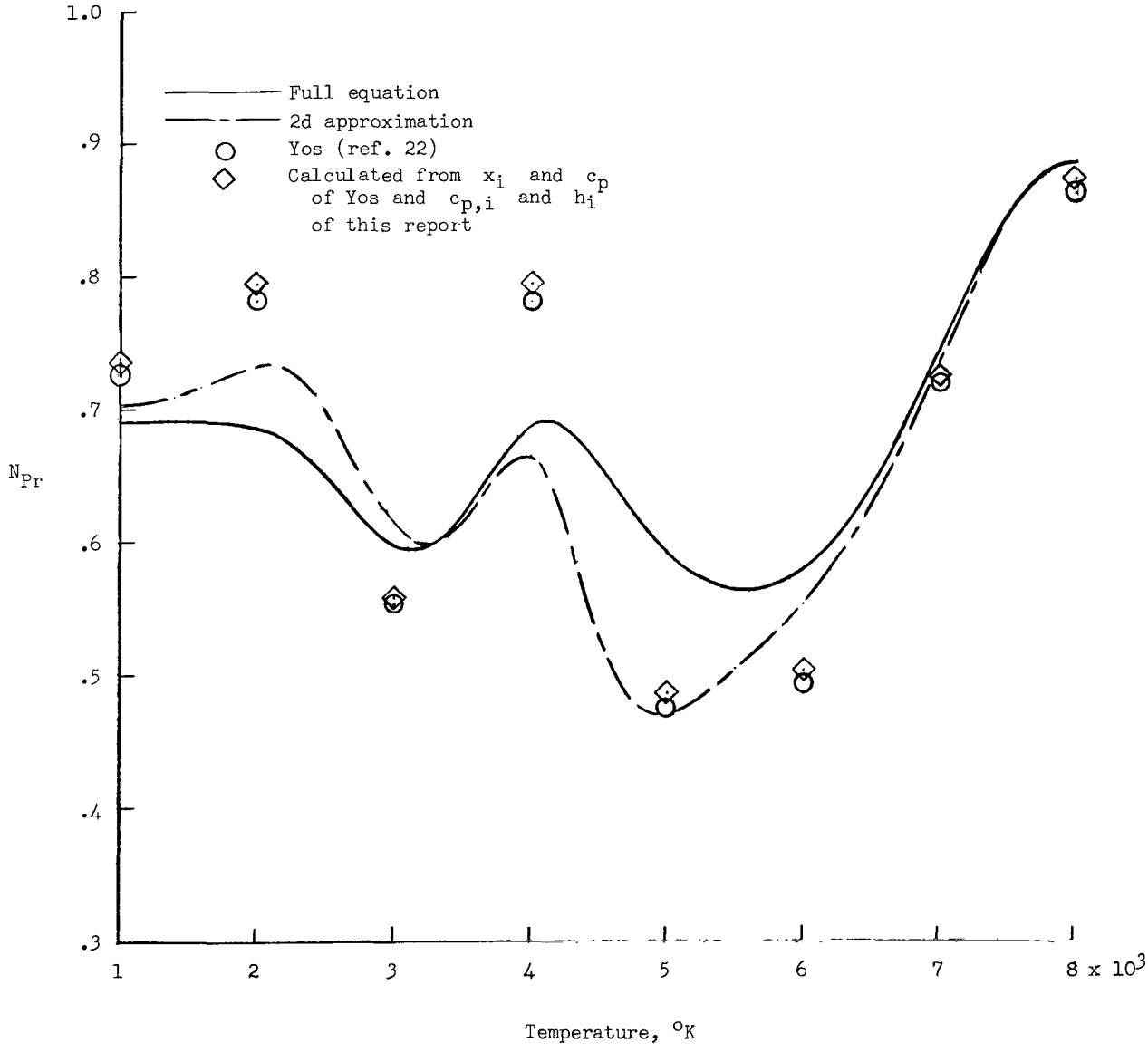

Figure 31.- Comparison of full-equation and approximate calculations of Prandtl number of air with modified data of Yos for p = 1 atm.

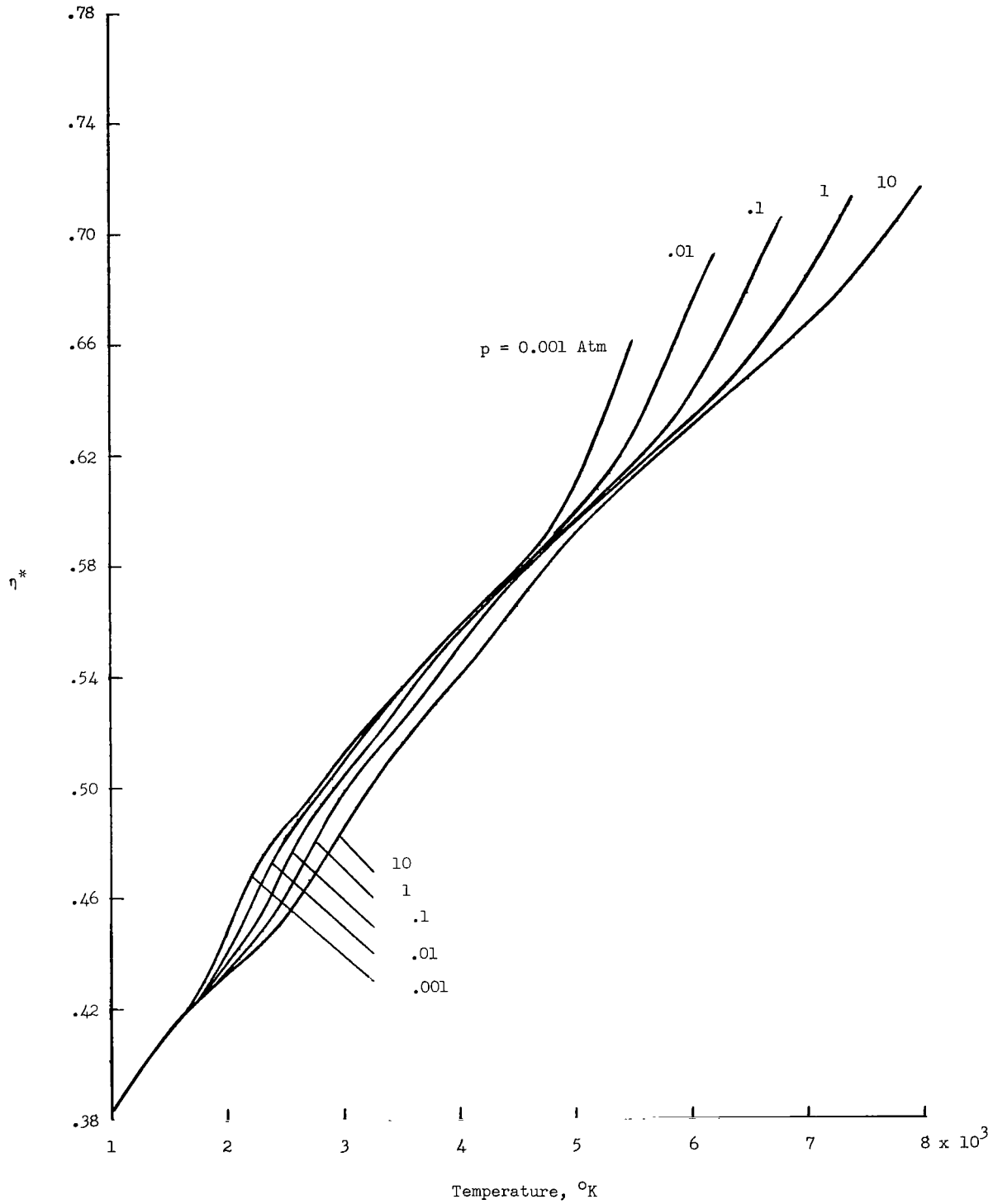

Figure 32.- Variation of nondimensional viscosity of CO_2 with temperature.

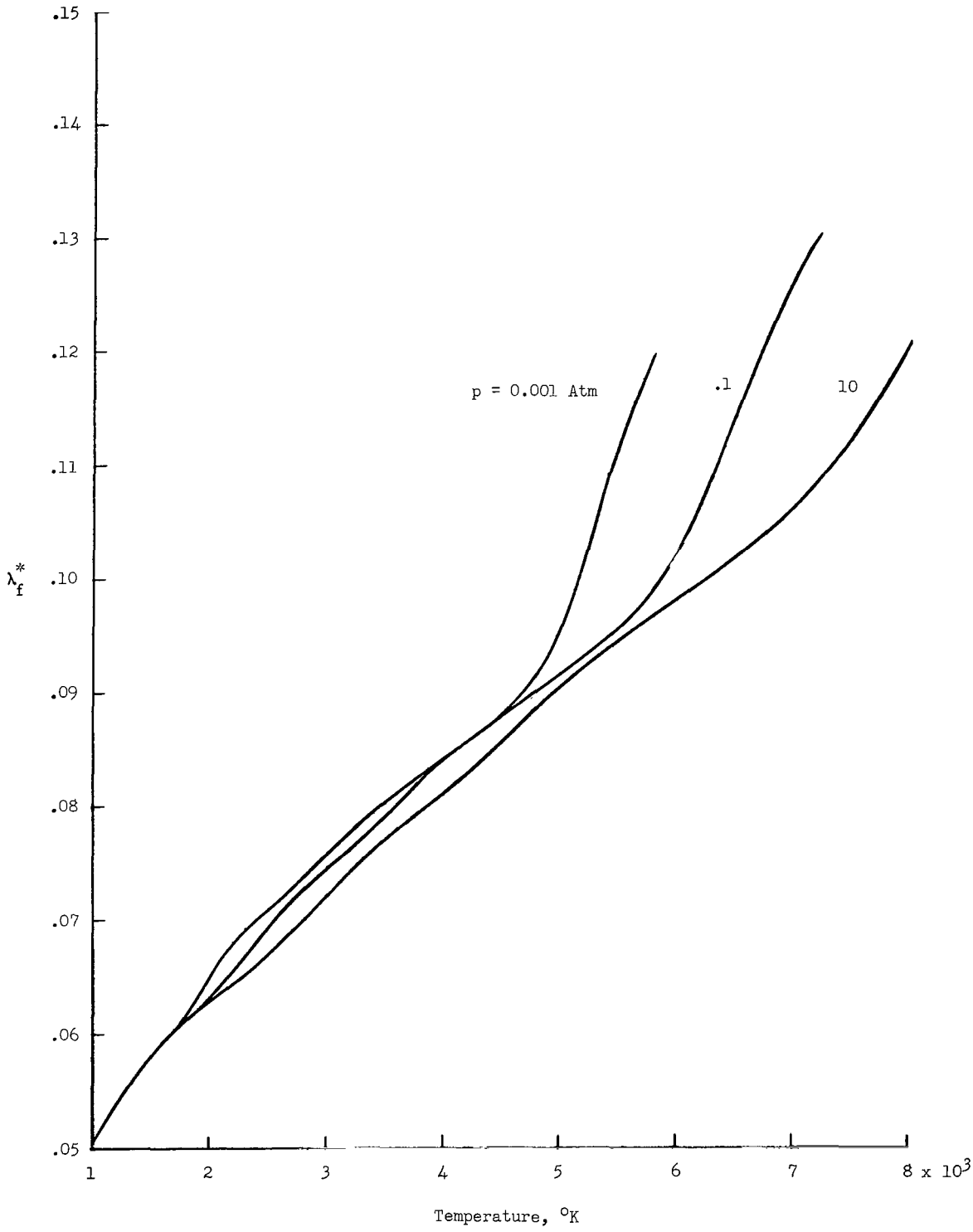

Figure 33.- Variation of nondimensional frozen conductivity of CO_2 with temperature.

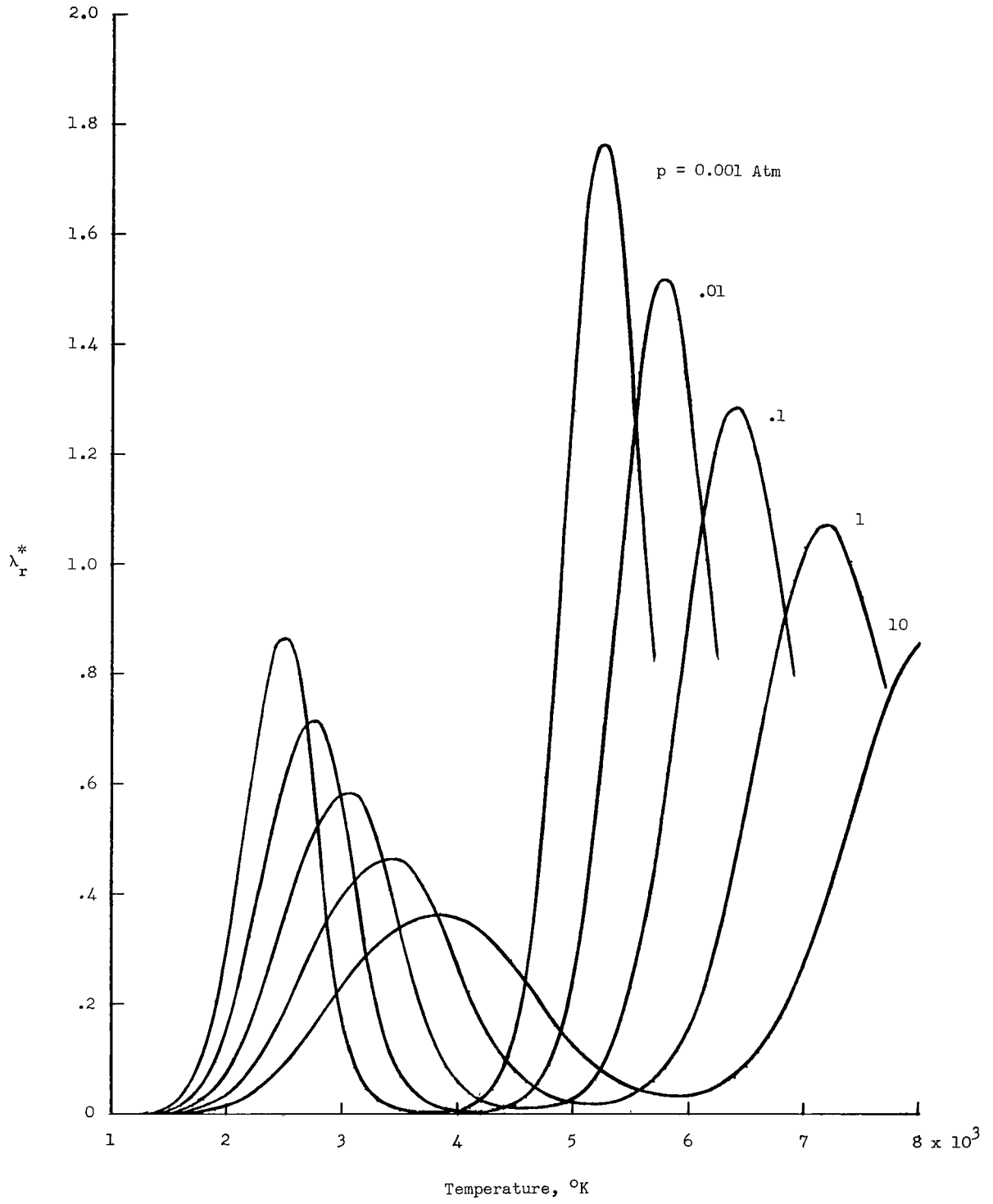

Figure 34.- Variation of nondimensional reactive conductivity of CO_2 with temperature.

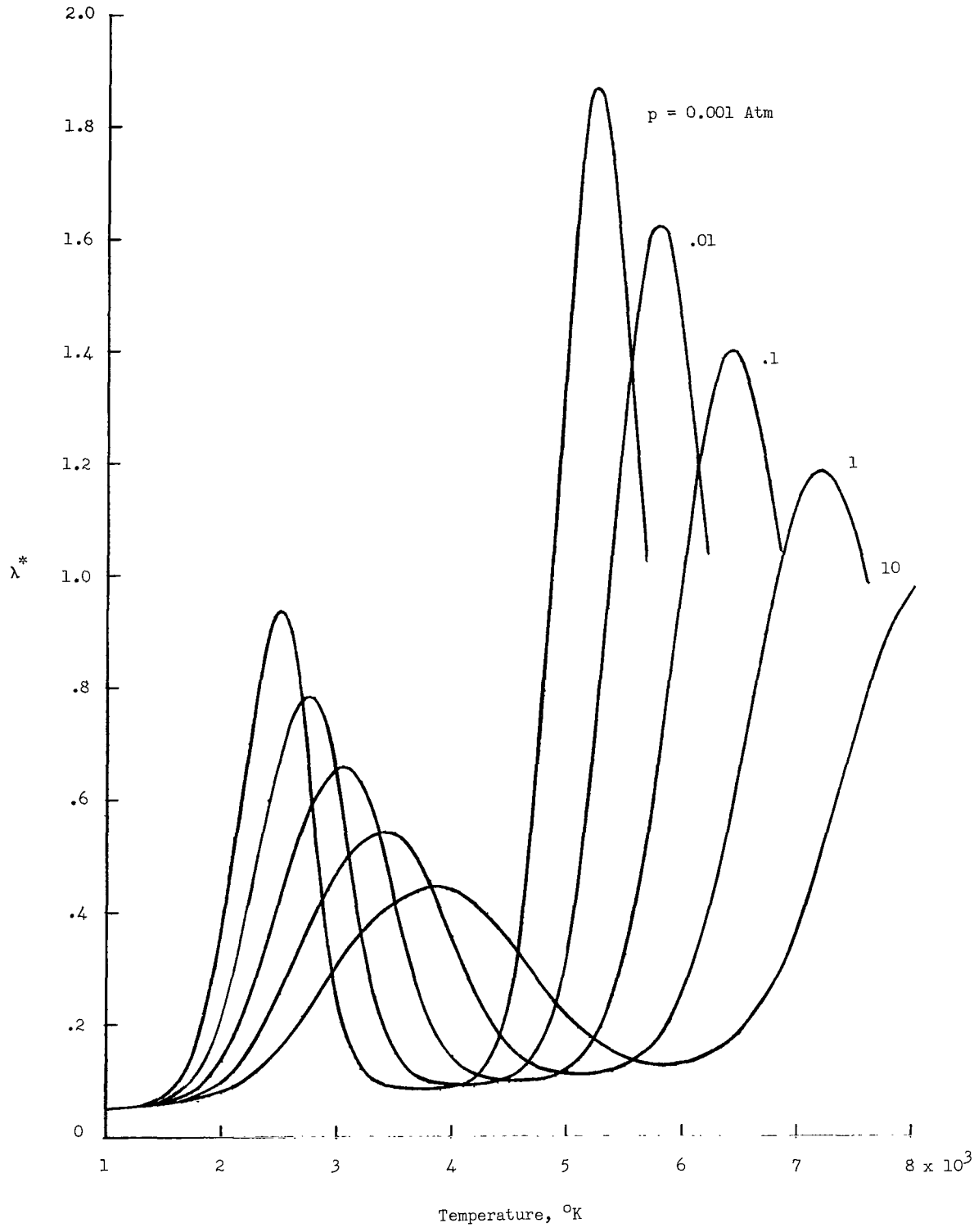

Figure 35.- Variation of nondimensional total conductivity of CO_2 with temperature.

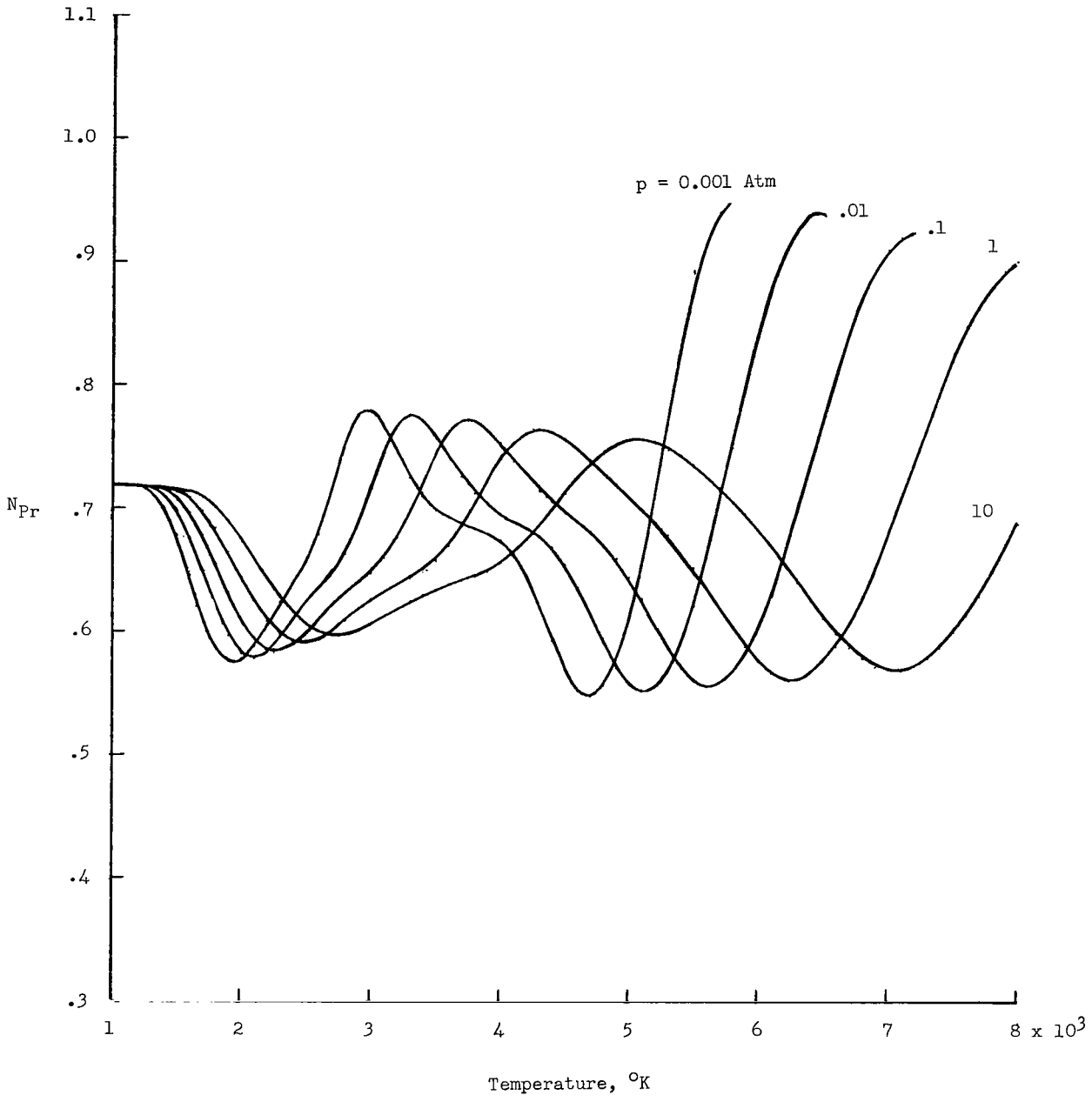

Figure 36.- Variation of Prandtl number of CO_2 with temperature.

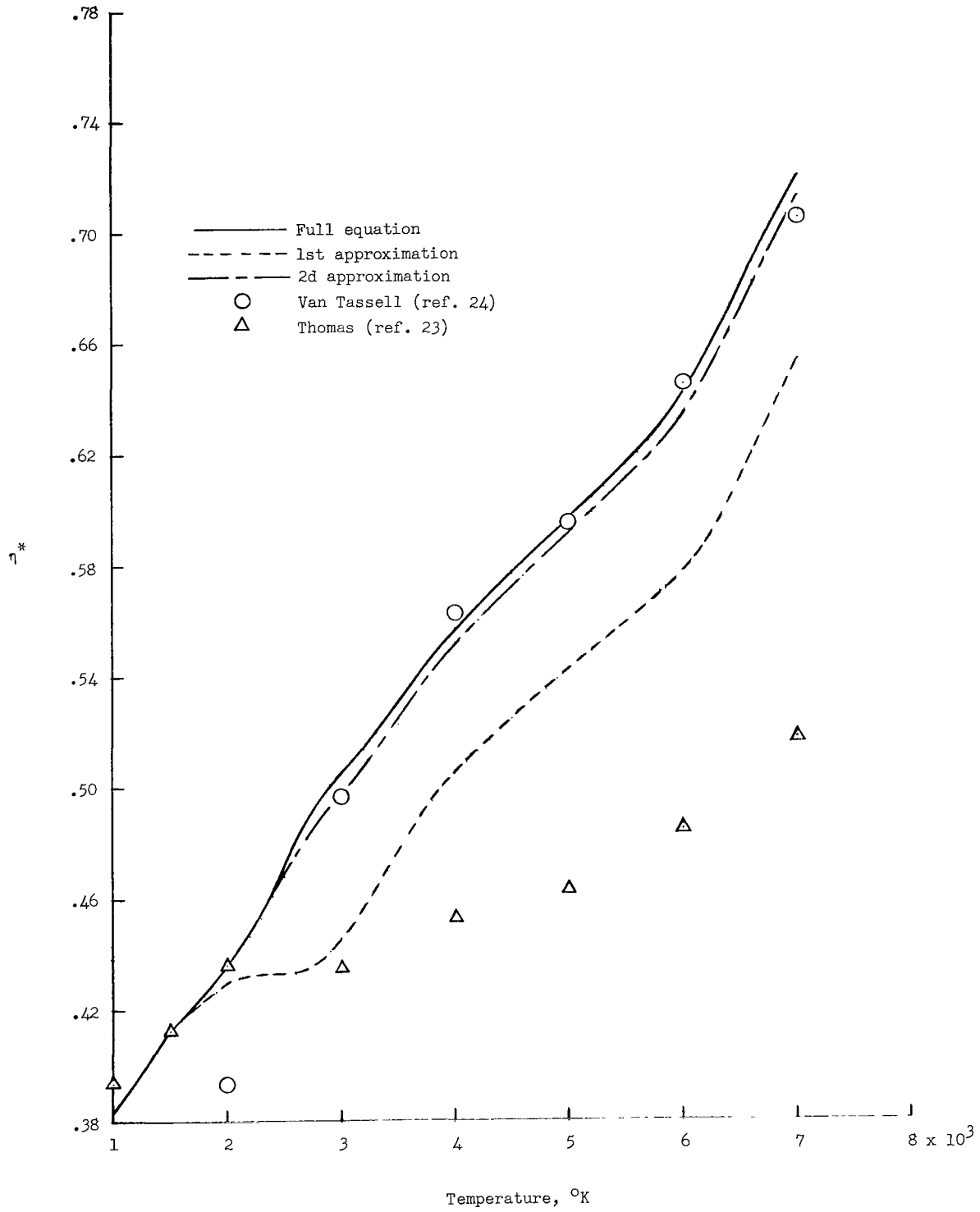

Figure 37.- Comparison of full-equation calculation of nondimensional viscosity of CO_2 with approximate calculations and previous results for p = 0.1 atm.

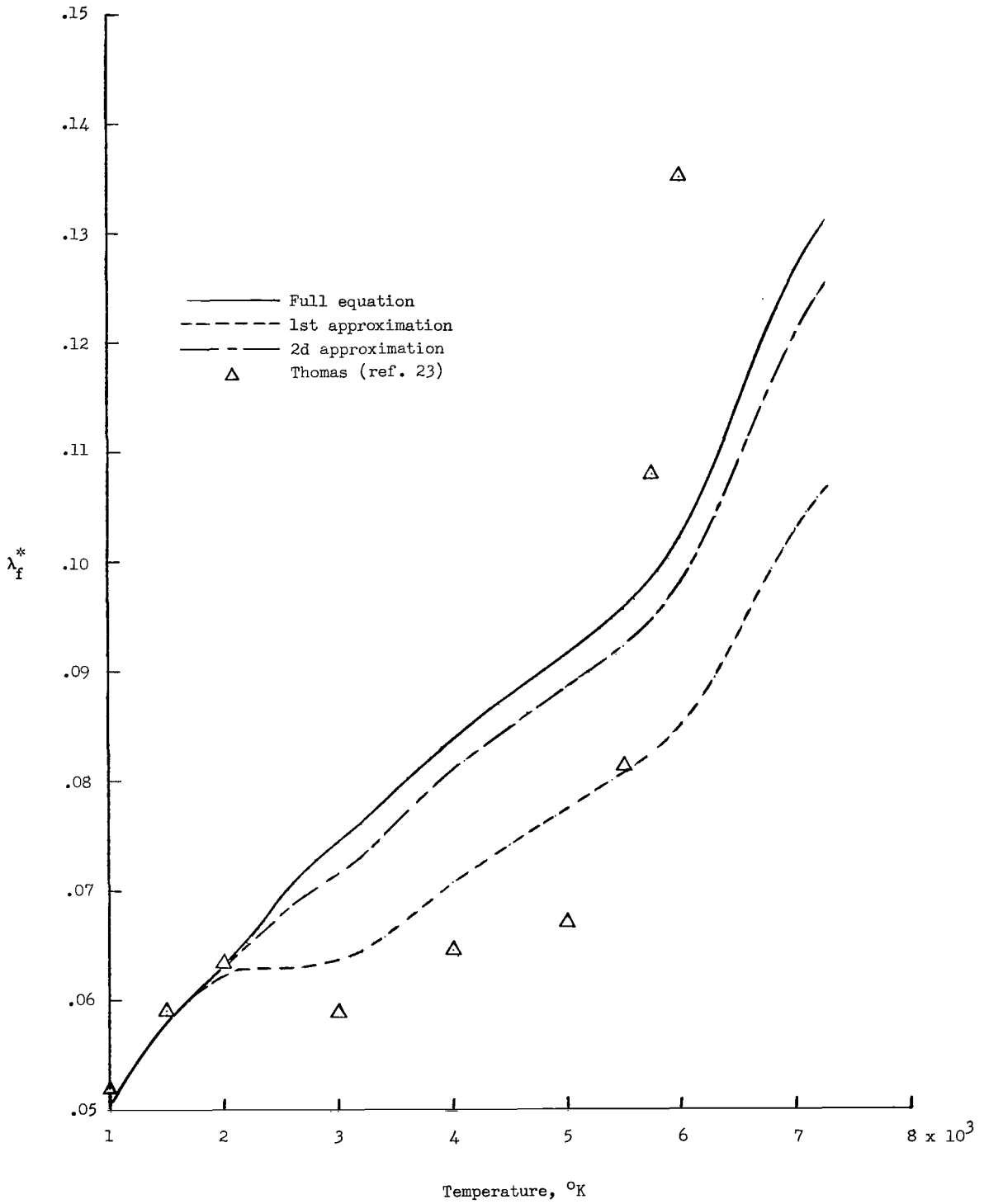

Figure 38.- Comparison of full-equation calculation of nondimensional frozen conductivity of CO_2 with approximate calculations and previous results for p = 0.1 atm.

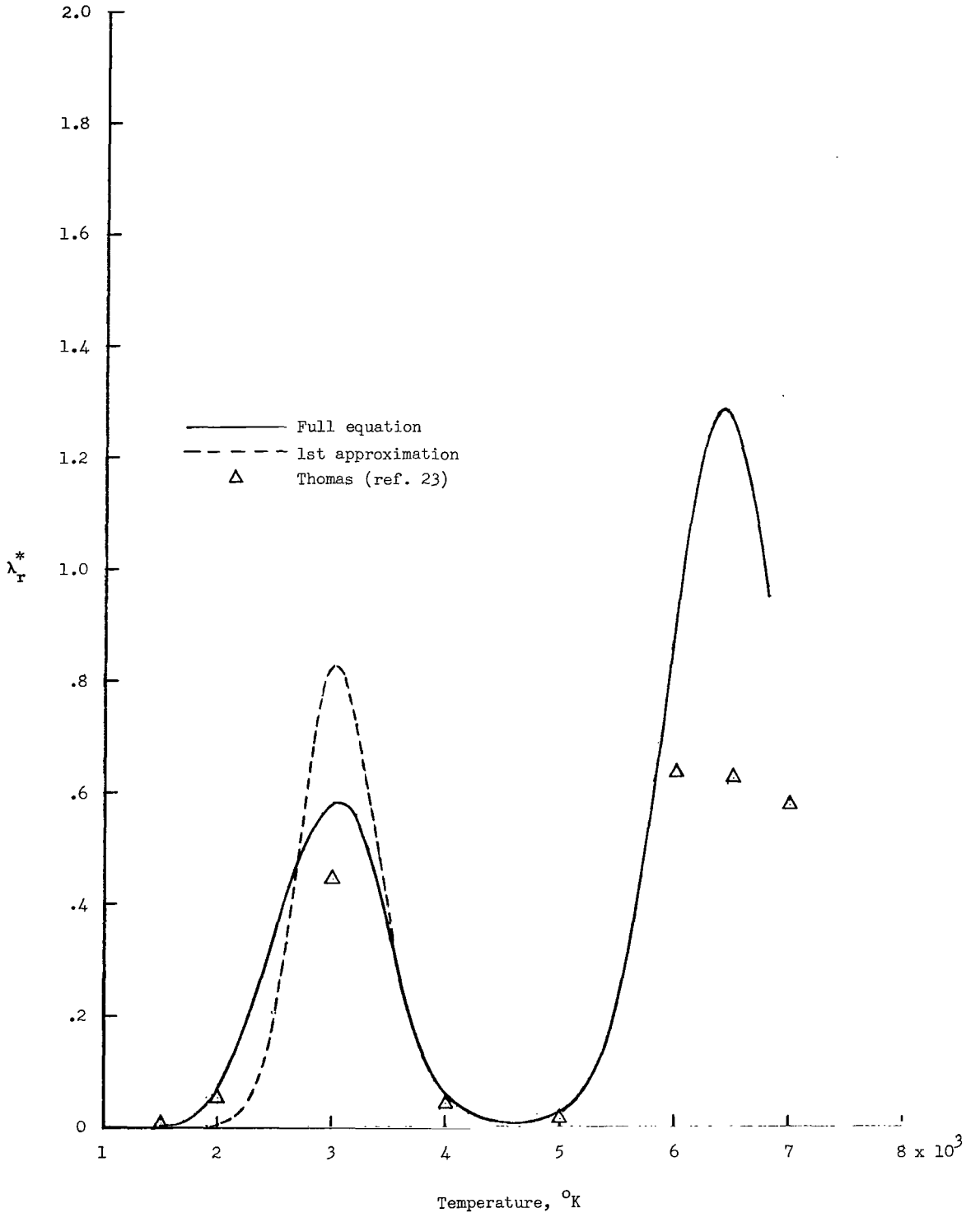

Figure 39.- Comparison of full-equation calculation of nondimensional reactive conductivity of CO_2 with approximate calculations and previous results for p = 0.1 atm.

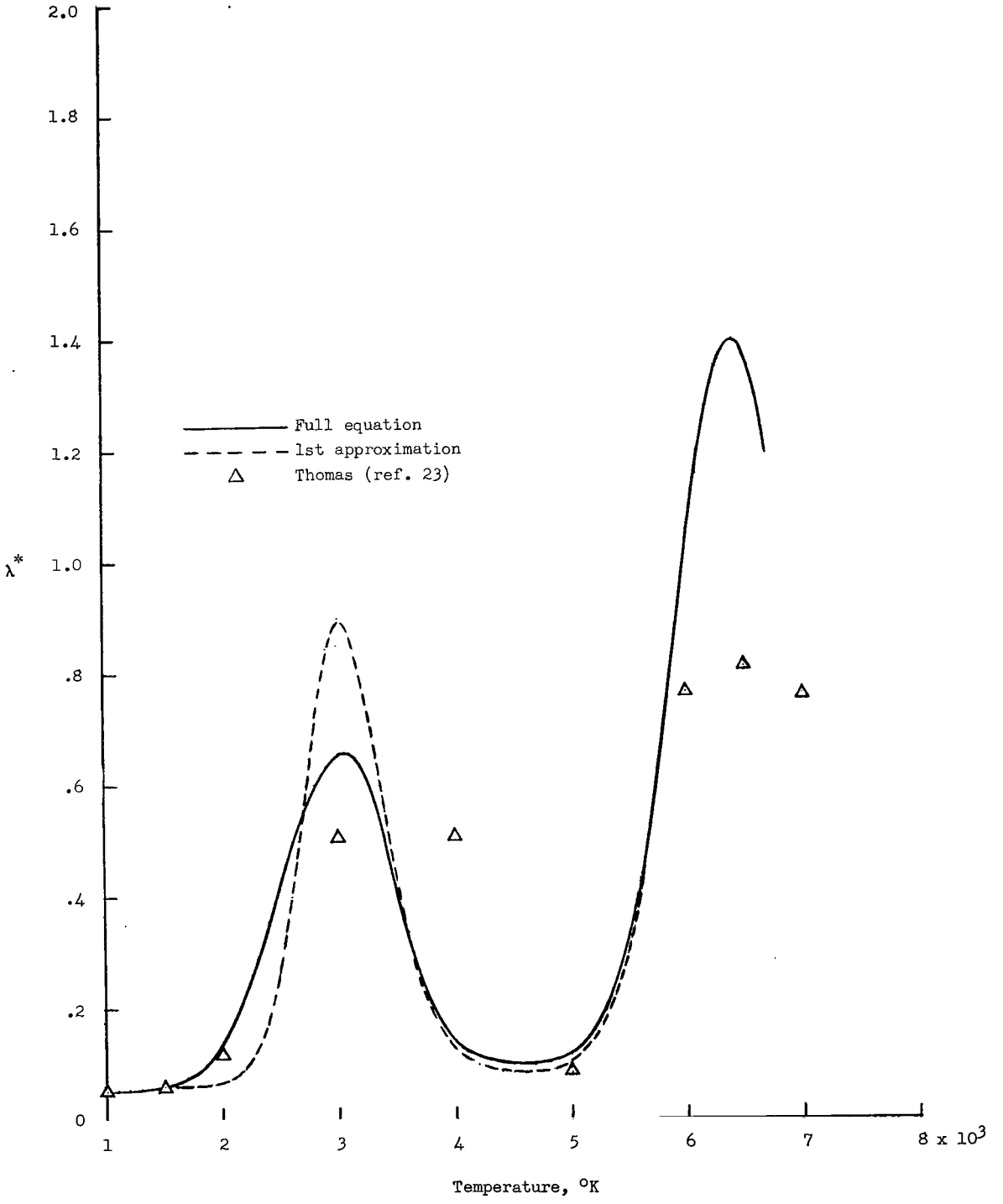

Figure 40.- Comparison of full-equation calculation of nondimensional total conductivity of CO_2 with approximate calculations and previous results for p = 0.1 atm.

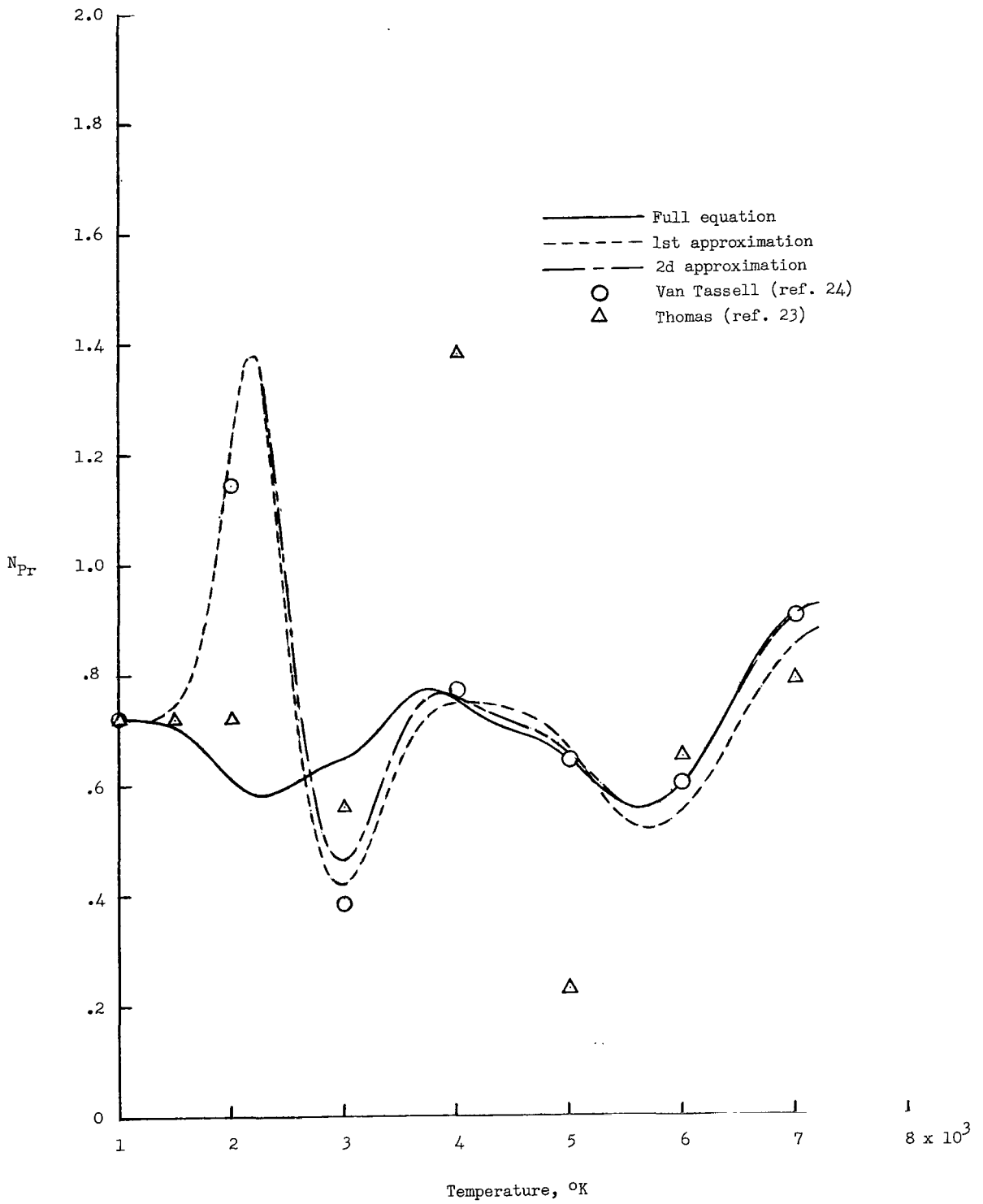

Figure 41.- Comparison of full-equation calculation of Prandtl number of CO_2 with approximate calculations and previous results for p = 0.1 atm.

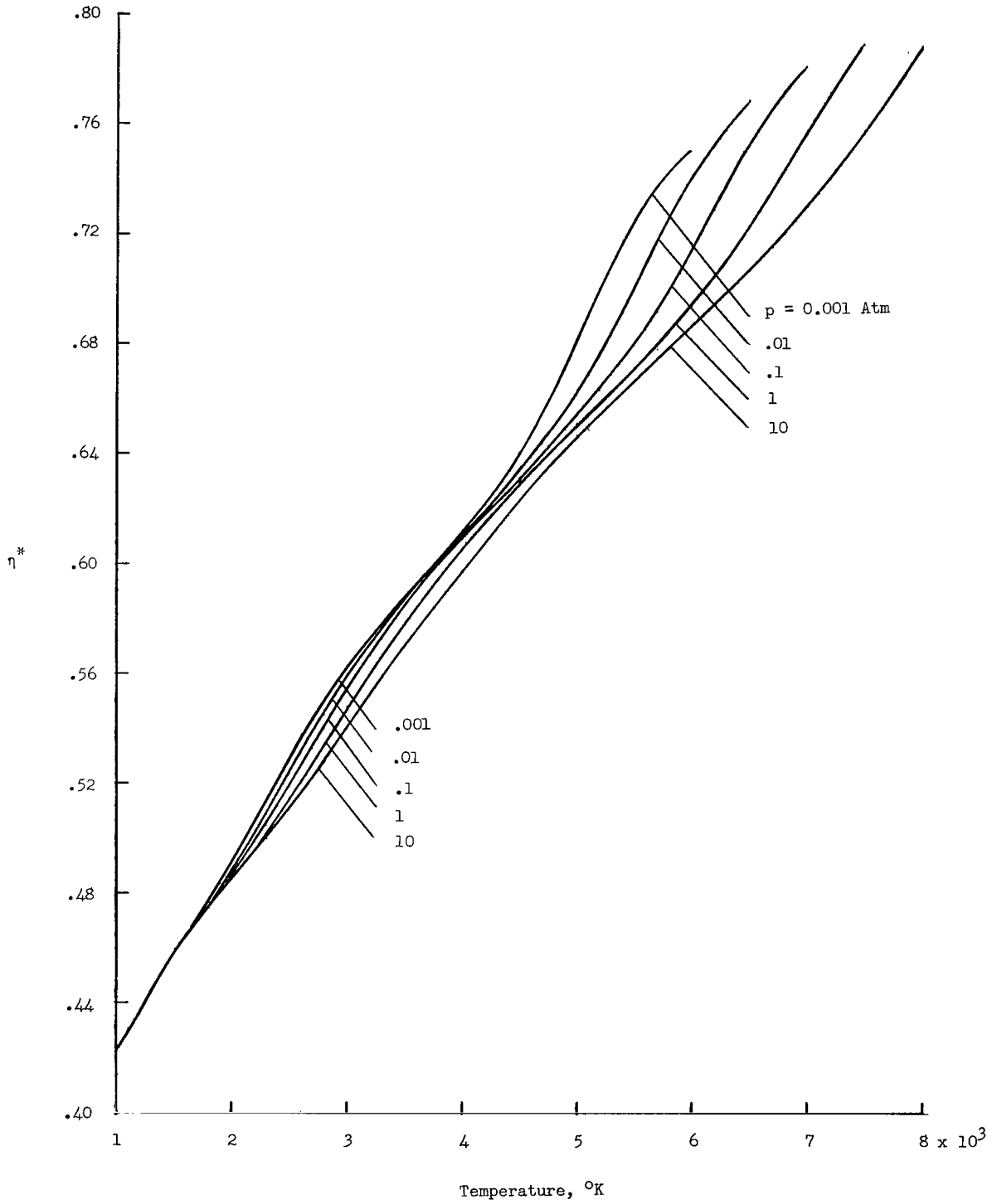

Figure 42.- Variation of nondimensional viscosity of the Mars model atmosphere with temperature.

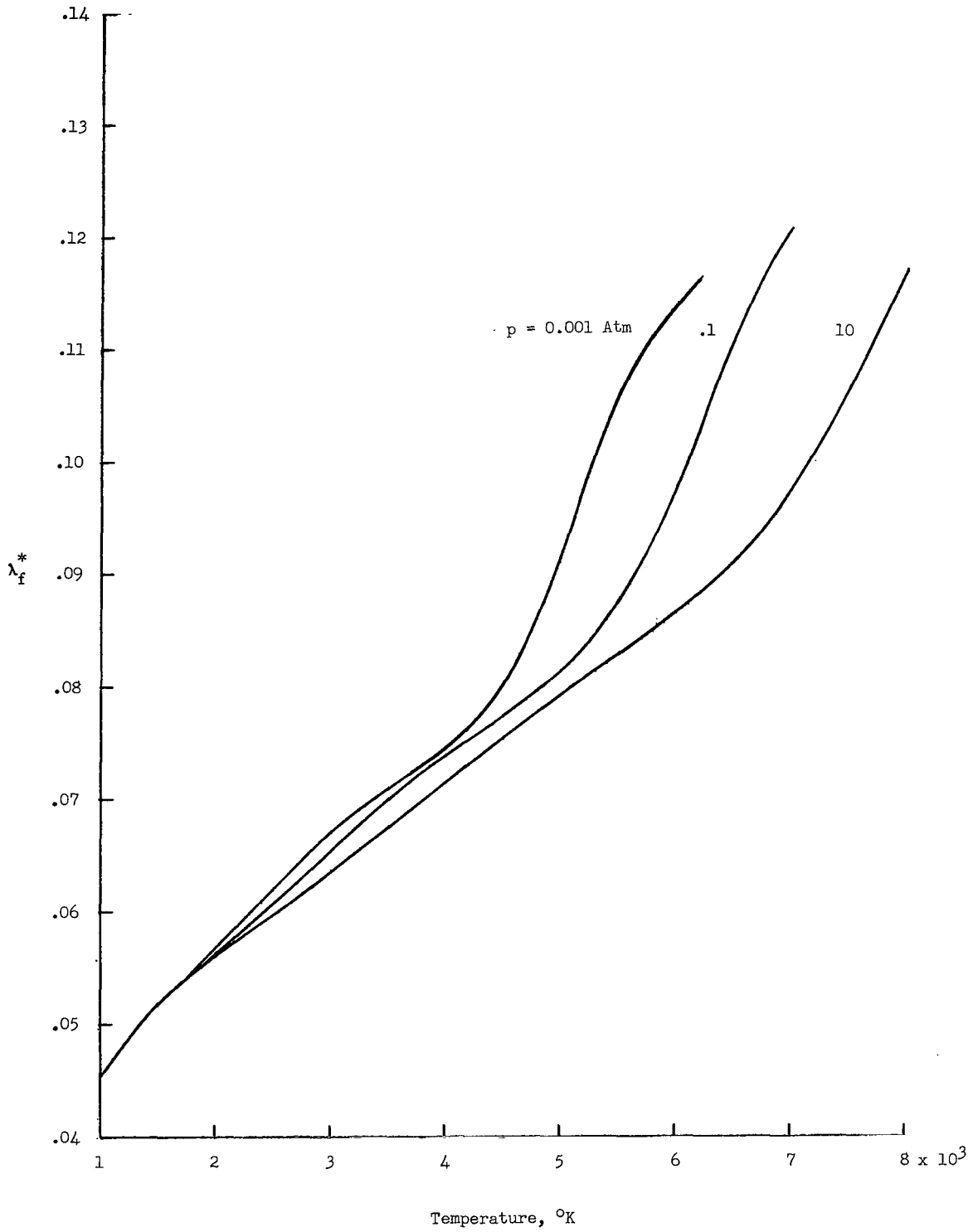

Figure 43.- Variation of nondimensional frozen conductivity of the Mars model atmosphere with temperature.

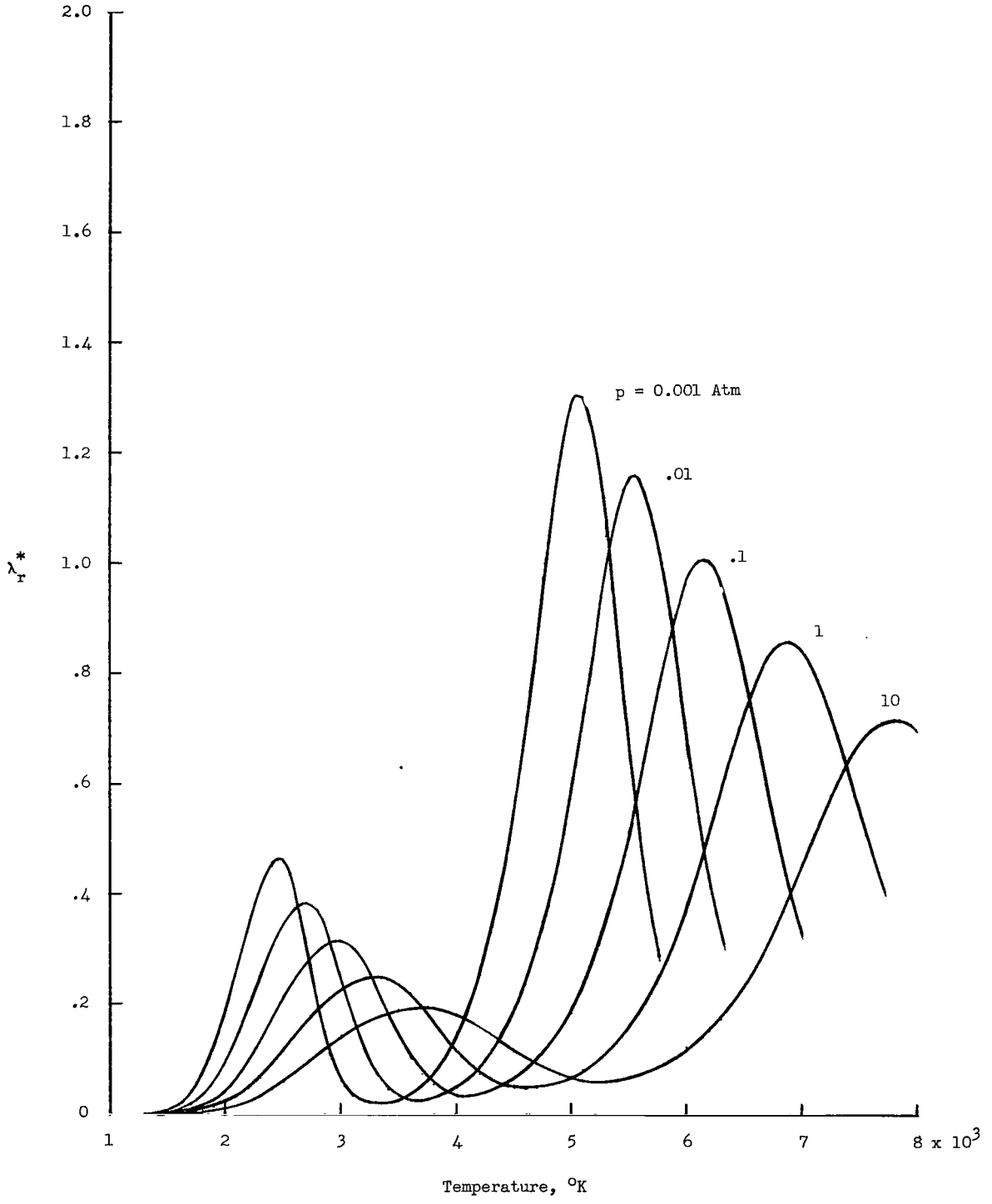

Figure 44.- Variation of nondimensional reactive conductivity of the Mars model atmosphere with temperature.

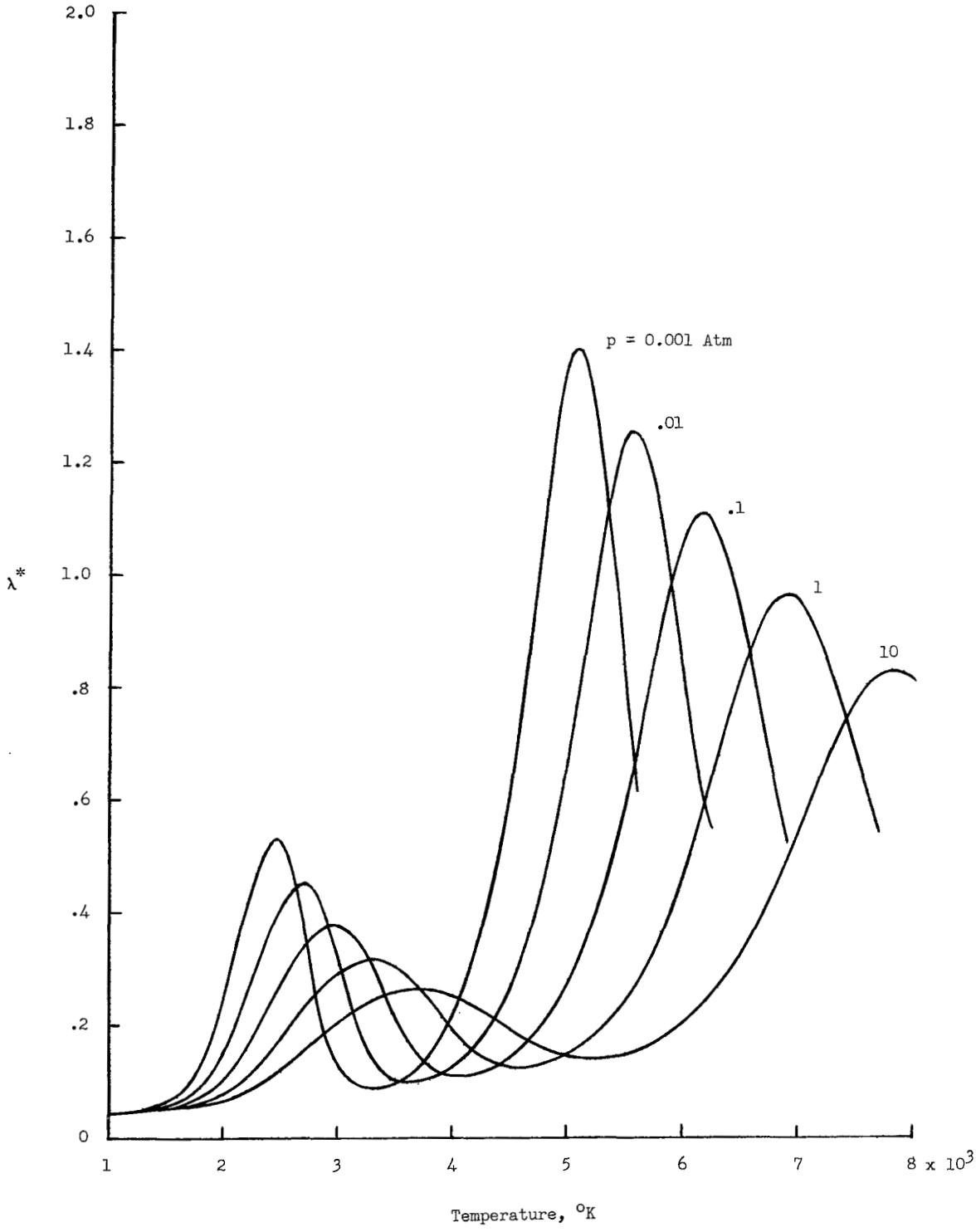

Figure 45.- Variation of nondimensional total conductivity of the Mars model atmosphere with temperature.

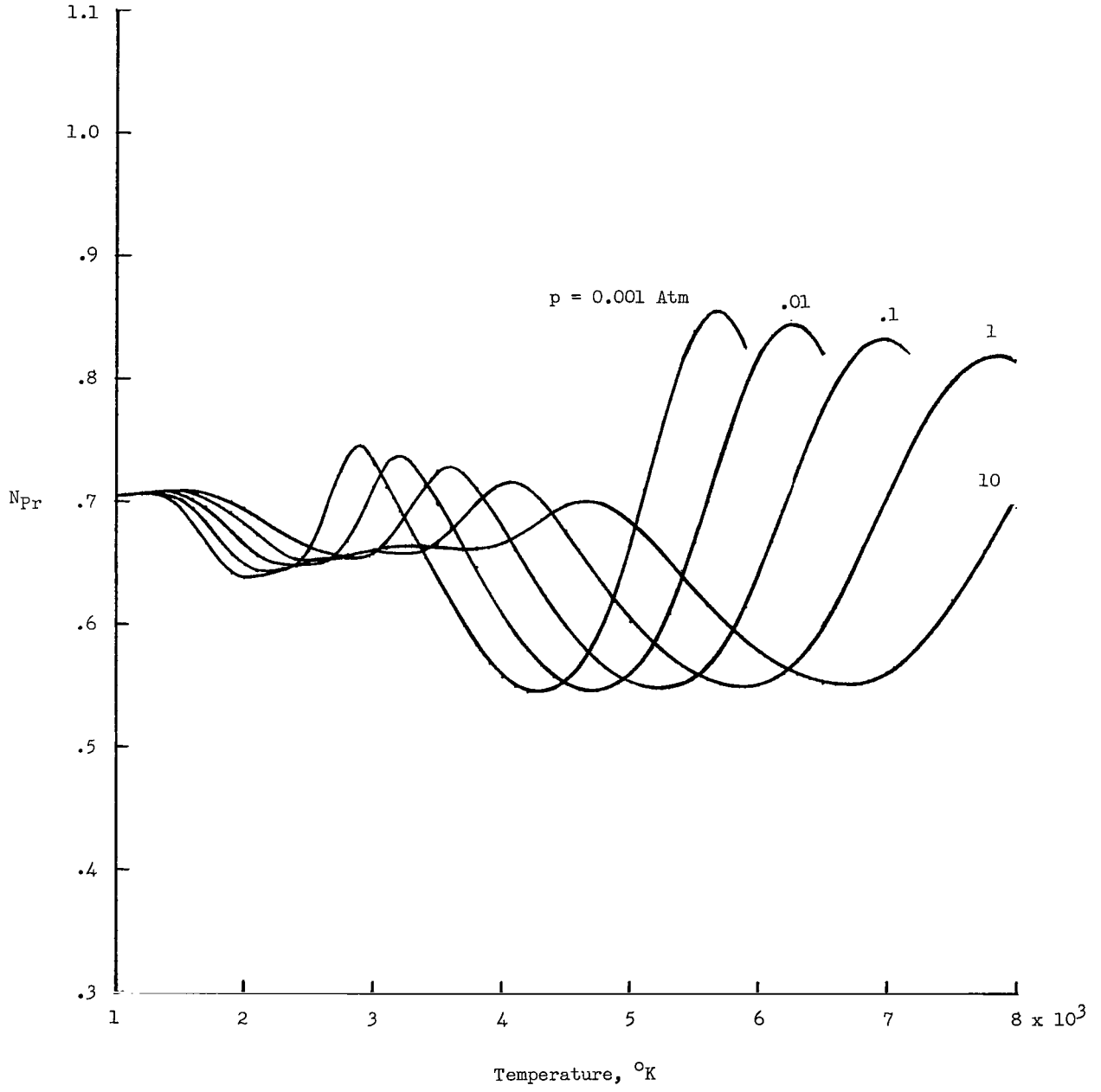

Figure 46.- Variation of Prandtl number of the Mars model atmosphere with temperature.

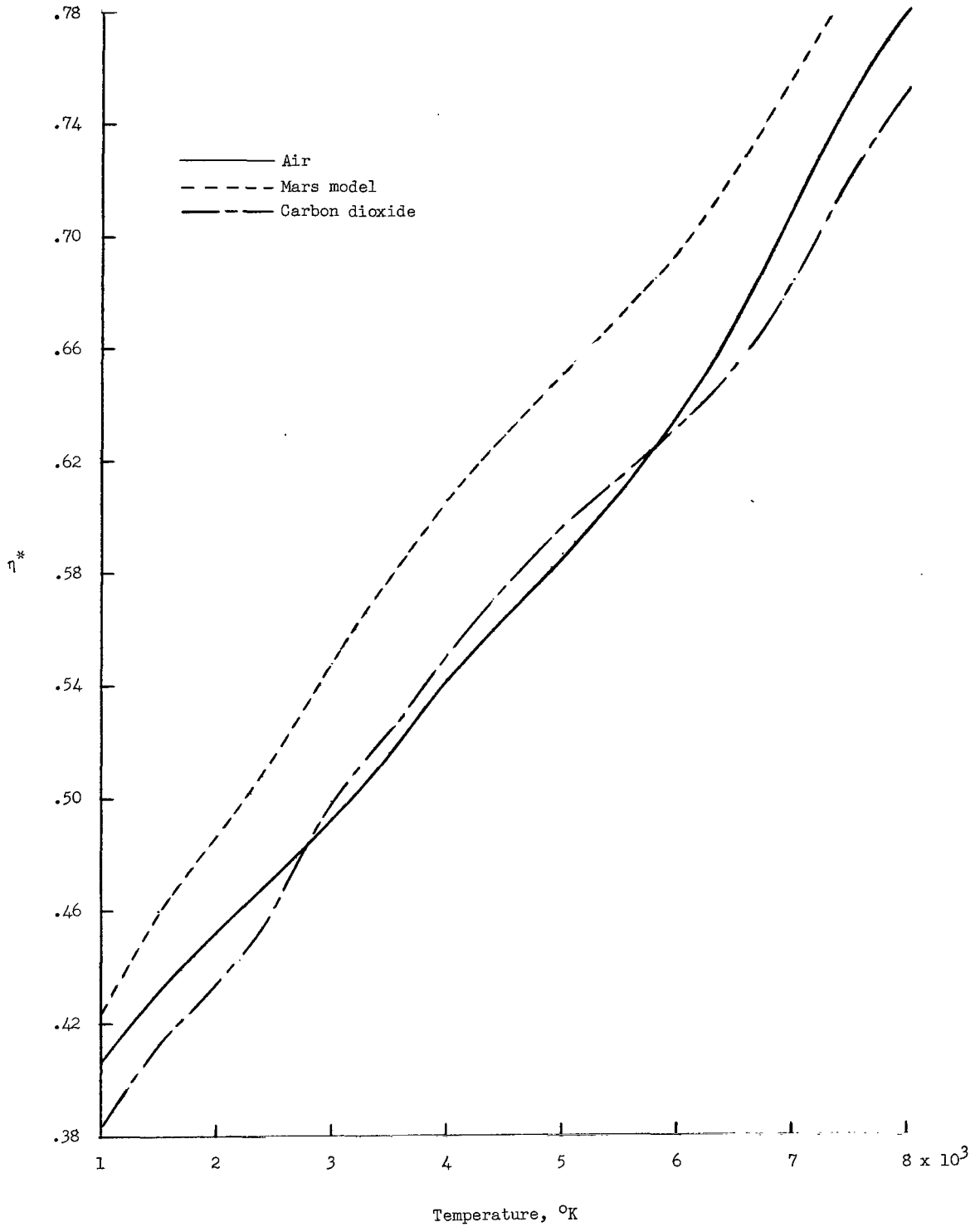

Figure 47.- Comparison of nondimensional viscosities of air, CO_2, and the Mars model atmosphere for p = 1.0 atm.

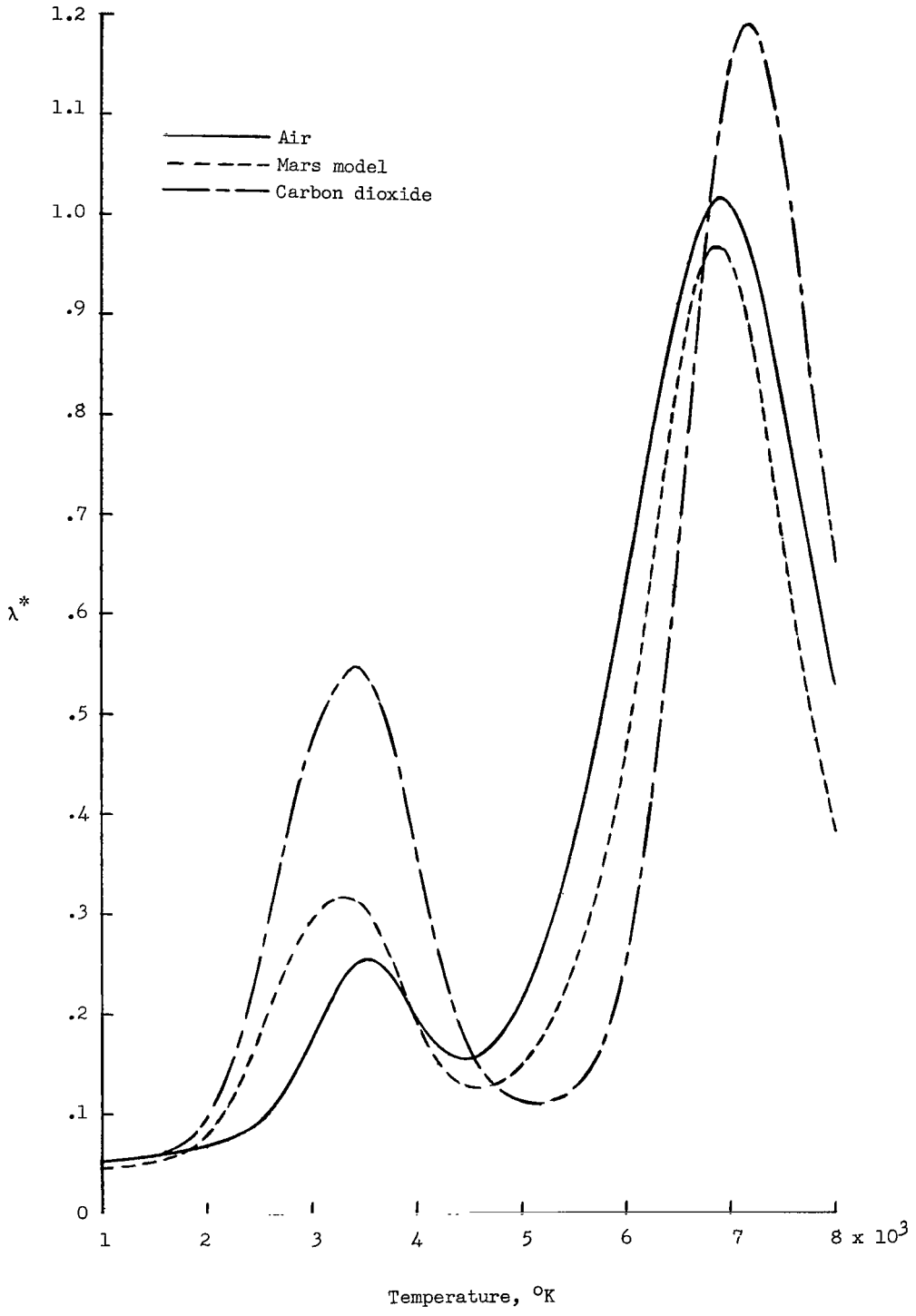

Figure 48.- Comparison of nondimensional total conductivities of air, CO_2, and the Mars model atmosphere for p = 1.0 atm.

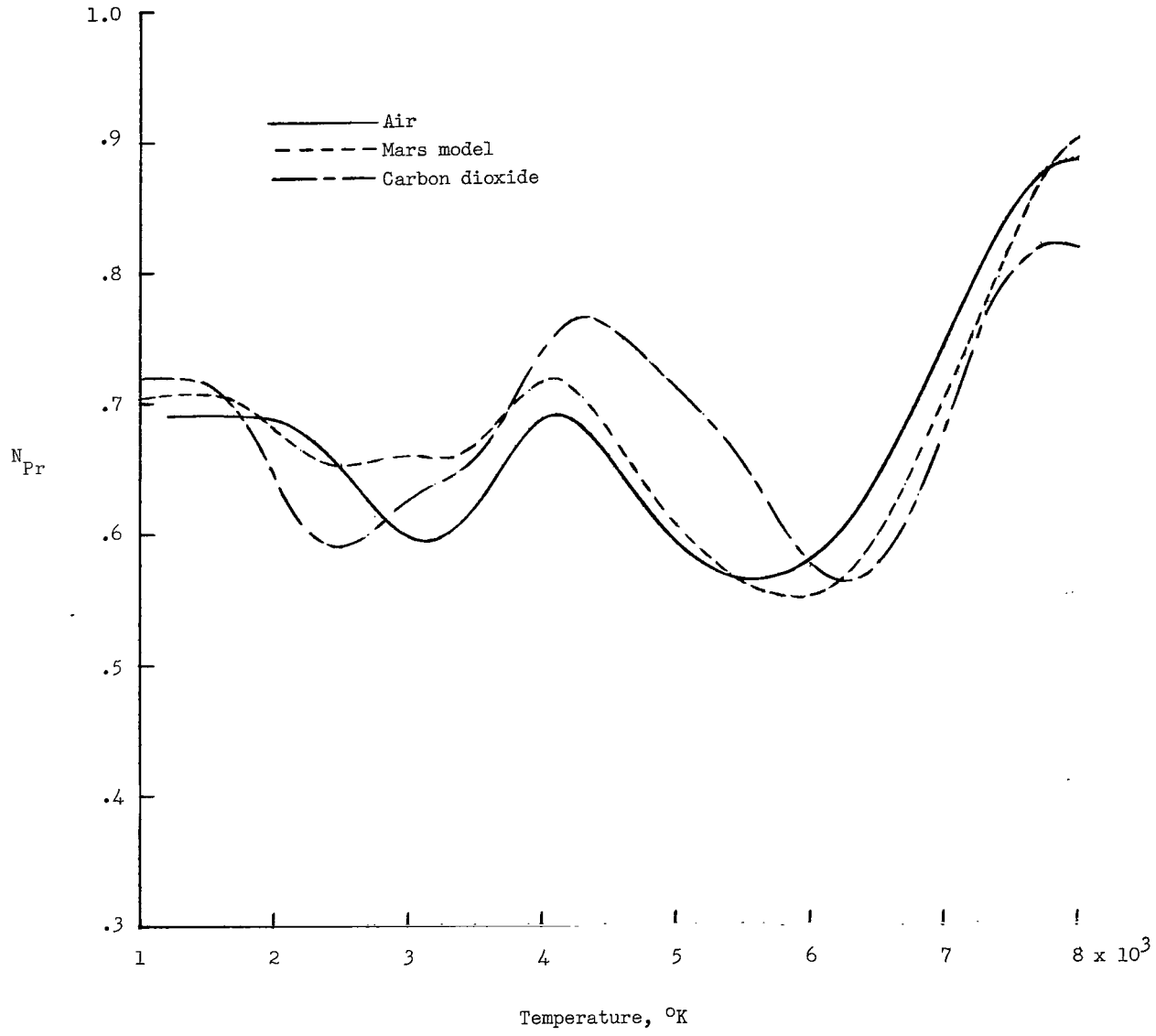

Figure 49.- Comparison of Prandtl numbers of air, CO_2, and the Mars model atmosphere for $p = 1.0$ atm.

"The aeronautical and space activities of the United States shall be conducted so as to contribute . . . to the expansion of human knowledge of phenomena in the atmosphere and space. The Administration shall provide for the widest practicable and appropriate dissemination of information concerning its activities and the results thereof."

—NATIONAL AERONAUTICS AND SPACE ACT OF 1958

NASA SCIENTIFIC AND TECHNICAL PUBLICATIONS

TECHNICAL REPORTS: Scientific and technical information considered important, complete, and a lasting contribution to existing knowledge.

TECHNICAL NOTES: Information less broad in scope but nevertheless of importance as a contribution to existing knowledge.

TECHNICAL MEMORANDUMS: Information receiving limited distribution because of preliminary data, security classification, or other reasons.

CONTRACTOR REPORTS: Scientific and technical information generated under a NASA contract or grant and considered an important contribution to existing knowledge.

TECHNICAL TRANSLATIONS: Information published in a foreign language considered to merit NASA distribution in English.

SPECIAL PUBLICATIONS: Information derived from or of value to NASA activities. Publications include conference proceedings, monographs, data compilations, handbooks, sourcebooks, and special bibliographies.

TECHNOLOGY UTILIZATION PUBLICATIONS: Information on technology used by NASA that may be of particular interest in commercial and other non-aerospace applications. Publications include Tech Briefs, Technology Utilization Reports and Notes, and Technology Surveys.

Details on the availability of these publications may be obtained from:

SCIENTIFIC AND TECHNICAL INFORMATION DIVISION

NATIONAL AERONAUTICS AND SPACE ADMINISTRATION

Washington, D.C. 20546